Fabrication of a New Model Hybrid Material and Comparative Studies of its Mechanical Properties

by

Daniel Robert Andrew Cluff

A thesis
presented to the University of Waterloo
in fulfillment of the
thesis requirement for the degree of
Master of Applied Science
in
Mechanical Engineering

Waterloo, Ontario, Canada, 2007

AUTHOR'S DECLARATION

I hereby declare that I am the sole author of this thesis. This is a true copy of the thesis, including any required final revisions, as accepted by my examiners.

I understand that my thesis may be made electronically available to the public.

Abstract

A novel aluminum foam-polymer hybrid material was developed by filling a 10 pore per inch (0.39 pores per millimeter), 7 % relative density Duocel® open-cell aluminum foam with a thermoplastic polymer of trade name Elvax®. The hybrid was developed to be completely recyclable and easy to process. The foam was solution treated, air quenched and then aged for various times at 180˚C and 220˚C to assess the effect of heat treatment on the mechanical properties of the foam and to choose the appropriate aging condition for the hybrid fabrication. An increase in yield strength, plateau height and energy absorbed was observed in peak-aged aluminum foam in comparison with under-aged aluminum foam. Following this result, aluminum foam was utilized either at the peak-aged condition of 4 hrs at 220˚C or in the as-fabricated condition to fabricate the hybrid material. Mechanical properties of the aluminum foam-polymer hybrid and the parent materials were assed through uniaxial compression testing at static ($\dot{\varepsilon} \approx 0.008 s^{-1}$) and dynamic ($\dot{\varepsilon} \approx 100 s^{-1}$) loading rates. The damping characteristics of aluminum foam-polymer hybrid and aluminum foam were also obtained by compression-compression cyclic testing at 5 Hz. No benefit to the mechanical properties of aluminum foam or the aluminum foam-polymer hybrid was obtained by artificial aging to peak-aged condition compared to as-fabricated foam. Although energy absorption efficiency is not enhanced by hybid fabrication, the aluminum foam-polymer hybrid displayed enhanced yield stress, densification stress and total energy absorbed over the parent materials. The higher densification stress was indicative that the hybrid was a better energy absorbing material at higher stress than the aluminum foam. The aluminum foam was found to be strain rate independent unlike the hybrid where the visco-elasticity of the polymer component contributed to its strain rate dependence. The damping properties of both aluminum foam and the aluminum foam-polymer hybrid materials were found to be amplitude dependant with the hybrid material displaying superior damping capability.

Acknowledgements

I would like to gratefully thank my academic supervisor Shahrzad Esmaeili for her valuable guidance throughout this work. Her advice, support and patience have made all the difference in my completing this degree.

I would like to thank Dupont™ Scientist Dr. Sassan Hojabr and Dupont™ for both their advice in the polymer selection and for providing sufficient quantities of polymer to perform the required experiments. A special thanks goes to Norval Wilhelm and Amin Eshraghi for their help during experimental testing. Good conversations made the testing always enjoyable.

I am grateful for the financial support NSERC and the University of Waterloo provided for this work.

I can not forget to thank all the friends I have made while studying at the University of Waterloo. Specifically I would like to thank my group mates Panthea Sepehrband, Ashkan Shadkam and Roger Carrick as well as past group mates David Poetter and Brian Langelier. I would also like to thank my office mates Ramtin Movassaghi and Amir Poursaee for good conversations and afternoon tea. There are many others without whom I would not nearly have had as many fond memories of my time at Waterloo.

Finally and most importantly I would like to thank my family. My wife Ashleigh and my son Brennick who helped me keep my feet on the ground and showed me what is really important in life. We could not have made it through this without the support of both of our parents and I am grateful for all their assistance.

Table of Contents

List of Tables

.

List of Figures

Chapter 1
Introduction

Although currently there are over 40 000 materials available for a designer to choose from [Ashby 1992] gaps in material properties still exist. The presence of gaps is especially true when a combination of properties (e.g. weight and stiffness) is required [Ashby and Bréchet 2003]. These gaps can be filled by producing new alloys and polymers, however this can be difficult and expensive, or an easier way is the design of new hybrid materials [Ashby and Bréchet 2003]. Hybrid materials, an amalgamation of two or more monolithic materials combined in a predetermined shape and scale, display properties which are a combination of those displayed by the parent materials [Kromm *et al.* 2002]. In filling in the gaps in material properties hybrid materials open new design possibilities and concepts hitherto not possible with monolithic materials. There is therefore much interest in the development and production of hybrid materials.

The term hybrid material encompasses both traditional composite materials, like carbon fiber reinforced polymer matrices and shape based material combinations, such as sandwich panels (i.e. solid face sheets separated by a foam core) [Ashby and Bréchet 2003]. This term was chosen as the combination of the two materials in this work fits well with its definition. Similar materials reported on in literature are also referred to as hybrid materials throughout the course of this work.

Aluminum foam, a hybrid material in its own right (i.e. metal-air), is used on its own or as a component in other hybrid structures in both structural and impact applications due to its high mass specific stiffness and excellent energy absorption properties [Harte *et al.* 1999, Hassen *et al.* 2000, Andrews *et al. 2001*, Tagarielli *et al.* 2004, and Wang *et al.* 2006]. It can be fabricated with open (i.e. interconnected network of empty space) or closed cells (i.e. empty space closed off from neighboring cells) [Gibson and Ashby 1997]. An open cell network leaves open the possibility of filling with a

second material. Thermosetting polymers with their relatively low weight and high energy absorption and damping capacities have been utilized by other researchers to create a new hybrid material showing an increase in energy absorption [Cheng and Han 2003, and Kwon *et al.* 2003]. Increasingly however, environmental considerations are also factors in material selection. As thermosets are not recyclable it is the aim of this study to produce an aluminum foam-polymer hybrid material from a thermoplastic polymer which can be separated from the aluminum via melting and allow both materials to be recycled separately.

There has been much interest in aluminum foam and aluminum foam based hybrids for structural and impact protection applications in the automotive, railway and aerospace industries [Banhart 2001, Cheng and Han 2003, Krishna 2007]. These newly developed materials could help contribute to increased safety, comfort and weight savings. Important in the design for these applications is the knowledge of the mechanical response of the hybrid materials under static and dynamic loading conditions as well as the hybrid's ability to absorb vibrations (i.e. damping capacity). With a newly developed hybrid the material properties are not known. It is therefore an aim to characterize the mechanical response of the model hybrid material under static and dynamic loading conditions, and to determine the damping capacity by way of cyclic testing.

Chapter 2
Literature Review

2.1 Introduction

The present research focuses on producing an aluminum foam-polymer hybrid material and the examining of its mechanical properties in comparison with its parent materials. In this chapter the concept of hybrid materials is presented followed by background on the types of mechanical testing performed on the model hybrid material. These include static and dynamic compression testing as well as damping capacity studies. Aluminum foam is the backbone of the hybrid material and therefore a solid background on aluminum foam is provided. Polymer properties followed by a brief summary of some aluminum foam composite materials round off the chapter.

2.2 Hybrid Material Concept

Hybrid materials expand the range of properties over those provided by monolithic materials [Ashby 1992]. A hybrid material is an amalgamation of two or more existing materials in a predetermined geometry and scale [Ashby and Bréchet 2003]. The properties of the resultant material are a combination of the parent materials' [Ashby and Bréchet 2003]. All materials which fit this description in literature will be labeled as hybrid materials for the purpose of this study. From the concept introduced by Ashby and Bréchet [2003] a schematic of possible hybrid properties, based on the component materials, is seen in Figure 2.1. In the ideal case the hybrid material possesses the best properties of the component materials shown as 'A'. This occurs in composites such as galvanized steel where the full strength of steel is retained along with the corrosion resistance of zinc. In many structural composites, such as long fiber reinforced composites loaded in the direction of the fibers, the "rule of mixtures" is the best that can be achieved. This is shown as 'B'. The point 'C' denotes the

harmonic mean of the component properties, a relationship found in particle reinforced composites. The worst case scenario is ‘D’ where the worst properties of each component are demonstrated in the hybrid material.

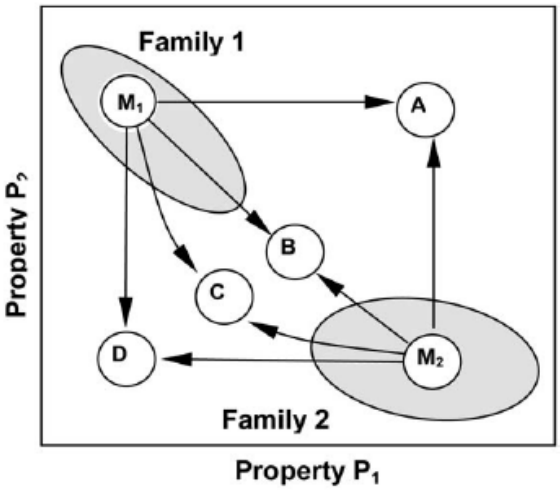

Figure 2.1: Hybrid properties due to possible combinations of hybrid component properties. The combination of the best of the component properties result in ‘A’ and the combination of the worst result in ‘D’. [Ashby and Bréchet 2003]

The expanded range of properties allow for the development of new design possibilities to meet the demanding requirements of present and future applications [Ashby and Bréchet 2003]. In the majority of structural and crashworthiness applications, aluminum foam is combined with other materials such as aluminum extrusions and aluminum face sheets [Hanssen *et al.* 2002]. Components made from aluminum foam and aluminum foam hybrid materials are used in light weight construction of structural panels and energy absorbing devices in the automotive, aerospace and railway industries [Gioux *et al.* 2000, Fuganti *et al.* 2000, Banhart 2001, Kretz *et al.* 2002, Miyoshi *et al.* 2002, Hanssen *et al.* 2002a, Fraunhofer USA—Delaware 2002, Chirwa *et al.* 2003, Wang *et al.* 2006 and NASA]. The following provides exemplar applications. The car manufacturer Karmann use 3-D foam

sandwich panels to replace the front bulk head and rear wall in a prototype car [Banhart 2001]. Kretz *et al.* [2002] show how lining the inside of an automobile A-pillar with foam can reduce injury to the head of an occupant in roll-over situations (~ 20 km/hr). Automotive crash boxes made from aluminum foam filled extrusions can reduce damage to the chasis under low speed impacts (~ 15 km/hr) [Fuganti *et al.* 2000]. NASA utilizes open-cell aluminum foams in the design of blast containers [NASA]. Trains in Japan have 2.3 m^3 of aluminum foam to improve crash energy absorption [Banhart 2001]. Sandwich panels can also be employed as energy absorbers for blast waves [Vaidya 2006] and as construction components in mobile military protective structures allowing for blast protection and easy portability [Sierakowski and Hughes 2006]. Machine designers make use of the damping capacity of aluminum foam to reduce the noise and vibrations produced [Banhart 2001].

2.3 Testing Methods

In the applications listed for aluminum foam and aluminum foam hybrid materials the components are usually subject to compressive loading at various rates of deformation. This is reflected in the testing performed on the model hybrid material. This section gives background on the types of mechanical testing performed and includes static and dynamic compression testing as well as damping capacity studies.

2.3.1 Static Compression Testing

A simple way to obtain material deformation behaviour under an imposed load is to perform a static test [Doman 2004]. The most common types of testing apparatuses employ hydraulic, pneumatic or servo-mechanical power to compress or extend the specimen [Doman 2004]. Typically to be considered a static test, the strain rate must be less than 10^{-1} s^{-1} [Dieter 1986]. The engineering

strain rate ($\dot{\varepsilon}$) is a function of crosshead speed ($v_{crosshead}$) and specimen height ($h_{specimen}$) in the following manner [Tan *et al.* 2005]

$$\dot{\varepsilon} = \frac{v_{crosshead}}{h_{specimen}} \tag{2.1}$$

The important properties obtained from the static tests are the elastic modulus, yield strength, plateau strength and the absorbed energy at a certain stress or strain.

2.3.2 Dynamic Compression Testing

Dynamic testing is performed to determine the behaviour of materials at high strain rates [Doman 2004]. This knowledge is important when designing for crash or blast loadings [Doman 2004]. There are many dynamic tests available each with advantages and limitations. One such method for low velocity impacts is a falling weight impactor [Cronin 2006]. There is a variety of falling weight impactors. Some masses are hung on the bottom of a pendulum producing a horizontal impact [Montanini 2005]. A drop tower produces a vertical impact [Lifshitz *et al.* 1995]. The actual impactor can be either a “dart” or an “anvil”. A “dart” impactor is spherical. Typically a plate is clamped and tested for penetration [Lifshitz *et al.* 1995]. Impacting with an “anvil” is the configuration that is used for the aluminum foam and model aluminum foam-polymer hybrid in this study. The drop tower contains a mass and an anvil (or dart) which is raised above the specimen. The weight maintains horizontal alignment with guide rails. Upon release the mass falls impacting the specimen. It is assumed that the mass of the specimen is negligible with respect to the falling weight [Hsaio and Daniel 1998]. The benefit of such testing devices is the ability to test final parts (if size permits and the correct clamping mechanisms are employed) and the ease with which the strain rate is varied [Hsiao and Daniel 1998].

There are many methods of instrumenting a falling weight impactor. An accelerometer can be placed in the anvil [Lifshitz *et al.* 1994]. The accelerations produced on the known mass of the anvil are utilized to determine the load [Hsiao and Daniel 1998]. The acceleration signal can also be integrated twice to get displacement [Hsiao and Daniel 1998]. Displacement of the anvil can be measured with optical sensors [Lifshitz *et al.* 1994]. The signal can then be differentiated twice to yield acceleration of the anvil [Lifshitz *et al.* 1994]. With the acceleration and the known anvil mass, the load is determined. Load cells in the base can also be used [Found *et al.* 1998].

These impact devices are sensitive to contact conditions and produce ringing and vibrations in the signal upon impact [Hsiao and Daniel 1998]. Lifshitz *et al.* [1994] and Shin *et al.* [1999] state that the high frequency ringing is due to one of the natural modes of vibration of the impactor and does not represent actual loads placed on the specimen. Filtering of data can be performed. However, it is noted that filtering of the data must be done very carefully to not discard actual test data [Found *et al.* 1998].

2.3.3 Damping Capacity Studies

The knowledge of material damping capacity is important for material selection in applications such as reducing noise from machine vibrations [Banhart 2001]. When cyclic loading is applied, inelasticity results in energy dissipation, which is reflected in different parts of the loading and unloading curves and the resultant hysteressis loop [Lazan 1964]. Sub-resonant and resonant experiments are performed to obtain this stress-strain hysteresis loop [Nowick and Berry 1972]. Sub-resonant experiments were utilized in this study for reasons of machine availability.

Sub-resonant experiments involve placing a specimen in forced vibration and measuring the stress and strain amplitudes. The square of the frequency of the forced vibration w^2, must be much smaller than the square of the specimen resonant frequency w_r^2 (i.e. $w^2 << w_r^2$). These experiments,

although the best way to measure visco-elasticity or anelasticity, are difficult if the damping is small [Nowick 1972]. This method works for polymers and on metals at high stress amplitudes where the plastic strain energy is large enough to be measured accurately [Morrow 1964]. Sub-resonant tests on metals and polymers can be performed on conventional uniaxial testing machines capable of cyclic loading [Morrow 1964 and Shen *et al.* 2001]. The most common resonant experiment is free vibration [Nowick and Berry 1972]. Such experiments excite vibrations in the specimen and then measure the frequency and decay of the free vibrations upon removal of the excitation force [Nowick and Berry 1972]. Damping is related to the decay of these free vibrations [Nowick and Berry 1972].

It should be noted that damping measurements are affected by many factors such as damping of the testing device, damping due to air resistance as well as the damping of the specimen [Banhart *et al.* 1996]. This makes comparison between the results of tests performed on different machines difficult and a comparison of results can only accurately be performed on specimens tested on the same machine or on machines that have eliminated all extraneous sources of damping [Banhart *et al.* 1996].

2.4 Aluminum Foam

Foams belong to a group of materials called cellular solids. Cellular solids are defined as having a porosity > 0.7 [Gibson and Ashby 1997]. Natural foams are produced by plants and animals such as cork or bone [Ashby 1983]. Man made foams can be manufactured from a variety of materials such as ceramics, polymers and metals [Ashby 1983]. There are two categories of foams: open-cell and closed-cell foams [Gibson and Ashby 1997]. In this work the foams of interest are open-cell aluminum foams. However, closed-cell foams are cheaper to produce [Banhart 2001] and much more prevalent in literature and are therefore also reviewed. Included in this section are fabrication methods, foam characteristics, mechanical properties and some applications of aluminum foams.

2.4.1 Fabrication Methods

There are many methods of fabricating aluminum foams. The following section highlights five of the most common methods for both open and closed-cell foam fabrication. Figure 2.2 shows the foam structure produced by each method.

As the name suggests open-cell foams contain an interconnected network of cells or pores. The most common open-cell foams available are those produced by casting [Montanini 2005]. Casting aluminum into a foam structure is performed in one of two ways: a) through the use of space holders, b) through investment casting. Space holder material varies from soluble salts and sand pellets to polymers. The space holders form an interconnected network which is preheated then infiltrated under pressure or vacuum with molten aluminum. The space holders are then removed. The use of space holders allows tight control over the distribution of pore sizes. However maximum porosities of only 80% can be achieved [Banhart 2001]. Investment casting allows for the same homogeneous distribution of cell sizes produced by casting around space holders but can produce porosities up to 97% [Banhart 2001]. In investment casting methods, polymer foam of desired porosity and pore size is filled with plaster which is then fired to burn off the polymer. Molten aluminum is allowed to fill the voids in the plaster. The plaster is removed revealing an exact copy of the polymer foam made out of aluminum. Duocel® and M-PORE® are commercially available foams manufactured by investment casting [Montanini 2005].

Closed-cell foams have closed pores. There are numerous methods of producing closed-cell foams. For direct foaming of metals, liquid metal is foamed and cooled while maintaining the foam structure [Banhart 2001]. In these methods thickening of the aluminum melt with ceramic particles before foaming is performed to help maintain the foam structure until solidification occurs [Banhart 2001]. Foaming is accomplished by one of two methods, either by injecting gas or adding blowing agents into molten aluminum. In the first method gas is injected while the liquid is rapidly mixed. The foam

floats to the top where it is extracted and rapidly quenched to retain its structure [Banhart 2001]. This process can produce average cell sizes varying between 3 to 20 mm in diameter and porosities as high as 97%. Gravity induces gradients in density, pore size and pore elongation [Banhart 2001]. Foams produced by this method have been available from Alcan®, Norsk-Hydro® and Cymat® [Montanini 2005]. Gravity effects can be reduced by using a blowing agent, as used in the second method of direct foaming. In this method a blowing agent, typically titanium hydride (TiH_2), is added to liquid aluminum. The liquid is held at constant pressure and the heat releases the blowing agent. The pressure is maintained until solidification is complete. These foams, available under the trade name Alporas®, produce some of the most homogeneous closed-cell foams with porosities up to 94% and cells sizes ranging from 2 to 10 mm [Banhart 2001].

Another method of producing closed-cell foam is the powder compact melting technique developed at the Fraunhofer-Institute. The process involves premixing metal powders and blowing agents. The powders are compacted and placed in a mold. Heat melts the powders and the blowing agents decompose. This process can produce foams with porosities between 75% and 90% [Banhart 2001]. Commercially available Alulight® and Schunk® foams are produced in this manner.

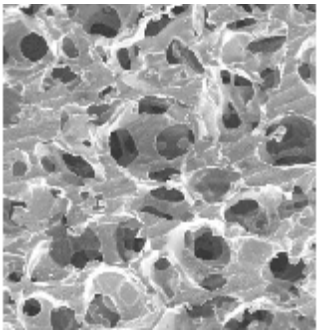

a) [San Marchi and Mortensen 2001]

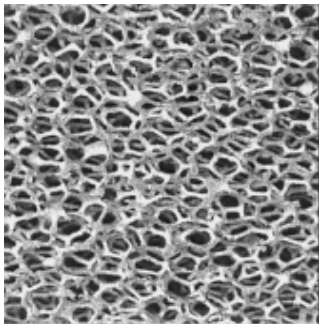

b) [Andrews *et al.* 1999]

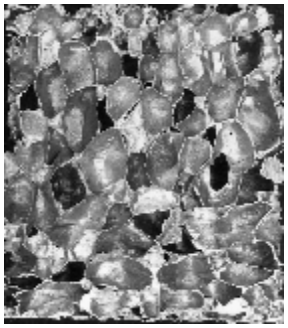

c) [Beals and Thompson 1997]

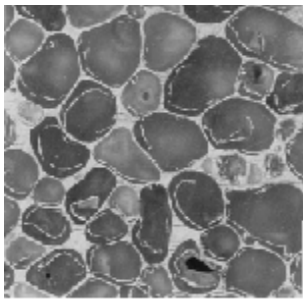

d) [Miyoshi *et al.* 1999]

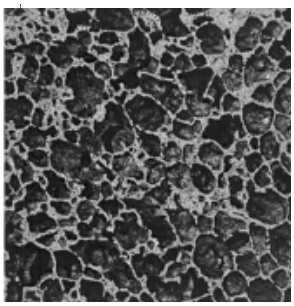

e) [Andrews *et al.* 1999]

Figure 2.2: Images of aluminum foams produced using the five methods described: a) casting around space holders, b) investment casting, c) foaming by gas injection, d) foaming with blowing agents, e) powder compact melting technique.

2.4.2 Foam Characteristics

Relative density, foam morphology and pore size depend on the method of fabrication. These characteristics affect foam physical and mechanical properties. Among these relative density is the most important characteristic which affects mechanical properties of foams [Gibson and Ashby 1997]. Relative density is the ratio of foam density (r^*) to solid material density (r_s), i.e. r^* / r_s, and relates to porosity simply by ($1 - r^* / r_s$) [Gibson and Ashby 1997]. Considering foam morphology, although cell shapes can vary substantially in variously fabricated foams, they are idealized as tetrakaidecahedral for theoretical analysis of foam deformation [Andrews *et al.* 1999, Li *et al.* 2006, and Gong and Kyriakides 2006]. In real foams, equiaxed cells produce isotropic material

response and, conversely, elongated cells produce anisotropic material response [Gibson and Ashby 1997]. From Figure 2.2 b) it is seen that the cells in open-cell foams produced through investment casting have a relatively uniform shape. Duocel®, which is the foam used in this study, is found to contain few morphological defects such as cracks in cell walls and cell wall wiggles [Andrews *et al.* 1999, Nieh *et al.* 2000]. Closed-cell foams have varying cell shape and show significant morphological defects [Sugimura *et al.* 1997, McCullough *et al.* 1999, Andrews *et al.* 1999, Olurin *et al.* 2000 and Gioux *et al.* 2000]. In Fraunhofer foams major defects including cracks spanning 10 cells or more are also found [Andrews 1999]. Although there are exceptions pore size generally has little importance on most mechanical properties and is given in pores per inch (ppi) or pores per millimeter (ppm) [Gibson and Ashby 1997].

Some of the key physical properties of aluminum foam are those considered as thermal and electrical properties. Gibson and Ashby [1997] mention that in general foams have low thermal conductivities which are proportional to relative density. This is confirmed by both Paek *et al*. [2000] and Feng *et al.*[2003]. Paek *et al*. [2000] also find the permeability to fluid flow of the foam varies with porosity and cell size, increasing as both foam parameters increase. The effect of porosity has the same impact on electrical conductivity [Gibson and Ashby 1997, Goodall *et al.* 2006]. Dharmasena and Wadley [2002] confirm this and note conductivity is further decreased with larger node (i.e. point where ligaments connect) sizes.

2.4.3 Mechanical Properties of Aluminum Foams

2.4.3.1 General Considerations

Mechanical properties of foams are the focus of this work and hence they are described in detail in the following sections. As Duocel® open-cell foam is studied in this work, both on its own and as part of the model hybrid material (due to its open network), the main focus of the section on

mechanical properties will be on open-cell foams. However since many of the aluminum foam hybrid materials produced utilize closed cell foams [Gioux *et al.* 2000, Fuganti *et al.* 2000, Banhart 2001, Miyoshi *et al.* 2002, Hanssen *et al.* 2002, Fraunhofer USA—Delaware 2002, Chirwa *et al.* 2003, Wang *et al.* 2006], important related findings of researchers on closed-cell foams are also included.

In section 2.4.3.2 the stress-strain behaviour of aluminum foams under static and dynamic compressive loading is reviewed with attention given to the elastic modulus, yield and plateau strength. Section 2.4.3.3 details the energy absorption of aluminum foam under compressive loading conditions and includes research findings at both static and dynamic loading conditions. This is followed by a review of the possibility of age hardening aluminum foam to alter the stress-strain and energy absorption behaviour at static and dynamic loading conditions in section 2.4.3.4. Finally in section 2.4.3.5 damping mechanisms and damping of aluminum foam is covered.

2.4.3.2 Stress-Strain Behaviour Under Compression

Gibson and Ashby [1997] develop a simple cubic unit cell model to predict many normalized mechanical properties of foam structures. The cubic unit cell depicting an open-cell foam can be seen in Figure 2.3. In the model, the cell has a side length l and a square wall cross section of thickness t. The purpose of the model is to yield scaled relationships based on bulk material properties and relative density. The relative density of the unit cell is given by [Gibson and Ashby 1997]:

$$\frac{r^*}{r_s} \propto \left(\frac{t}{l}\right)^2 \tag{2.2}$$

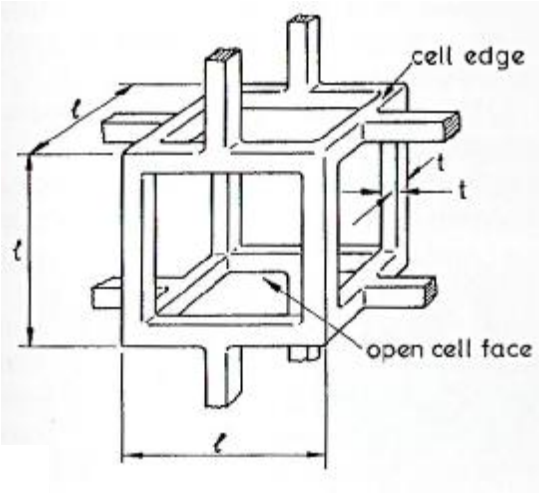

Figure 2.3: Cubic unit cell model of an open-cell foam with square cell edges with thickness t, and length l developed by Gibson and Ashby [Gibson and Ashby 1997]

Compressive deformation of aluminum foam produces a distinctive type of stress-strain curves. Important mechanical properties including the elastic modulus, yield and plateau strengths are obtained from these curves. Figure 2.4 a) shows a schematic of a typical aluminum foam stress-strain curve displaying the three regions characteristic of a plastic foam [Gibson and Ashby 1997]. Region I is linear-elastic followed by a plastic collapse plateau in Region II. Region II is truncated by densification of the foam in Region III. The stress-strain curve for brittle foams has a similar shape and contains the same three regions. However, a significant stress peak is observed at the end of Region I and Region II is rough with many stress peaks and valleys shown in Figure 2.4 b) [Gibson and Ashby 1997].

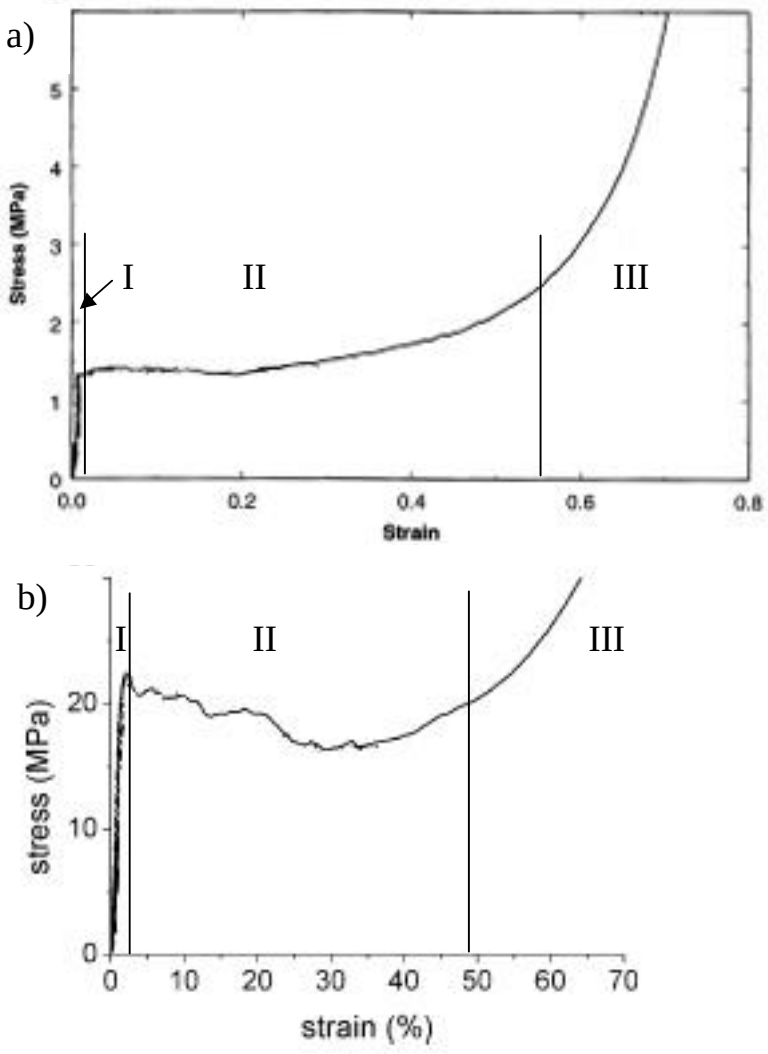

Figure 2.4: a) A typical stress-strain curve for a plastic open-cell aluminum foam [from Andrews et al. 1999] and a schematic presentation of various deformation regimes. b) A typical stress-strain curve for a brittle aluminum foam [from Lehmus and Banhart 2003] and a schematic presentation of various deformation regimes.

Golovin and Sinning [2003] break Region I down further into two sub regions. Figure 2.6 shows the two sub regions on a log-log plot. Region Ia is purely elastic while Region Ib is elasto-plastic showing microplastic deformation. The initial linear-elastic behaviour of aluminum foam is dependant on relative density. For open-cell foams the initial linear-elastic deformation produces a

heterogeneous strain distribution [Zhou *et al.* 2004a] and is controlled by cell wall bending [Gibson and Ashby 1997]. The equation the elastic modulus (E^*) for open-cell foam normalized by the elastic modulus of the bulk material (E_S) is

$$\frac{E^*}{E_s} = (\frac{r^*}{r_s})^2 \tag{2.3}$$

In the region beyond linear-elasticity but before yielding (or according to Golovin and Sinning [2003] Region Ib) no visible permanent deformation is observed, however dislocation slip bands can be seen on the surface of some of the struts under scanning electron microscopy (SEM) [Zhou *et al.* 2004b].

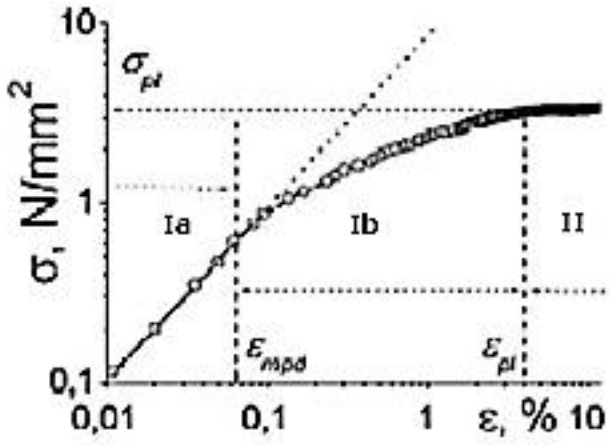

Figure 2.5: The subdivision of Region I into a linear elastic region (i.e. Region Ia) and an elasto-plastic region (i.e. Region Ib). [Golovin and Sinning 2003]

Plastic collapse of cell walls occurs when the moment exerted on the cell edges is higher than their plastic moment leading to the formation of plastic hinges and subsequent cell wall buckling [Gibson and Ashby 1997] and signals the end of Region I and the beginning of Region II. The plastic collapse strength occurring at the beginning of Region II is taken as the foam yield strength (s^*) by some researchers [Andrews *et al.* 1999 and Olurin *et al.* 2000]. Lehmus and Banhart [2003] define the yield

stress as the maximum observed stress up to a strain of 0.05. The model predicting s^* for open-cell foams is related to the bulk aluminum yield strength (s_s) by [Gibson and Ashby 1997]

$$\frac{s^*}{s_s} = C_2 \left(\frac{r^*}{r_s}\right)^{3/2} \tag{2.4}$$

where C_2 =0.3 is a constant [Gibson and Ashby 1997]. Ideally a constant stress of s^* is assumed over the length of the plateau. In reality a steady increase in stress due to hardening of the cell wall material is observed [Sugimura *et al.* 1997], although the stress may initially drop slightly from s^* [Zhou *et al.* 2005a]. During compression in the plateau region Duocel® open-cell foam displays heterogeneous deformation [Zhou *et al.* 2004a and Krishna *et al.* 2007]. The foam crushes in discrete bands in which the localized strain is greater than the macroscopic strain level [Zhou *et al.* 2004a].

At the end of Region II the collapse and deformation of cell walls becomes significant enough that the walls begin to touch, i.e. densification begins [Gibson and Ashby 1997]. Region III is characterized by the densification process of the foam where by porosity is removed [Gibson and Ashby 1997]. However the removal of all porosity from the foam during a compression test is difficult and rarely achieved [Brydon *et al.* 2005]. The densified foam behaves as a solid material requiring large stresses for further compression. Foam densification occurs at the densification strain e_d. The point at which the foam densifies is not well defined and the definition is found to vary between researchers. Common methods of determining the densification strain (or stress) based on the stress-strain response are by visual inspection [Maiti *et al.* 1984 and Nieh *et al.* 2000], at a stress 1.5 times the stress value at a strain of 0.5 [Andrews *et al.* 1998 and Krishna *et al.* 2007]. The former method utilizes the point of intersection of the slope of the plateau region and that of the densification region as the point of densification. This is can be inaccurate as the slope of the plateau can be suppressed by increasing the scale on the stress axis thus changing the point of densification. The

latter method is better as the point of densification remains constant regardless of the choice of scale, however as noted by the authors this method is arbitrary. Other researchers choose an arbitrary strain and utilize this as the densification point [Paul and Ramamurty 2000 and Lehmus *et al.* 2002a]. In structural applications the densification point is not as important as the yield point. However in energy absorption applications the point of densification is important and compression beyond densification is to be avoided due to the sharp increase in stress [Gibson and Ashby 1997]. The Cushion factor (C) is the ratio of peak stress to energy absorbed [Gibson and Ashby 1997]. It is fully defined in Section 2.4.3.3. In this study the point of densification is chosen as the point where the minimum Cushion factor occurs. This methodology is similar to the one employed by Hansson *et al.* [2000] and Fuganti *et al.* [2000] who define that the maximum useful displacement (d_{max}) occurs at the point of maximum Total Efficiency (T_E). Where T_E is approximately equivalent to 1/C. Hansson *et al.* [2000] also define a Stroke Efficiency (S_E) as d_{max} divided by the total length (l). This is equivalent to the definition of densification strain utilized in this work. Gibson and Ashby [1997] also use a similar definition where the densification stress is taken as the shoulder of the energy absorption curve (i.e. the point of highest energy absorbed to peak stress). Although ideally these are the same points, reading the shoulder point from the graph can give different results depending on what scale for the axis is chosen.

2.4.3.2.1 Stress-Strain Behaviour under Static Compression Testing

Duocel® open-cell foams display the characteristic stress-strain curve of typical plastic foams shown in Figure 2.4 a) [Andrews *et al.* 1999]. The elastic modulus of Duocel® foam is well predicted by equation 2.3 [Andrews *et al.* 1999, Despois *et al.* 2006]. Similar to the elastic modulus, the yield strength of Duocel® foam is closely predicted by equation 2.4 due to the homogenous cell structure [Andrews *et al.* 1999, Despois *et al.* 2006]. The strong dependence of Duocel® foam elastic modulus

and yield strength on relative density and little dependence of these properties on cell size are confirmed by Nieh *et al.* [2000]. Higher relative densities are also found shorten the plateau in open-cell aluminum foams [Gibson and Ashby 1997]. Unlike Duocel®, in open-cell foams created by the space holder method, foam yield strength and plateau height show a dependence on pore size [Bin *et al.* 2007].

The stress-strain curves of closed-cell foams display either plastic or brittle fracture depending on foam fabrication and microstructure [Sugimura *et al.* 1997, Miyoshi *et al.* 2002 and Banhart and Baumeister 1998]. Variations in porosity of closed-cell foams result in heterogeneous elastic modulus and yield strength values throughout the specimen [Beals and Thompson 1997, Koza *et al.* 2003]. Many researchers have noted the low experimental values of elastic modulus and yield strength compared to the values predicted by the mechanical models developed for closed cell foams [Yu *et al.* 1998, Andrews *et al.* 1999, McCullough *et al.* 1999, Lu and Ong 2001, Olurin *et al.* 2000, Sugimura *et al.* 1997, and Werther *et al.* 2006]. This is attributed to stress concentrations occurring at the nodes [McCullough *et al.* 1999] and morphological defects in the foam such as curvature in the cell edges and cracks [Yu *et al.* 1998, Andrews *et al.* 1999, Lu and Ong 2001, Olurin *et al.* 2000, Sugimura *et al.* 1997, and Werther *et al.* 2006]. As with open-cell foams, higher relative densities shorten the plateau [Gibson and Ashby 1997].

2.4.3.2.2 Stress-Strain Behaviour under Dynamic Compression Testing

Strain rate sensitivity of foam mechanical behaviour is highly dependant on cell morphology and cell wall microstructure [Dannemann and Lankford Jr. 2000]. Duocel® is found to be strain rate insensitive (i.e. independent of strain rate) over a wide range of strain rates and therefore displays mechanical properties such as yield and plateau strengths similar to those observed in static testing [Deshpande and Fleck 2000, Dannemann and Lankford Jr. 2000, McArthur *et al.* 2003, Lee *et al.*

2006]. The strain rate up to which the mechanical properties of Duocel® remain insensitive is inconsistent among published data. Deshpande and Fleck [2000] find the mechanical properties of a 7% relative density foam with 20 ppi to be insensitive to strain rate up to strain rates of 5000 s^{-1}. However, a 40 ppi foam with the same relative density is found to have mechanical properties that are insensitive to strain rate only up to strain rates of approximately 1200 s^{-1} [Dannemann and Lankford Jr. 2000, McArthur *et al.* 2003]. McArthur *et al.* [2003] note that a noticeable increase in the mechanical properties occurs for the same porosity and relative density with strain rates at and above 1500 s^{-1} (i.e. strain rate dependant). They also test a 10 ppi and 11% relative density Duocel® foam and find the mechanical properties to be insensitive to strain rate for strain rates up to 1500 s^{-1} (maximum rate tested for this foam). The authors suggest that perhaps the pore size has an effect on strain rate sensitivity. This assumption is in contradiction with the findings of Zihua *et al.* [2006] who report strain rate sensitivity does not vary with cell size and find little strain rate sensitivity of mechanical properties for strain rates up to 1900 s^{-1} for higher relative densities (r^* / r_s = 25% to 30%). Lee *et al.* [2006] perform a series of tests on Duocel® 7% relative density foam with 40 ppi at strain rates up to 3300 s^{-1} and observe that the mechanical properties are insensitive to strain rate supporting the findings of Deshpande and Fleck [2000]. Similar to Duocel®, the mechanical properties of M-PORE® investment cast open-cell aluminum foam are found to be strain rate independent up to a strain rate of 100 s^{-1} for relative densities ranging between 5 and 8 % [Montanini 2005]. Yi *et al.* [2001] test open-cell foams fabricated by a powder metallurgical method at strain rates of 10^{-3} s^{-1} to 2600 s^{-1}. The rate sensitivity of the foam mechanical properties are found to be r^* / r_s dependant with higher relative densities producing a larger dependence of mechanical properties on strain rate [Yi *et al.* 2001].

The rate sensitivity of the mechanical properties in strain rate dependant closed-cell foams is due to the suppression of the compliant buckling modes of failure and gas trapped in the pores [Dannemann and Lankford Jr. 2000, Tan *et al.* 2005]. Closed-cell Alporas® foams are sensitive to strain rate displaying an increase in yield stress from rates as low as 3×10^{-5} s^{-1} up to 2.5×10^{3} s^{-1} [Mukai *et al.* 1999, Dannemann and Lankford Jr. 2000, Paul and Ramamurty]. Recently Mukai *et al.* [2006], note that the sensitivity of the yield strength increases for larger relative densities. However the plateau stress of the lower density foam shows higher rate sensitivity. Cymat® is found to be insensitive to strain rate in the ranges of $10^{-3}-10$ s^{-1} [Ruan *et al.* 2002]. However at higher strain rates (~ 100 s^{-1}) the yield stress of Cymat® is found to increase and the stress plateau becomes shorter even though the height of the plateau remains unchanged [Montanini 2005]. Montanini [2005] tests Schunk® foams at 100 s^{-1} and finds significant rate sensitivity. This is in contrast to Alulight®, produced by a similar process as Schunk®, which is found to be rate insensitive under strain rates up to 5000 s^{-1} [Deshpande and Fleck 2000]. A study by Miyoshi *et al.* [2002] illustrates the effect microstructure has on rate sensitivity by adding zinc and magnesium to a closed-cell aluminum foam. The base foam exhibits slight rate dependence at 1.38×10^{2} s^{-1} while the new alloy shows no rate sensitivity.

2.4.3.3 Energy Absorption under Compression

The long stress plateau typical of the stress-strain curves of aluminum foams gives rise to excellent energy absorption properties [Gibson and Ashby 1997 and Song and Nutt 2005]. Damage to an object is caused when a critical force (or acceleration) level is exceeded [Gibson and Ashby 1997]. The ability to absorb energy at a force below this critical level is paramount to the protection of the object [Gibson and Ashby 1997, Fuganti *et al.* 2000]. The force of an impact is directly related through geometry to the stress in the foam [Gibson and Ashby 1997]. Figure 2.6 shows why foams are much better than solid materials at providing damage protection. For a given stress foams always absorb

more energy than a solid due to the bending, buckling and fracture of the foam cell walls [Gibson and Ashby 1997]. The following section is based on the analysis of energy absorption properties of cellular materials by Gibson and Ashby [1997].

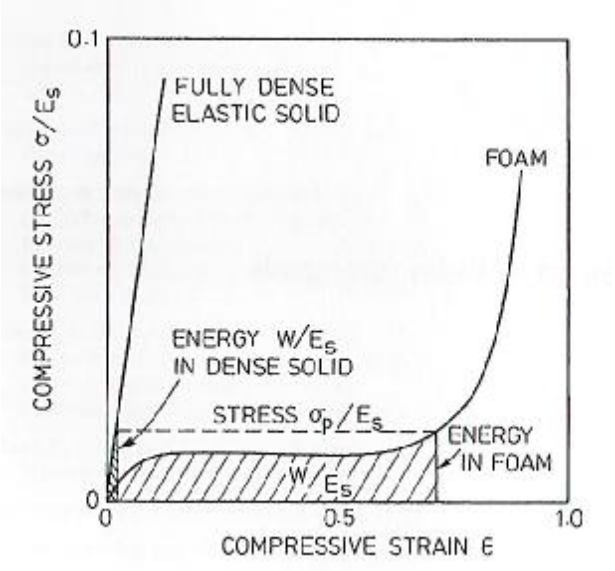

Figure 2.6: Stress-strain curves for both an elastic solid and a foam showing the difference in energy per unit volume absorbed at the same stress level [Gibson and Ashby 1997].

The compression of aluminum foam under an applied force results in work. The work per unit volume (W) up to a strain of e is the area under the stress-strain curve. It is calculated in the following manner

$$W = \int_0^e s\,(e)de \tag{2.5}$$

Little energy absorption occurs in the initial linear elastic region. Energy absorption in the plateau region accounts for the majority of energy absorbed by the specimen. Plastic deformation of aluminum foams at near constant stress in the plateau region translates into energy dissipated at near constant stress. Ideally for better energy absorption the stress-strain curve would be perfectly

horizontal from $e = 0$ to e_d. After densification modest increase in energy absorption is accompanied by large stress increases.

Considering impact conditions (i.e. strain rates in the range of 10^1 to 10^4 s^{-1}), there is an optimum foam density to absorb energy efficiently [Gibson and Ashby]. This is illustrated in Figure 2.7 where three foams of different relative densities are shown schematically. The stress and strain at which an amount of energy W is absorbed is shown for all three densities. This shows that if too weak of a material is chosen the required amount of energy absorbed is more than that under the plateau, the foam densifies and the force increases sharply before all energy is absorbed. If however too strong of a material is chosen the load becomes too large before all the required energy is absorbed. The most efficient foam is shown to have the middle density. Here the full plateau is employed in energy absorption while $e < e_d$ and the load transferred to the object is minimized (i.e. $(s_p)_2 < (s_p)_1$ and $(s_p)_3$ where s_p represents the peak, i.e. highest recorded stress for the chosen value W calculated from 0 strain)

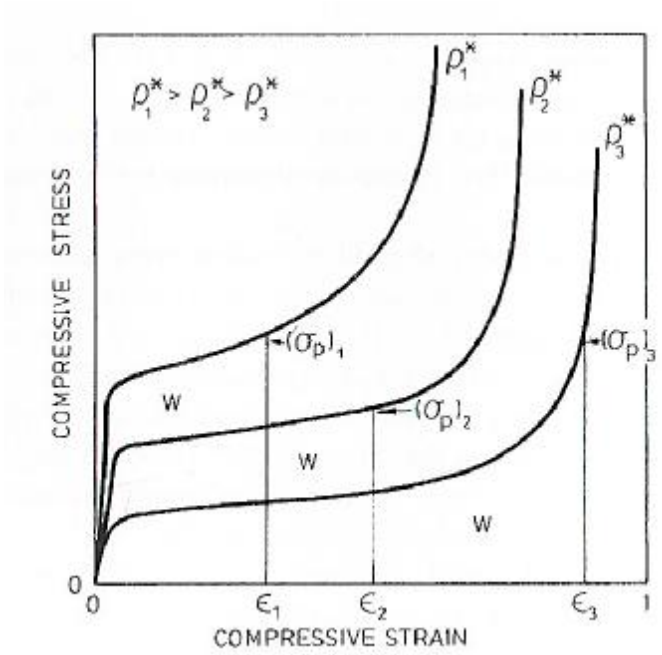

Figure 2.7: Schematic of three different relative density stress-strain curves. The curves show the stress levels for the equal energy absorption (W) for each case. The middle foam absorbs the amount of energy W at the lowest peak stress ($(s_p)_2$). [Gibson and Ashby 1997]

Figure 2.8 shows energy absorption (W) vs. s_p curves of ideal open-cell plastic foams at various relative densities, at a constant strain rate. It should be emphasized that the curves are plotted using log scale on both axes and both W and s_p are normalized by the bulk material elastic modulus (E_s) [Gibson and Ashby 1997]. The initial parts of the curves display the energy absorbed in the linear-elastic regime. The plateau regime is responsible for the vertical slope displaying large increases in energy absorption with no increase in stress. In real foams, however, the plateau is not horizontal and therefore the slope in this region of the energy absorption curve deviates slightly from the vertical trend, showing a reduction in slope. At the end of this region (i.e. when the vertical part of the curve changes to horizontal) a shoulder in the energy absorption curve is observed [Gibson and Ashby

1997]. The shoulder occurs at the foam densification stress s_d (i.e. the stress at which e_d occurs) [Gibson and Ashby 1997]. The horizontal slope following the shoulder is due to the densification of the foam. This is for idealized foams, in real foams this slope is greater than zero.

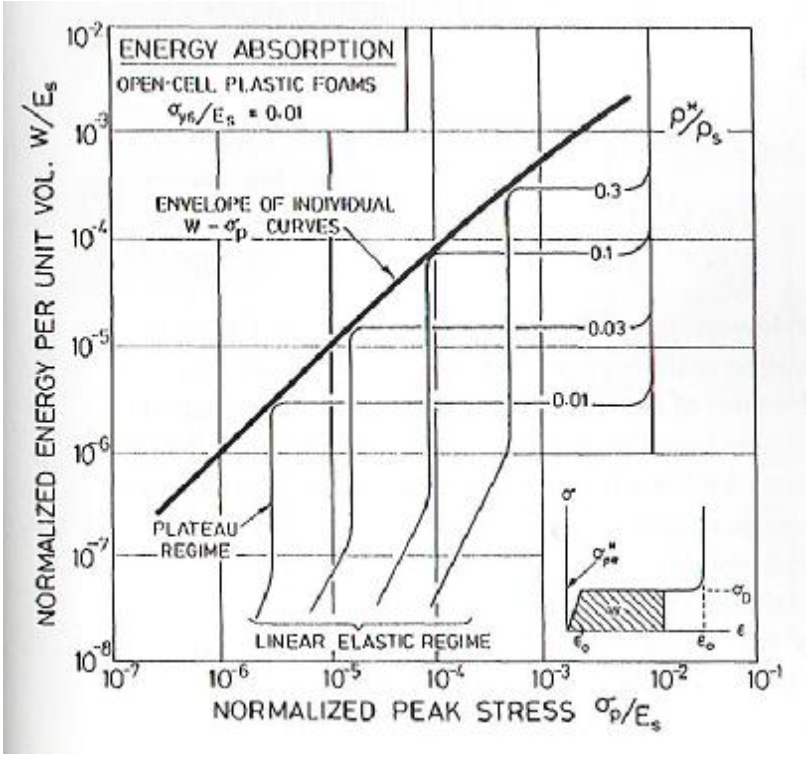

Figure 2.8: Energy absorption curves for ideal open-cell plastic foams at a constant strain rate for various relative densities. [Gibson and Ashby 1997]

Two methods of comparing and choosing foams for energy absorption applications will be reviewed. The first method involves comparing the energy absorption efficiency of the different materials. There is a range of methods that determine the efficiency of energy absorption. One such method is discussed by Lehmus and Banhart [2003]. Here the efficiency (x) up to a strain e is determined as

$$x(e) = \frac{\int_0^e s(e)de}{s_p e} \tag{2.6}$$

The numerator is simply W, while the denominator represents the energy absorbed by an ideally horizontal stress-strain curve. This method is only beneficial when comparing materials at the same strain and does not correlate well to maximum energy absorbed at a maximum allowable load. Another measure of efficiency is the Cushion factor [Gibson and Ashby 1997]. The Cushion factor relates the amount of energy absorbed to peak stress. It is determined in the following manner [Gibson and Ashby 1997]

$$C = \frac{s_p}{W} \tag{2.7}$$

The lower the value of C the more energy a foam can absorb in relation to its peak stress and the more efficient it is considered [Gibson and Ashby 1997]. This relation is important as it correlates directly to the level of energy to be absorbed and the allowable load limit of impacts [Gibson and Ashby 1997]. The Cushion factor also takes into account both deviations from the ideal stress-strain curve for energy absorption (i.e. horizontal stress-strain curve) and the amount of strain up to densification. In this investigation when two materials have similar densification stresses a comparison of the Cushion factors will be used to determine the most appropriate material for energy absorption applications.

A second method for choosing a suitable material for energy absorption applications are the energy absorption curves [Maiti *et al.* 1984]. This method is well suited for comparing materials which have different densification stresses [Gibson and Ashby 1997]. The most suitable material is the one that absorbs the most energy at the maximum allowable stress of impact. Ideally the densification stress of the material (or shoulder of the energy absorption curve) is the same as the maximum allowable stress

[Gibson and Ashby 1997]. This method will also be utilized in this investigation when comparing two materials with different densification stresses. Gibson and Ashby [1997] show in detail how energy absorption curves are utilized.

2.4.3.3.1 Energy Absorption under Static Compression Testing

Energy absorption is affected by the shape of the stress-strain curve. The increase in plateau stresses due to increased relative densities result in higher values of energy absorbed [Maiti *et al.* 1984, Gibson and Ashby 1997, Song and Nutt 2005]. However, the energy absorption efficiency as defined by equation (2.16) is unaffected by relative density but changes with loading direction in anisotropic foams [Olurin *et al.* 2000]. The defects in closed cell foams decrease the energy absorption efficiency [Beals and Thompson 1997, Miyoshi *et al.* 1999]. Beals and Thompson [1997] find density gradients within the foam also decrease the efficiency of energy absorbed. By careful control of foam production Miyoshi *et al.* [1999] are able to produce closed-cell Alporas® with small cell sizes and, reduced density gradients, cell wall curvature and corrugation. The modified foam with fewer defects not only shows an increase in energy absorption over the unmodified foam with similar relative density, it also displays an increase in energy absorption efficiency.

2.4.3.3.2 Energy Absorption under Dynamic Compression Testing

Dannemann and Lankford Jr. [2000], and Montanini [2005] report no change of energy absorption with strain rate in the rate insensitive Duocel® and M-PORE® foams respectively. For strain rate sensitive foams such as Alporas® and Schunk®, the amount of energy absorption increases as the plateau stress increases [Mukai *et al.* 2006, Montanini 2005]. Although Dannemann and Lankford Jr. [2000] view the increase in energy absorption as an enhancement Mukai *et al.* [2006] point out that to

design an efficient energy absorbing structure with rate sensitive foam the exact strain rate observed upon impact must be known. This is not always an easy task.

2.4.3.4 Mechanical Damping Capacity Studies

Few materials behave in a perfectly elastic manner regardless of stress level [Granato 1964]. This inelasticity results in the dissipation of energy (or damping) and is due to internal friction mechanisms within the specimen [Nowick 1964]. Relevant damping mechanisms to aluminum foams are reviewed. This will be followed by the stress-strain behaviour of closed-cell aluminum foams under cyclic loading and the damping properties (i.e. energy absorption) of closed-cell aluminum foams due to the lack of literature on damping of open-cell aluminum foams.

2.4.3.4.1 Mechanical Damping Mechanisms

Mechanical damping is caused by internal friction mechanisms [Granato 1964]. These mechanisms can be classified as linear (i.e. strain/stress amplitude independent) or non-linear (i.e. strain/stress amplitude dependent) [Lazan 1964] and are generally related to the movement of atoms and defects [Nowick 1964].

The two major relevant mechanisms of linear internal friction are thermo-elastic effects (or thermal gradients) and dislocation damping [Lazan 1968, Golovin and Sinning 2004]. Thermo-elastic effects produce damping due to elastic stress gradients in non-uniformly stressed specimens [Lazan 1968, Golovin and Sinning 2004]. The elastic stress gradients set up temperature gradients which in turn lead to thermal currents, dissipating energy as heat [Golovin and Sinning 2004]. Damping due to thermo-elastic effects reaches a maximum at a resonant frequency that is dependant on the well defined bulk specimen thickness [Lazan 1968, Golovin and Sinning 2004]. The damping capacity quickly drops as the difference between testing frequency and resonant frequency increases. An

accepted model of dislocation damping is the vibrating string dislocation model proposed by Koehler [1952] and modified by Granato and Lücke [1956] [Fu-sheng *et al.* 1997]. In the model, at low strain/stress amplitudes the dislocations bow out between pinning points, dissipating energy as heat. The amount of energy dissipated is frequency dependant [Lazan 1968].

Relevant non-linear internal friction mechanisms include an extension of the vibrating string dislocation model and energy dissipation due to plastic strain [Lazan 1968, Morrow 1964]. In the vibrating string dislocation model, if the strain/stress amplitude is sufficiently high the dislocations break away from the pinning points [Granato and Lücke 1956]. Upon reversal of stress the dislocation contracts via a different path producing a hysteresis loop [Granato 1964]. Non-linear dislocation damping dissipates more energy than linear dislocation damping [Granato and Lücke 1956]. At stress amplitudes between the elastic limit and the true fracture strength of the material new dislocations are produced and the dissipation of energy is due predominantly to plastic strain [Morrow 1964]. Cyclic loading in this range is unstable as fatigue of the material eventually occurs [Morrow 1964].

Typically the internal friction mechanisms responsible for damping in bulk metals also results in damping in their respective cellular materials [Golovin and Sinning 2003]. However, the highly heterogeneous structure of cellular materials alters how these mechanisms occur and results in some new internal friction mechanisms [Banhart *et al.* 1996, Golovin and Sinning 2004]. For damping due to thermo-elastic effects, the cellular structure of foams disrupts the flow of the thermal gradients resulting in a distribution of apparent thickness values [Golovin and Sinning 2004]. Therefore there is a large range of apparent resonant frequencies which produces damping compared to the smaller frequency range seen in the bulk material [Golovin and Sinning 2004]. Little change occurs in the mechanism of dislocation damping. The higher localized strains/stresses produced by localized deformation means that amplitude dependant dislocation damping is more likely to occur at lower global strain/stress amplitudes than amplitude independent dislocation damping [Fu-sheng *et al.*

1997]. Similar to the observation by Morrow [1964] for bulk metals, Golovin *et al.* [2004b] note that testing beyond the elastic limit of foams, i.e. microplastic yielding (Region Ib in Figure 2.5), produces an increase in dislocation density and damping properties are not considered to be stable. One new internal friction mechanism thought to occur in foams is the interfacial friction between defects such as cracks [Banhart *et al.* 1996]. "Mode conversion", another new mechanism, is thought to produce amplitude dependant internal friction [Fu-sheng *et al.* 1997]. Under "mode conversion" the stress mode may be converted from tensile to shear at the pore boundaries. The shear deformation produces viscous flow with dislocation movement towards pore boundaries and dissipated as heat [Fu-sheng *et al.* 1997].

2.4.3.4.2 Stress-Strain Behaviour under Cyclic Loading

Under cyclic loading a loading and an unloading stress-strain curve constitutes a full cycle. The elastic modulus is found to decrease as the strain amplitude and the number of cycles increases [Fu-sheng *et al.* 1997, Golovin and Sinning 2003]. At high strain amplitudes (i.e. $e = 10^{-3} - 10^{-4}$) strain hardening of aluminum foam occurs in the first cycle which results in an open hysteresis loop. Also observed is a shift in the hysteresis loop to lower stresses which is attributed to an increase in dislocation density due to strain hardening [Golovin *et al.* 2004a, Golovin *et al.* 2004b].

2.4.3.4.3 Mechanical Damping characteristics of Aluminum Foam

The internal friction character of aluminum foam is found to be non-linear, increasing with increasing porosity and decreasing pore size [Banhart *et al.* 1996, Fu-sheng *et al.* 1997, Liu *et al.* 1998, Golovin and Sinning 2003, Golovin and Sinning 2004, Golovin *et al.* 2004a, Golovin *et al.* 2004b]. This is in contrast to the linear internal friction character of bulk aluminum which displays up to 10 times less mechanical damping capacity than aluminum foam when tested at the same

amplitudes (1.0 to 2.2 x 10^{-5}) [Fu-sheng *et al.* 1997, Liu *et al.* 1998]. Frequency is found to have no effect on mechanical damping of aluminum foam over a range of 200 Hz to 800 Hz [Banhart *et al.* 1996] however a decrease in damping is observed when the frequency was increased from 1 kHz to 3 kHz [Liu *et al.* 1998]. Amplitude independent thermo-elastic effects are found to contribute little to the overall damping of aluminum foams [Golovin and Sinning 2003, Golovin and Sinning 2004]. The amplitude dependence and the major source of damping can be interpreted using Granato-Lücke vibrating string dislocation model and mode conversion [Banhart *et al.* 1996, Fu-sheng *et al.* 1997, Liu *et al.* 1998, Golovin and Sinning 2003, Golovin and Sinning 2004]. The difficulties in comparing measured mechanical damping values of aluminum foam tested on different machines are highlighted by the comparison performed by Banhart *et al.* [1996] of their results to those produced by Yu and He [1994] for the same relative density of aluminum foam. The lower mechanical damping values measured by Banhart *et al.* [1996] are attributed by the authors to either a different morphological cell structure in the foam or that some mechanical damping from the test apparatus used by Yu and He [1994] is included in their results [Banhart *et al.* 1996].

2.4.3.5 Effect of Age Hardening Treatment on Foam Mechanical Properties

Heat treating aluminum foam alters the yield strength and the plateau region without changing the relative density. The effect of heat treatment on the mechanical properties of Duocel® open-cell AA6101 aluminum foam is investigated by Zhou *et al.* [2004a, 2005]. The authors find increases to yield and plateau strengths over the as-fabricated condition are achieved by artificial aging. This is confirmed with tensile tests of individual foam struts [Zhou *et al.* 2005b]. Chan and Chan [2004] show open-cell AA6061 aluminum foam has a significant increase in yield strength and a shift from ductile to brittle fracture with aging at 160˚C for 18 hours. The effects of solution treatment and aging on closed-cell foams based on AA6XXX (AA6061 and AA6082) and AA7XXX (AA7020 and AA7075) wrought aluminum alloys are studied thoroughly by Lehmus *et al.* [2002a], Lehmus *et al.*

[2002b] and Lehmus and Banhart [2003]. An increase in yield strength is observed in the artificially aged specimens, and a solution treatment prior to aging, produces higher strengths than aging directly after solidification [Lehmus and Banhart 2003]. A shift in fracture mode from ductile to brittle is perceived in aged-hardened specimens [Lehmus and Banhart 2003]. Also, the stress plateaus of the directly aged foam specimens are more horizontal than solution treated foams. Chan and Chan [2004] record an increase in yield strength of 200% in SiCp reinforced A356 aluminum closed cell aluminum foam by artificial aging. More recently, Cao *et al.* [2006] investigate the mechanical response of artificially aged Al-Mg-Si and Al-Cu-Mg foams. They report that artificial aging with and without solution treatment increases the compression strength and shortens the plateau region compared to the corresponding properties of the as-fabricated foams.

Kanashi *et al.* (2001) investigate the effects of natural aging and artificial aging (9 hours at 160˚C) on the dynamic compressive properties of SG91A (9 mass% Si, 0.45 mass% Mg, 0.5 mass% Fe, 0.45 mass% Mn, remainder Al) open cell foam. They find the aging process reduced strain rate sensitivity and increased the yield strength over the properties of as-cast foams. Heat treating was also found to increase the ductility of the foam compared to the as fabricated condition.

The aged hardened foams studied by Lehmus and Banhart [2003] show an increase in energy absorption. Specimens aged following solution treatment absorb the most energy while the more horizontal stress-strain curves obtained through direct aging show the largest increase in energy absorption efficiency (according to equation (2.5)). Cao *et al.* [2006] report an increase in energy absorption of artificially aged foams due the increase in compression strength despite the shorter observed plateaus.

To the best of my knowledge the effect of artificial aging on mechanical damping properties has not been studied.

2.5 Polymers

2.5.1 General Considerations

Polymers can be either thermosets or thermoplastics [Nielsen 1974a, Gibson and Ashby 1997]. Thermosets are characterized by strong covalently bonded crosslinks between mononer chains [Gibson and Ashby 1997]. These bonds are not easily taken apart and therefore thermosets can not be melted and thus recycled through melting [Gibson and Ashby 1997]. Thermoplastics however have weak van der Waals bonding between monomer chains and can be melted and recycled repeatedly [Gibson and Ashby 1997]. Melting temperatures for some common thermoplastics are ~ 70˚C for ethylene vinyl acetate (EVA – with 28 % vinyl acetate) [Salyer and Kenyon 1971] and ~ 125˚C for polyethylene [Aklonis *et al.* 1972]. Polymers have an incredibly wide range of mechanical properties which vary not only from polymer to polymer [Nielsen 1974a] but also with manufacturer for the same polymer [Ashby 1992]. A significant change in mechanical properties in amorphous and semi-crystalline polymers occurs at the glass transition temperature (T_g) (i.e. the temperature at which the polymer becomes glassy) [Nielsen 1974a, Gibson and Ashby 1997]. Below T_g polymers display high elastic moduli values (~ 3 to 10 GPa) [Gibson and Ashby 1997]. Above T_g polymers are soft and flexible with an elastic moduli up to 1000 times smaller than glassy polymers [Nielsen 1974a]. Polymers which are utilized at temperatures above their T_g are considered elastomers [Nielsen 1974a]. EVA with a T_g of approximately -20˚C [Barbosa *et al.* 2005] is therefore considered an elastomer at room temperature. The polymer employed in this investigation is an EVA. EVA ranges from an amorphous to a semi-crystalline polymer [Salyer and Kenyon 1971]. Therefore in this work only the mechanical properties of amorphous and semi-crystalline thermoplastic elastomers are considered.

2.5.2 Mechanical Properties of Thermoplastic Elastomers

2.5.2.1 Stress-Strain Behaviour under Compression

The elastic modulus of an elastomer is taken as the initial slope of the stress-strain curve [Nielsen 1974a]. Elastomers are compliant with low moduli and no observable yield point [Gibson and Ashby 1997]. They show slowly increasing stiffness with increasing strain [Boyce *et al.* 2001]. The increase in stiffness becomes rapid at high strains [Nielsen 1974a]. Figure 2.9 shows a typical elastomeric stress-strain curve. Much of the deformation is recoverable however at large strains the elastic behaviour is non-linear [Gibson and Ashby 1997, Doman 2004]. In general increasing the molecular weight and the percent crystallinity, amongst other methods, will increase the elastic modulus in elastomers [Nielsen 1974a and Gibson and Ashby 1997]. The presence of crystals increases the stiffness by linking the amorphous matrix together; however, an increase in crystallinity reduces the amount of strain that is recoverable [Nielsen 1974a, Salyer and Kenyon 1971]. Hydrostatic pressure is also found to increase the apparent elastic modulus [Nielsen 1974a]. Typically elastomers are visco-elastic [Nielsen 1974a]. According to [Kaelble 1964] polymers show both elastic and viscous properties due to the large molecules producing long range molecular order. When loaded the elastic component shows an immediate increase in strain with increase in stress. However the increase in strain in the viscous component lags the increase in stress. When the loading rate is slow the viscous component relaxes out some of the stress reducing the apparent stiffness of the polymer. At higher loading rates there is less time for stress relaxation and as such the apparent elastic modulus increases. Decreasing the test temperature is equivalent to increasing the rate of loading and increases the elastic modulus [Kaelble 1964].

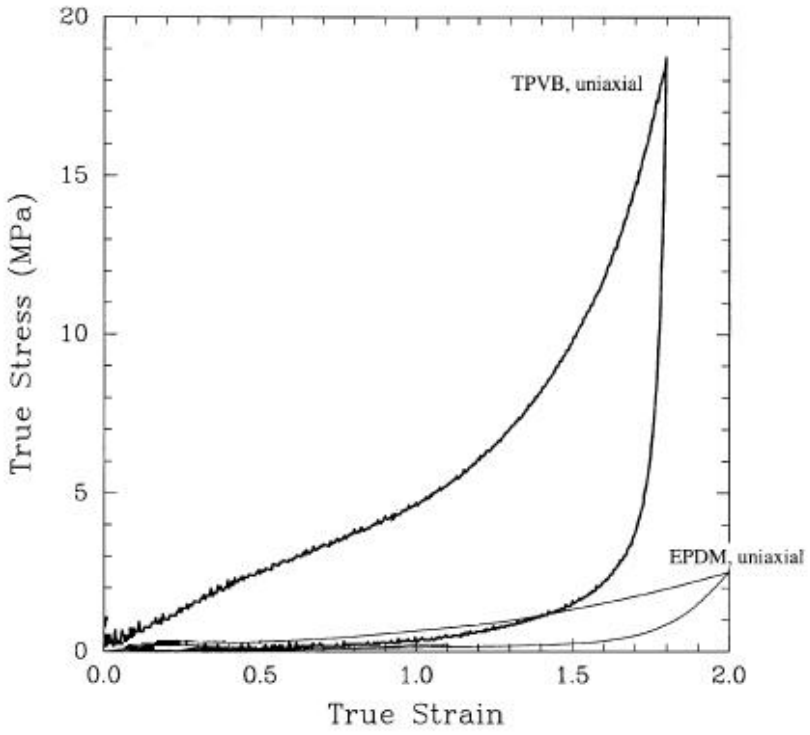

Figure 2.9: Typical elastomeric uniaxial compressive true stress - true strain curve [adapted from Boyce et al. 2001]. Upper curve is the loading curve, lower curve is the unloading curve.

2.5.2.2 Energy Absorption in Thermoplastic Elastomers

Upon loading, deformation occurs by the movement of polymer chains relative to one another, dissipating some of the energy as heat [Nielsen 1974a] and some of the energy remains stored in the specimen as elastic energy [Gibson and Ashby 1997]. Due to the non-linear elastic behaviour of elastomers, the release of the elastic energy resulting in the strain recovery during unloading is time dependant [Gibson and Ashby 1997]. This is seen by the drastically different unloading curve in Figure 2.9. The total energy dissipated is therefore the area between the loading and unloading curves [Gibson and Ashby 1997]. However in this investigation the calculation of energy absorption per unit

volume for polymers is the same as that of aluminum foams, i.e. area under the stress-strain curve during loading as unloading curves could not be measured.

The mechanical damping capacity of a thermoplastic elastomer is dependant on many factors such as stress amplitude, temperature and frequency [Nielsen 1974a]. The main mechanism in the mechanical damping of elastomers is the movement of polymer chains and side groups relative to each other dissipating energy as heat [Nielsen 1974a]. Typically in amorphous polymers the maximum observed mechanical damping capacity occurs at the glass transition temperature [Kaelble 1964]. However in elastomers chain movement readily occurs, maintaining a high level damping [Kaelble 1964]. There is a local maximum in mechanical damping capacity above T_g [Nielsen 1974a, Barbosa *et al.* 2005, Khonakdar *et al.* 2004]. This peak is thought to be associated with melting of the crystalline phase allowing the rotation of the long chain segment about their axis [Nielsen 1974a, Khonakdar *et al.* 2004]. Increasing the frequency has the same effect as decreasing the temperature [Nielsen 1974a, Gibson and Ashby 1997].

2.6 Selected Hybrid Materials

2.6.1 General Considerations

Although there are many different hybrid materials, in this section only the mechanical properties of a select few which are relevant to this research are presented. The hybrids reviewed are interpenetrating network composites (or Interpenetrating phase composites [Wegner and Gibson 2001]), sandwich panels and foam filled extrusions.

2.6.2 Interpenetrating Network Composites

In interpenetrating network composites (INCs) each phase forms a continuous network with itself while being interconnected to all other phases [Wegner and Gibson 2001]. All hybrids in this section

meet this description and will be referred to as INCs. Both aluminum foam and the model aluminum foam-polymer hybrid produced in this work meet the description of an INC and are therefore INCs as well. Typically an open pore structure is infiltrated by a second material yielding the characteristic INC structure [Zhou *et al.* 1998, Prielipp *et al.* 1995]. Due to the continuous network of both phases, many of the classical models used to describe regular hybrid materials are not valid [Feng *et al.* 2004] and the prediction of mechanical properties of INCs based on composite microstructure is not well understood [Tilbrook *et al.* 2005].

Wegner and Gibson [2000, 2001] investigate what effect an interpenetrating network of stainless steel in a resin matrix has on the hybrid mechanical properties. The elastic modulus and yield strength are found to increase with increasing volume fraction of steel. It is noted however, that the increase in mechanical properties is likely due to the increase of the phase with the higher mechanical properties (i.e. stainless steel). Prielipp *et al.* [1995], Travitzky [2001] and Zhang *et al.* [2006] find that the ceramic-metal INC created produce strengths that are above those expected by the rule of mixtures. This is attributed to the interpenetrating network structure [Zhang *et al.* 2006]. Boczkowska *et al.* [2006] credit the increase in upper yield strength over the parent materials of a silica oxide and urea-urethane elastomer INC to strong hydrogen interfacial bonds produced by the polar polymer and the silica oxide.

Cheng and Han [2003] and Kwon *et al.* [2003] combine open-cell aluminum foam with a thermoset elastomer. Both note that the elastic filler has a larger contribution to enhancing the strength than to changing the elastic modulus. The increase in strength is due to the resistance imposed to cell wall deformation by the elastic filler [Cheng and Han 2003, and Kwon *et al.* 2003]. Cheng and Han [2003] distinguish five regions in the hybrid stress-strain curve seen in Figure 2.10. The regions include an initial linear elastic region (Region I) in which the response of the aluminum foam and the hybrid are almost identical. Region II is assumed by the authors to be a plateau where again the aluminum foam

stress-strain curve and the hybrid stress-strain curve are similar. In Region III however the hybrid displays an increase in stress over the base foam. According to the authors this region is the transition from the plateau in Region II to another plateau in Region IV. As the hybrid compresses at near constant stress in Region IV the base foam material begins to densify at a strain of 0.46. The hybrid densifies in Region V, at a strain of 0.6. This delayed densification in the hybrid is the result of awaiting the force to be large enough to break the cell walls. Many broken cell beams are observed after compression. The densification stress is lower and the energy absorbed up to densification is higher in the hybrid [Cheng and Han 2003].

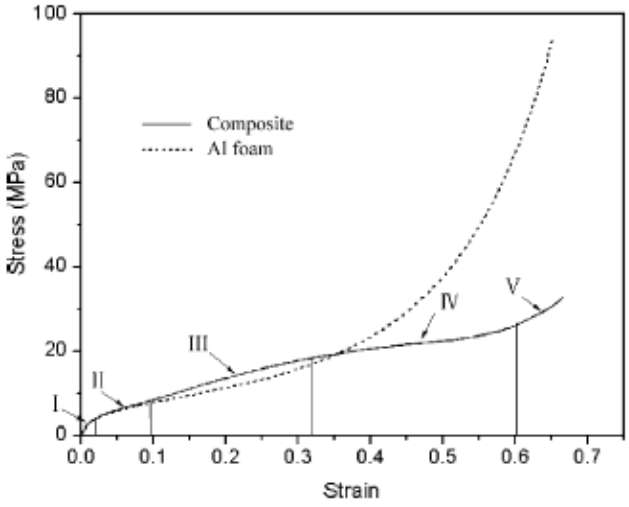

Figure 2.10: Aluminum foam-silicate rubber hybrid compressive stress-strain response showing the five distinct regions and the response of the base foam [Cheng and Han 2003].

Xie *et al.* [2002] find the damping in a woodceramic-magnesium INC to be larger than that predicted by the rule of mixtures. Dislocations produced in the metal at the interface during cooling are the one possible source of increased mechanical damping at low temperatures. Mechanical damping due to interfacial interactions is also suggested to be present. Although the strength of the bond is not given it is noted that at weakly bonded interfaces relative movement between each

material provides damping due to friction Xie *et al.* [2002]. For strongly bonded interfaces interfacial damping occurs due to the mobility of incoherent microstructures [Lavernia *et al.* 1995].

2.6.3 Sandwich Panels

Sandwich panels are composed of a light stiff core bonded between face sheets and produce a gain in stiffness by a factor of 3 over the most efficient fibrous composite [Ashby and Bréchet 2003]. The core must be strong enough to handle the shear stresses when the sandwich panel bears load [Ashby and Bréchet 2003]. Aluminum foam possesses the material properties required of a core material, and is therefore commonly used in sandwich panels [Ashby and Bréchet 2003].

Aluminum foam sandwich panels with aluminum face sheets examined under static three point bending test [Tagarielli *et al.* 2004, Yu *et al.* 2003] and four point bending test [Harte *et al.* 2000, Chen *et al.* 2001] show three modes of failure depending on panel geometry. One method of failure, i.e. face yield, occurs when the stress in the face sheets attains the yield strength of the face sheet. The panel deforms plastically, similar to the plastic bending of a solid plate, with little change in thickness of the foam core (i.e. only the outer panels deform plastically). Core shearing is another method of sandwich panel failure. Similar to face yield the panel deforms analogous to a solid plate, however the face sheets do not yield but the core shears plastically along the neutral axis. The other failure mechanism observed is indentation [Tagarielli *et al.* 2004, Yu *et al.* 2003]. Only the top face sheet deforms plastically compressing the foam beneath it and penetrating into the core thickness. In a stretch bending tests where the panel ends are clamped, plastic face stretching is the dominant mechanism for deformation regardless of the initial mode of failure [Tagarielli *et al.* 2004].

The mechanical response and failure of sandwich panels fabricated with aluminum face sheets and aluminum foam cores to dynamic three point bending is presented by Yu *et al.* [2003]. At impact speeds of 4 m/s the panels display large local indentation and debonding of the skin. These have

deleterious effects on energy absorption such that specimens absorb more energy when statically loaded. Radford *et al.* [2006] report the efficiency of stainless steel face sheets and aluminum foam core sandwich panels in energy absorption during blast loading. Testing is performed on two sandwich panels with different thicknesses but with the same areal mass (i.e. mass/area). The thicker core sandwich panels have a higher shock resistance permitting less core strain and showing smaller deflections of the bottom plate for the same impact energy.

Cantwell *et al.* [2000] and Kiratisaevee and Cantwell [2003] produce sandwich panels with thermoplastic composite face sheets and an aluminum foam core. Localized crushing and fracture of the core along with fiber buckling and skin fracture are found to be the major methods of energy absorption. Vaidya *et al.* [2006] note from tests on thermoset face sheets that a face sheet which does not allow penetration on impact but deforms spreading out the strain to the foam core increases the energy absorption of the panel.

2.6.4 Foam Filled Extrusions

There have been many studies on the strength and energy absorption of aluminum foam filled columns [Hanssen *et al.* 2000, Fuganti *et al.* 2000, Hanssen *et al.* 2002a, Hanssen *et al.* 2002b, Chirwa *et al.* 2003, Wang *et al.* 2006, Shahbeyk *et al.* 2007]. Notable results are obtained by Hanssen, Langseth and Hopperstad [2000] who find that due to the interaction of the two materials, the force-displacement curve of the hybrid is higher than the linear summation of the force-displacement curves for the two base materials tested individually. The filled aluminum tubes also absorb more energy and display higher energy absorption efficiencies, as calculated by equation (2.16), over unfilled tubes. Little strain rate sensitivity is displayed in stress-strain curves up to 25 m/s in axial crushing. Similar results are found for carbon skinned nose cones filled with aluminum foam

[Chirwa *et al.* 2003]. This composite displays stress-strain curves insensitive to strain rate for impact speeds up to 6.26 m/s [Chirwa *et al.* 2003].

Chapter 3
Scope and Objectives

The present work aims at utilizing open-cell aluminum foam to design a new metal-polymer hybrid material and to assess the potential enhancement in the mechanical properties of the hybrid material in comparison with the base aluminum foam and the filling polymeric material.

To achieve the goal of a new metal-polymer hybrid, design parameters for the polymer should be set and experimental trials carried out. A method of fabrication based on the two materials should then be designed and implemented. To asses mechanical properties, testing of the hybrid, as well as the two base materials, will be conducted under static compression, dynamic compression and compression-compression, cyclic loading. The stress-strain behaviour, the yield strength and the energy absorption properties of the materials will be investigated. The mechanical properties of aluminum foam vary with artificial aging. The effects of ageing on the aluminum foam will be investigated using static and dynamic compression testing to see if the properties of the hybrid material can be augmented further through age-hardening.

The process of filling an open cell aluminum foam with a thermoplastic is a novel process which holds the promise of producing a new recyclable material with enhanced mechanical properties. The mechanical properties of the hybrid material given in this work can be used in the design of new approaches to existing and future applications. A closer inspection of some of the trends and mechanisms in hybrid deformations will lead to an optimization of aluminum foam-polymer hybrid materials.

The ensuing chapter will describe the design and fabrication of the metal-polymer hybrid. The experimental methods which describe the materials, the equipment employed in the testing, heat treatment, as well as the testing procedures will be presented in Chapter 5. The results of

experimental characterization of mechanical testing will be brought in Chapter 6. The experimental results will be discussed in Chapter 8 and a comparison of the mechanical properties between the hybrid and the base materials will be given. Subsequently conclusions will be drawn and recommendations for future work will be provided.

Chapter 4
Design and Fabrication of a Metal-Polymer Hybrid Material

4.1 Introduction

There is a desire to fabricate structures with good energy absorption capabilities from light weight materials. Hybrid materials such as sandwich panels and fiber reinforced composites show that combining two materials can improve upon the parent material properties. It has been shown that aluminum foams display high specific strength and stiffness as well as excellent energy absorption properties. The interconnected pores in an open-cell foams have the ability to be infiltrated by a second material. Polymers are light and also display excellent energy absorption properties. An attempt is made to combine the two materials. Simple criteria are utilized to choose a polymer and design the fabrication process. The process of choosing the polymer and the procedure with which the foam is filled are laid out in this chapter.

4.2 Choosing the Polymer

The mechanical properties of polymers are so incredibly vast varying from soft rubbers to hard plastics. When choosing a polymer the following important considerations are taken into account. There is increasing concern by people all over the globe for the environment, therefore the model hybrid must be environmentally friendly. To preserve the mechanical properties of the aluminum foam the structural integrity of the ligament must be preserved. This is accomplished by filling the foam with liquefied polymer under the force of gravity alone. These considerations lead to following simple criteria for the polymer:

1) It must be recyclable through melting (i.e. a thermoplastic polymer). Thermoplastic polymers melt in ranges which might further induce age hardening in the aluminum foam.

2) It must have a low viscosity in order to fill the foam pores easily and efficiently (i.e. high Melt Index (MI))

The above criteria was discussed with Dupont™'s technical staff, who suggested and provided Elvax® 205W pellets. Elvax® is an ethelyne vinyl acetate (EVA) copolymer, a thermoplastic which is produced in many different grades with varied MI and melting points. Elvax® 205W has an MI of 800 [Dupont 2005a] and a melting temperature of 74˚C [Dupont 2005b]. It therefore meets the above selection criteria.

4.3 Foam Filling Procedure

Filling of the foam requires a mold to hold the specimen and a hopper to hold the filler material (i.e. Elvax® pellets). The design of these two components is described below followed by the finalized procedure utilized to fill the aluminum foam and finally problems encountered during the fabrication process.

4.3.1 Mold Design

The mold was designed around the requirement that the aluminum foam, with a size required for mechanical testing, be filled under gravity. To accommodate this, the mold was designed with an open top allowing polymer to drip into the mold for specimens of height 50.8 mm and maximum nominal widths (specimens have a square cross sectional area) of 42 mm. The final inside dimensions of the mold are 52 mm x 44 mm x 44 mm (l x w x h). An extra 1 mm in length and 2 mm in width was added to ensure the foam would not be damaged when placed in the mold. The mold was designed such that it could be dismantled after filling the specimen. The finalized mold can be seen in Figure 4.1. The mold is constructed of 6.35 mm thick aluminum plate (1/4 inch) with an open top and removable sides and bottom.

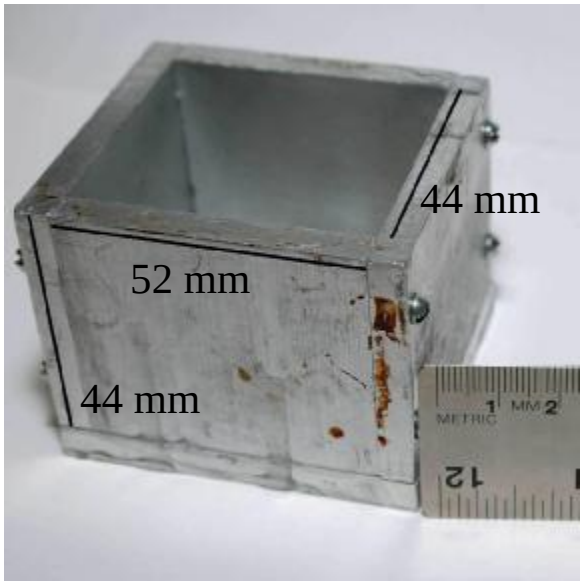

Figure 4.1: Finalized mold with dimensions employed in the production of the model hybrid.

4.3.2 Hopper Design

The hopper was designed with a flange to fit inside the mold and to hold the required amount of polymer to fill the aluminum foam specimen in the mould. To reduce the amount of entrained air in the polymer due to initial hopper designs a V shape was placed in the hopper. This allows air to escape the mold as the polymer fills it. The hopper is shown in Figure 4.2. Figure 4.3 a) and b) shows how the hopper fits inside the mold

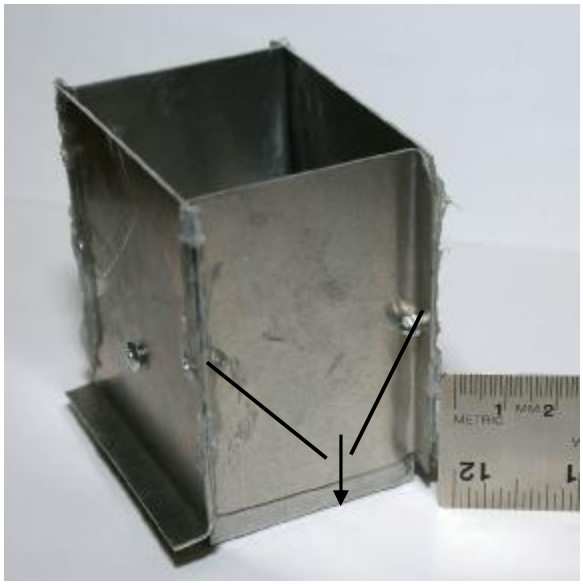

Figure 4.2: Picture of the hopper employed in the production of the model hybrid. Included is a schematic of the V shape and an arrow indicating the polymer flow.

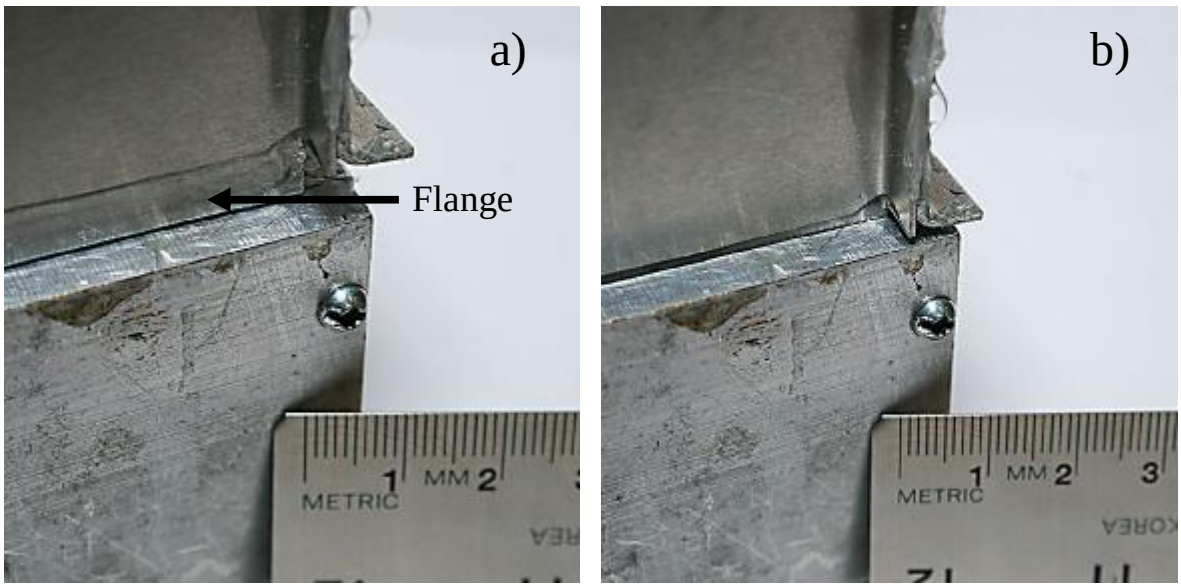

Figure 4.3: Picture of a) the flange sitting on top of the mold and b) the flange tucked inside the mold to hold the hopper in place.

4.3.3 Finalized Step by Step Procedure

Producing the aluminum foam-polymer hybrid material is performed with the following steps:

1. Assemble the mold and lubricate it with silicone spray and stearate powder
2. Place the aluminum foam specimen in the mold
3. Place the hopper on top of the mold and fill it with approximately 160 ml of Elvax® pellets
4. Place the mold and hopper in the furnace for 3 hours at 115˚C
5. Remove the mold and hopper from the furnace
6. Remove the hopper from the mold and allow the polymer to cool
7. Dismantle the mold removing the hybrid specimen

Figure 4.4, Figure 4.5 and Figure 4.6 show the procedure at various stages. The process produces a specimen with excess polymer due to the differences in mold and aluminum foam specimen size. This can be seen in Figure 4.7 a). The excess polymer is removed in two stages. A rough cut is performed using the band saw. This is followed by cutting the polymer off close to the foam with a knife. This process results in specimens with an average increase in width of 1 mm over non-filled aluminum foam samples due to a thin layer of polymer coating the outside surface of the foam. It is desirable to have the foam exposed on the top and bottom of the specimen to allow direct contact between the foam and the platens attached to the testing device. This eliminates the effect the thin layer of pure polymer on the top and bottom of the specimen has on the results. This process is performed by milling to ensure the top and bottom surface remain parallel. A finished specimen ready for testing can be seen in Figure 4.7 b).

Figure 4.4: Assembled and lubricated mold with an aluminum foam specimen placed inside (i.e. step 2).

Figure 4.5: Hopper filled with Elvax® pellets placed on top of the mold (i.e. step 3).

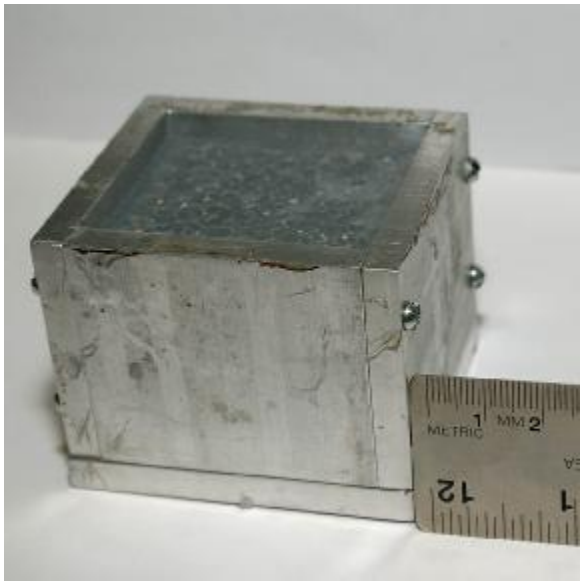

Figure 4.6: Mold before disassembly and removal of the hybrid specimen (i.e. step 6).

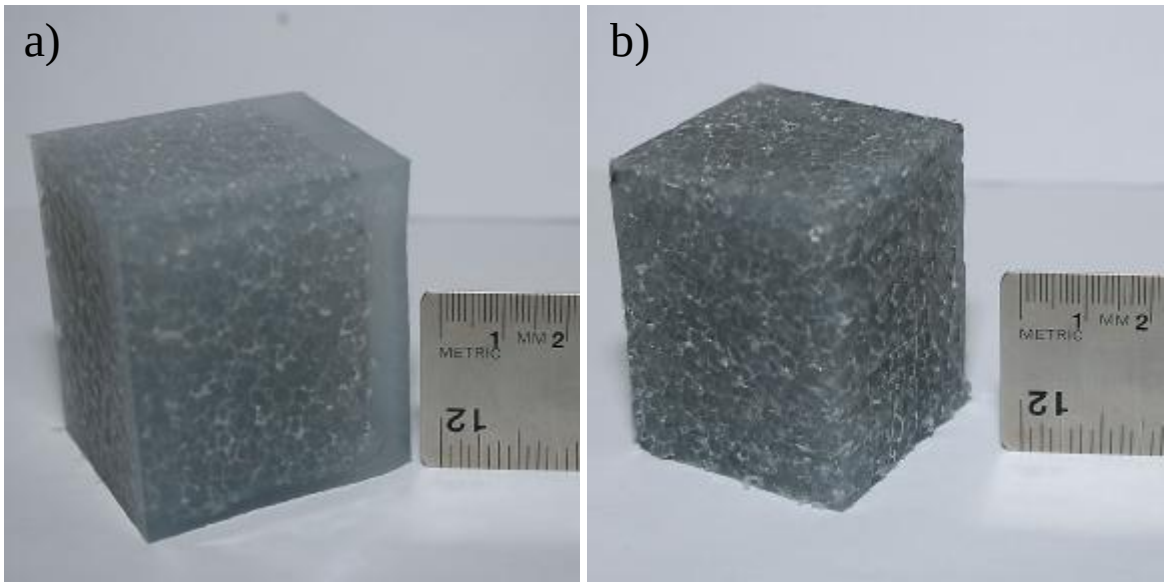

Figure 4.7: a) As fabricated aluminum foam-polymer hybrid. b) Prepared aluminum foam-polymer hybrid specimen ready for mechanical testing.

4.3.4 Problems Encountered

The two major problems that occurred during the fabrication of the hybrid specimens are low polymer viscosity and the polymer adhering to the mold walls. The polymer is still too viscous at temperatures close to the melting point. Through trial and error the viscosity of Elvax® at 115˚C is found to be acceptable for filling purposes and so this temperature was used to fill the foam. The problem of specimens sticking to the mold is solved by using a silicon spray and stearate powder on the mold walls before filling. This eliminates specimens sticking to the mold walls and makes the removal of the hybrid specimen easy.

Chapter 5
Experimental Methodology

5.1 Introduction

The chapter on experimental methods is comprised of four main categories: materials, specimen preparation, thermal processing and testing procedures. A description of the materials which include aluminum foam and a thermosplastic polymer of trade name Elvax® are given. This is followed by the handling of and modifications to the materials for preparing test specimens. The thermal processing of the aluminum specimens is described in detail. Finally experimental procedures are explained. The mechanical tests carried out on the aluminum foam, hybrid and polymer materials include static compression testing, dynamic compression testing and compression-compression cyclic testing. The procedures of all three preceding experimental techniques are described individually.

5.2 Materials

5.2.1 Aluminum Foam

AA6101 Duocel® open cell aluminum foam with a nominal relative density of 6-8% is used. The foam has a pore size of 10 pores per inch (ppi), corresponding to 0.39 pores per millimeter. The nominal alloying element content of AA6101 is given by the ASM handbook as: 0.35-0.8 wt% Mg, 0.30-0.70 wt% Si, maximum 0.1 wt% Cu [ASM 1992]. Blocks, with the dimensions 2x10x10 inches (50.8x254x254 mm), are received from ERG Materials and Aerospace Corporation, Oakland, California in as fabricated condition with no prior heat treatment performed. Open cell foam with a large pore size was chosen to allow infiltration of the pores with a polymer.

5.2.2 Polymer

For reasons described in Chapter 4 the polymer of trade name Elvax® was chosen. Elvax® is graciously provided by Dupont, Kingston, Onatrio in the form of pellets with an approximate diameter of 3mm. Elvax® is an ethylene vinyl acetate (EVA) copolymer blend and is available in various grades with a varying percentage of vinyl acetate [DuPont^{TM} 2005a]. The grade employed is 205W containing 28 wt% vinyl acetate leading to a density of 950 kg/m^3 [DuPont^{TM} 2005a]. A blocking agent is used to increase the melt index (MI) [DuPont^{TM} 2005a]. The polymer has an MI of 800 and a melting temperature of 74˚C [DuPont^{TM} 2005b].

5.3 Specimen Preparation

Testing is performed on aluminum foam, Elvax® and aluminum foam-polymer hybrid. Specimen preparation is required in order to achieve the desired dimensions for testing. The final dimensions of the specimens are produced by cutting to size with a band saw unless otherwise noted. This leads to variations in widths between specimens of up to 4% and along the length of individual specimens by less than 2%. Therefore, to achieve better accuracy and eliminate the effect of size discrepancies between specimens, the test results are reported in normalized form with respect to height and area. The errors caused by the variations in individual specimens are also reduced by taking the average of the specimen width at three locations along the length. The methods used to prepare the three specimen types are listed below.

5.3.1 Aluminum Foam Specimen

All three mechanical tests including static and dynamic compression testing as well as for cyclic loading experiments are carried out on aluminum foam. In initial trials specimens for static compression tests with dimensions of 42 mm x 42 mm x 50.8 mm (w x l x h) and 38 mm x 38 mm x 50.8 mm (w x l x h) are tested. The results for both specimens are identical. To save material only the

smaller sample size is used for all three reported experimental tests. The sample size choice is justified by the results reported by Andrews *et al.* [2001] who find that the mechanical properties become constant when an open cell foam has more than 8 cells in each direction. The aspect ratio chosen is similar to those found in literature [Lehmus *et al.* 2002 and Harte *et al.* 1999]. Relative densities are calculated for each specimen by dividing the measured mass by the measured volume of the specimens. The relative density for all specimens is found to be between 7.1 – 7.6 % with an average of 7.4 %.

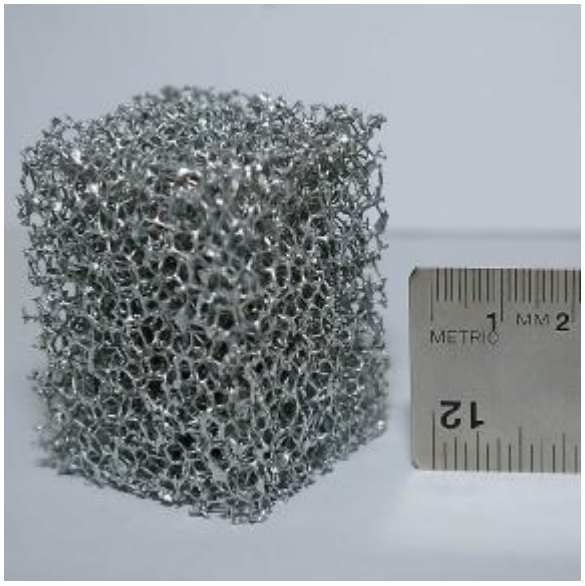

Figure 5.1: Typical aluminum foam specimen used in all mechanical tests

5.3.2 Polymer Specimen

Elvax® specimens are produced utilizing a similar procedure outlined in Chapter 4. The differences being that the mold is without the inclusion of aluminum foam and approximately 200 ml of Elvax® pellets are required. Without the foam in the mold the Elvax® contracts significantly upon cooling leaving a concave top face. Cutting the top side so that it is flat leaves the specimen approximately only 33 mm in width. The other two directions are cut such that the specimen

maintains the same aspect ratio. The approximate specimen size produced is 33 mm x 33 mm x 44 mm (w x l x h).

5.3.3 Aluminum Foam-Polymer Hybrid Specimen

The aluminum foam-polymer hybrid material is fabricated utilizing both as-fabricated and an age-hardened aluminum foam. The age-hardening condition is 4 hrs at 220˚C which provides the highest yield strength among specimens aged at 220˚C (i.e. peak-aged condition). Both foam conditions are tested in static and dynamic compression testing, however only the as-fabricated condition is employed in damping experiments. The production and processing of the aluminum foam-polymer hybrid is described in Chapter 4. In performing the milling operation the overall height of the specimen is reduced by up to 1.6 %. These procedures result in nominal hybrid specimen dimensions of 39 mm x 39 mm x 50 mm (w x l x h). Figure 4.7 b) displays a finished specimen ready for testing.

5.4 Thermal Processing

As-fabricated foam samples do not receive any heat treatment. Foam samples are heat treated when age-hardened specimens are required. The initial stage of the heat treatment of the foam samples involves a solution heat treatment at 560˚C for 1 hour in an air furnace. This arrangement of time and temperature is chosen to ensure effective solutionizing before quenching and artificially aging the specimen [Esmaeili 2002]. The aluminum foam samples were removed from the furnace and quenched with forced air using a hair dryer.

Following the air quench the specimens are transferred to a furnace in which the ageing medium is air. A schematic representation of the aging profile is presented in Figure 5.2. For mechanical test specimens artificial aging is performed at 180˚C for 1, 2, 4, 5 and 7 hours and 220˚C for 0.5, 1, 2 and

4 hours respectively. After the desired aging time is reached the specimens are removed from the furnace and air cooled.

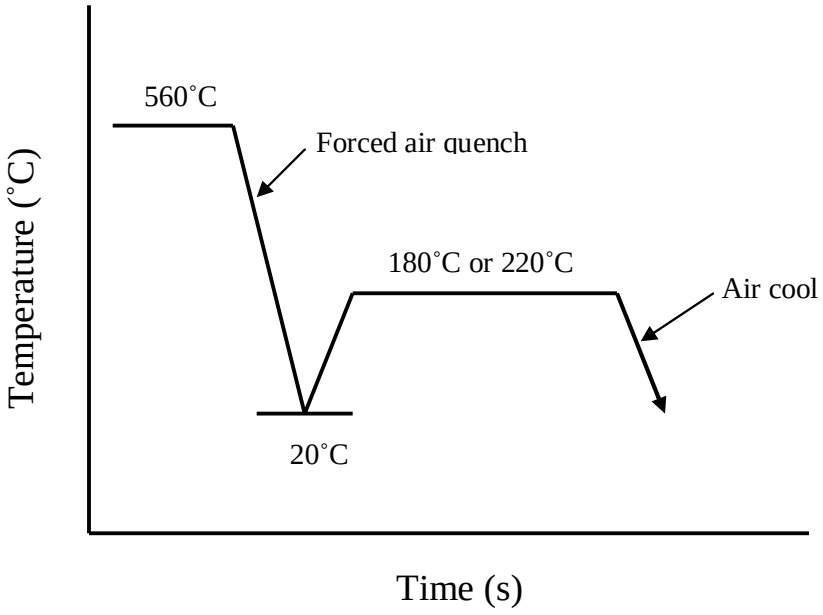

Figure 5.2: Schematic representation of the direct isothermal artificial aging treatment.

5.5 Experimental Procedures

The mechanical tests are performed at room temperature (~ 273 K). It is convention to utilize engineering stress and engineering strain when analyzing the stress-strain response of foams under these mechanical tests, even up to large deformations [Gibson and Ashby 1997]. The test data collected are the load (P) applied to the specimen and the change in specimen gage length, recorded as displacement (ΔX). This data is converted to engineering stress (s) and engineering strain (e) respectively. Engineering stress is determined from the load and the initial specimen area ($A_{specimen}$) by

$$s = \frac{P}{A_{specimen}} \tag{5.1}$$

Engineering strain is a function of the change in specimen gage length and the original gage length. In the compression tests performed the original gage length is the specimen height. Engineering strain is determined utilizing the following equation

$$e = \frac{\Delta X}{h_{specimen}} \tag{5.2}$$

Compressive engineering stress and compressive engineering strain will be employed for aluminum foam, as well as the polymer and hybrid specimens in order to maintain consistency and allow comparisons between specimens. This section outlines the testing procedures.

5.5.1 Static Compression Testing

The majority of compression testing is performed on a screw-driven Instron 4206 fitted with a 150 kN load cell. The remaining tests are performed on an Instron 8874 hydraulic machine capable of both axial and torsional loading. The 8874 machine uses a 25 kN load cell. Figure 5.3 shows pictures of both machines. The procedures for compression testing depend on the machine used.

a)  b)  c) 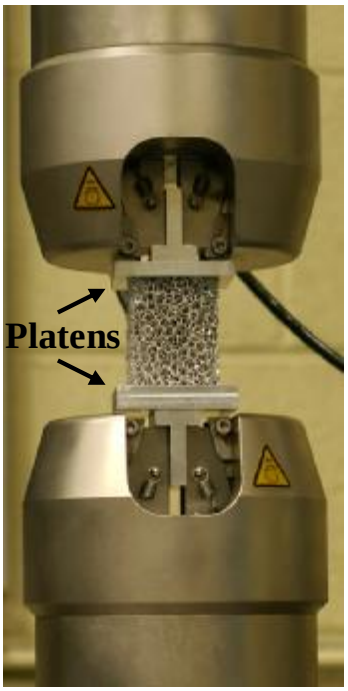

Figure 5.3 :Compression testing equipment: a) Instron 4206, b) Instron 8874, c) custom platens used for compression testing on Instron 8874.

For testing on the Instron 4206 the grippers are removed and replaced with platens. The crosshead moves at a user defined speed, in this case 25 mm/min (corresponding to an initial strain rate of $\dot{\varepsilon} = 0.008 s^{-1}$). The test is stopped automatically when a load of 70 kN is reached. The grippers on the Instron 8874 can not easily be removed. As a result custom platens, shown in Figure 5.3 c), were fabricated to produce a flat surface for the compression tests while fitting within the grippers. After the option for data acquisition on the Instron 8874 is turned on, the desired displacement of the crosshead and the time step over which the displacement is to occur are input into the machine. The maximum time step allowed is 100 s. This limits crosshead speed to 30 mm/min (initial strain rate of $\dot{\varepsilon} = 0.009 s^{-1}$) for specimens with a height of 50.8 mm. The load limit is set to stop testing when 20 kN is achieved. The results of testing on the Instron 4206 are comparable to those produced on the Instron 8874. Both machines have calibrated load cells and both show discrepancies between the

machines' measured displacement (i.e. from their linear variable displacement transducers (LVDT)) and the displacement measured by hand after testing (i.e. with calipers) of 1 %. Table 5.1 lists the static tests performed.

Table 5.1: List of compression tests performed including aging information.

Material Condition	Pore Size	Solutionizing Temp. (ºC)	Solutionizing Time (hr)	Aging Temp. (ºC)	Aging Time (hr)	Density (kg/m^3)	Machine (Instron)	Cross Head Speed (mm/min)	Number of tests
AA Al foam	10	560	1	N/A	0	196	4206	25	1
AA Al foam	10	560	1	220	0.5	196	4206	25	2
AA Al foam	10	560	1	220	1	196	4206	25	2
AA Al foam	10	560	1	220	2	196	4206	25	2
AA Al foam	10	560	1	220	4	196	4206	25	3
AA Al foam	10	560	1	180	1	196	8874	30	2
AA Al foam	10	560	1	180	2	196	8874	30	1
AA Al foam	10	560	1	180	2	196	4206	25	1
AA Al foam	10	560	1	180	4	196	8874	30	1
AA Al foam	10	560	1	180	5	196	4206	25	1
AA Al foam	10	560	1	180	7	196	8874	30	3
AF Al foam	10	N/A	N/A	N/A	N/A	196	4206	25	3
AA Foam-Hybrid	10	560	1	220	4	1080	4206	25	1
AF Foam Hybrid	10	N/A	N/A	N/A	N/A	1080	4206	25	2
Elvax®	N/A	N/A	N/A	N/A	N/A	950	4206	25	3

Note: AA - Artificially Aged
AF - As Fabricated

Two important points in the stress-strain curve are the yield point and the point of densification. Following Lehmus and Banhart [2003] the foam yield strength is defined in the present work in one of the two following ways. It is the maximum stress if the foam displays a stress peak followed by a valley at the intersection of the elastic region and the plateau region. Otherwise, it is taken as the stress at a strain of 0.05. This is shown schematically in Figure 5.4. This convention is also applied to the hybrid material. The point of densification is defined in this study as the stress at which the

cushion factor is a minimum. The cushion factor in this investigation is calculated in EXCEL using equation (2.17). For each set of data points (σ, e) the maximum observed stress from 0 strain up to e is divided by the energy absorbed (W) up to e. The cushion factor is also used to determine energy absorption efficiency. A typical stress-strain curve with the densification stress (σ_d) and strain (e_d) is shown schematically in Figure 5.5 a). The minimum cushion point is shown schematically in Figure 5.5 b).

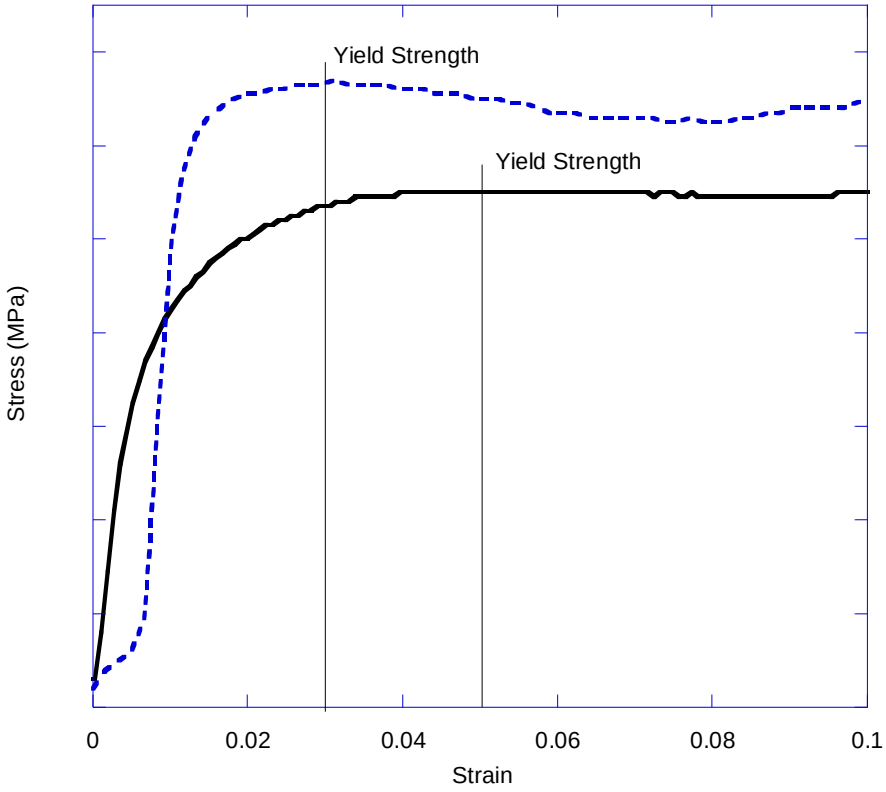

Figure 5.4: Yield strength definition schematic. Upper curve the yield strength is determined by the maximum stress value while the lower curve is determined by the stress value at 5% strain.

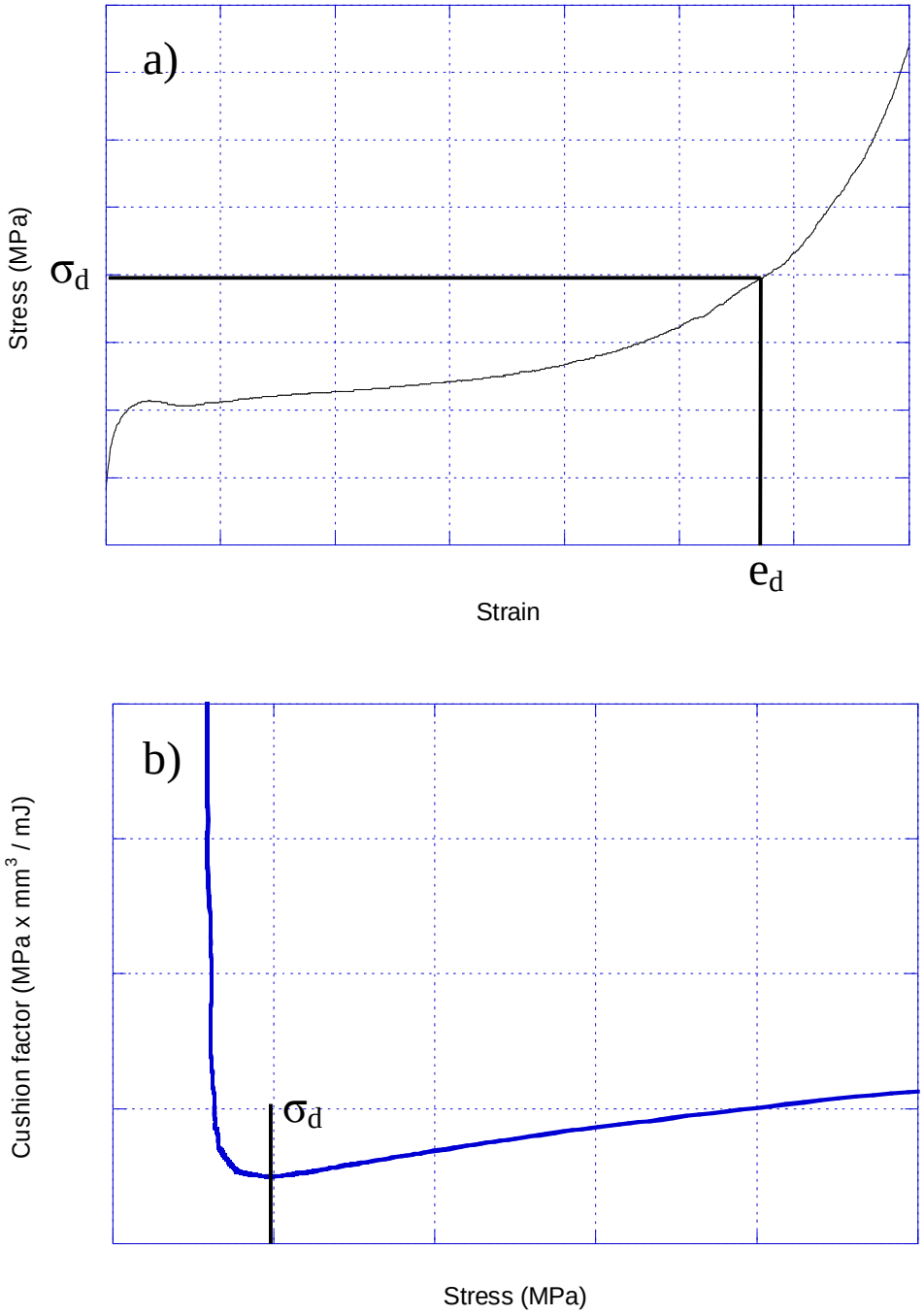

Figure 5.5: a) Schematic of a typical stress-strain curve showing densification stress (σ_d) and strain (e_d). b) Schematic presentation of the cushion factor (i.e. σ /W) vs. σ. Densification stress is defined as the stress at which the cushion factor is a minimum.

5.5.2 Dynamic Testing

Dynamic testing was performed on an Instrumented Falling Weight Impact Tester Type 5 H.V controlled by an Imatek controller. The machine is capable of testing specimens at strain rates in the approximate range of $\dot{\varepsilon} \approx 10^{1} - 10^{2}\, s^{-1}$ [Cronin 2006]. An anvil, restrained from horizontal motion by rails, is suspended above the specimen. The anvil is allowed to fall and impact the specimen. An optical sensor measures the displacement of the anvil. Both the initial height and the mass of the anvil are variable. Force (P) is obtained by differentiating the displacement (x) signal twice and multiplying by mass of the anvil (m_{anvil}) as follows [Lifshitz *et al.* 1994]:

$$P = m_{anvil} \times \frac{d}{dt}\left(\frac{dx}{dt}\right) \tag{5.3}$$

This is performed by the software that records the data. Figure 5.6 a) show the testing setup. The specimens are placed on the cone in the wide, lower chamber as shown in Figure 5.6 b).

a) 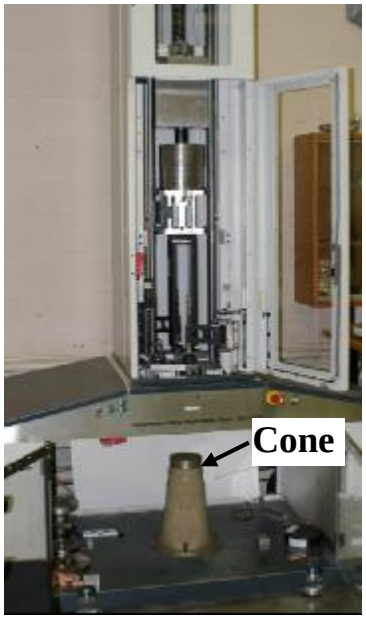

b) 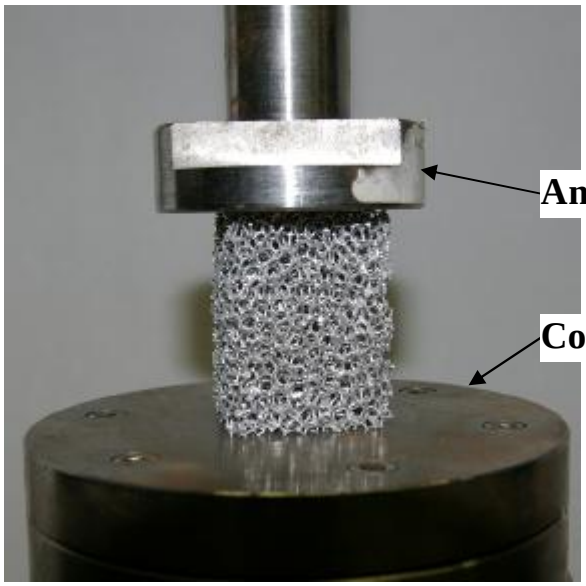

Figure 5.6: a) Falling Weight Impact Tester Type 5 H.V. used in performing dynamic compression tests. b) Close up of an aluminum foam specimen between the base cone and the anvil.

In this investigation the height and mass of the anvil are determined using the knowledge of specimen dimension, desired strain rate and approximate value of energy absorption of the specimen (E). The energy absorption of the specimen is approximated using the energy absorbed during a static test [Salisbury 2006]. Crash boxes in automobiles are utilized to absorb the energy of low velocity collisions (~ 15 - 18 km/hr) [Fuganti *et al.* 2000]. An approximate strain rate of 100 s^{-1} was chosen based on these velocities and the specimen dimensions through equation (2.1). With the strain rate and impact velocity (v_{anvil}) known the drop height of the anvil (h_{anvil}) is then calculated utilizing the following equation [Salisbury 2006]:

$$h_{anvil} = \frac{v_{anvil}^2}{2g} \tag{5.4}$$

where g is gravity. The mass required to produce an impact energy of E from a drop height of h_{anvil} is calculated as follows [Salisbury 2006]:

$$m_{anvil} = \frac{E}{gh_{anvil}} \tag{5.5}$$

The tests performed are listed along with the nominal testing parameters in Table 5.2. Tests are repeated twice to ensure repeatability. Two conditions of aluminum foam are used for testing. They include as-fabricated (i.e. “AF” in the table) and solutionized and artificially aged for 4 hours at 220˚C (ie. “AA 4 hrs 220˚C” in the table). The data collected is cut at the point where forward motion of the anvil is stopped.

Table 5.2: Dynamic testing parameters for each specimen type tested.

Material	Pore Size	Drop height (m)	Drop weight (kg)	Impact velocity (m/s)	Energy (J)	Density (kg/m3)
Solid Elvax	N/A	1.0	13	4.43	127.53	950.0
AF Foam	10	1.3	13	5.05	165.79	194.6
AA 4 hr 220°C Foam	10	1.3	13	5.05	165.79	194.6
AF Foam Hybrid	10	1.3	23	5.05	293.32	1080.0
AA 4 hr 220°C Foam Hybrid	10	1.3	23	5.05	293.32	1080.0

Dynamic testing on the drop tower produces initial vibrations caused by impact which are visible in the results (i.e. curve fluctuations) [Hsiao and Daniel 1998]. To avoid filtering out real data the results are left as is without filtering. The high rate of testing (~ 4430 mm/s) combined with the short linear-elastic region of the foam specimens ($e < 0.05$ equivalent to approximately 2.5 mm) result incomplete capture of this region. The initial curve fluctuations and the incomplete linear-elastic regions make accurately determining the yield strengths impossible. Therefore yield strength values are not determined for dynamic compression testing. At densification however the fluctuations in the curve are greatly reduced and therefore the densification stress and strain are determined utilizing the conventions employed in static testing.

5.5.3 Compression-Compression Cyclic Testing for Mechanical Damping Studies

The inelastic behaviour of materials under all loading conditions result in a hysteresis loop when cyclic loads are applied [Lazan 1964]. The area in the hysteresis loop is proportional to the damping capacity [Shen 2001, Lazan 1964]. To obtain damping properties of the aluminum foam and hybrid cyclic testing is performed on the Instron 8874 described previously.

All specimens are subjected to sinusoidal loading in an axial fixed-free vibration system. However the foam is not clamped to the fixed base to avoid damage to the foam. The specimens are tested for

190 cycles at 5Hz and at two different amplitudes. To maintain contact between the specimen and the platens a mean compressive strain that is larger than the applied amplitude is utilized, as described below.

For both aluminum foam and aluminum foam-polymer hybrid specimens only the as-fabricated condition of aluminum foam is tested. The specimens are tested by displacement control, under which a predetermined cyclic displacement is imposed by the machine on the specimens and the force values vary based on the specimen response. A mean compressive displacement d_M = 0.356 mm, corresponding to 0.7 % strain is applied to the specimens. Superimposed on this is the sine wave with either a "high" amplitude (i.e. test condition D5H) of d_A = 0.101 mm (0.2 % strain) or a "low" amplitude (i.e. test condition D5L) of d_A = 0.051 mm (0.1 % strain). These values are listed in Table 5.3. A schematic of the strain cycle applied to the specimens is shown in Figure 5.7. The schematic shows the two amplitudes employed at 5 Hz. When the polymer is strained under the above conditions, the differences in load values during loading and unloading are in the range of the load cell error, making the results unusable. Therefore polymer testing is not included.

Table 5.3: Cyclic testing displacement control parameters at the "low" amplitude (D5L) and "high" amplitude (D5H) conditions.

Test Condition	Frequency (Hz)	Displacement (mm)		Strain	
		Mean d_M	Amplitude d_A	Mean	Amplitude
D5L	5	0.356	0.051	0.007	0.001
D5H	5	0.356	0.101	0.007	0.002

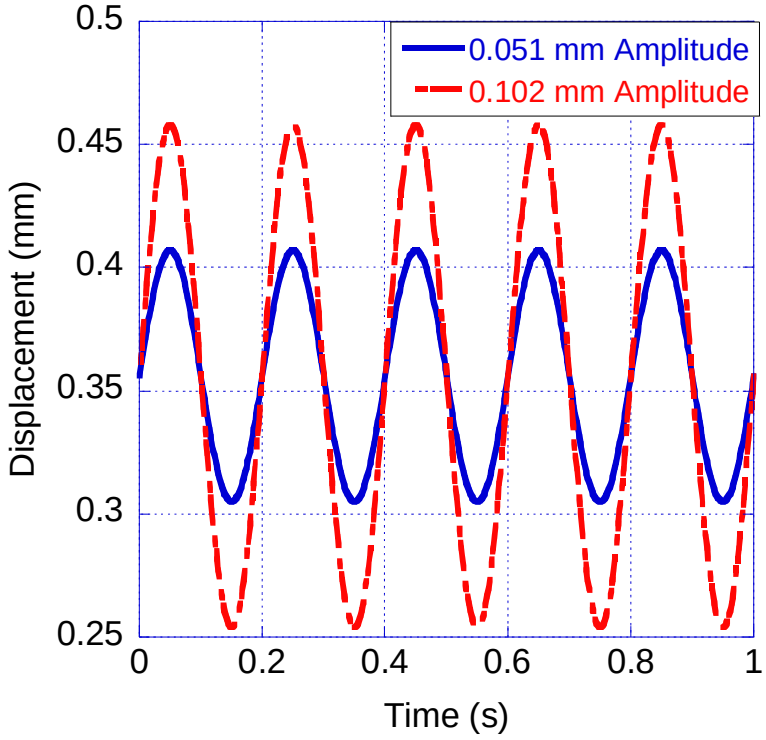

Figure 5.7: Schematic of input sinusoidal 5 Hz wave for cyclic testing at both amplitudes.

In this work both the unit damping (D) and the loss coefficient (h) of the specimens are utilized to compare the damping properties of the different materials. These two values are determined in the following manner. If the specimen is homogeneously stressed, i.e. the assumption made for uniaxial test specimens, D is defined as the area in the stress-strain hysteresis loop, and determined according to the following equation [Lazan 1968]

$$D = \oint s\,(e)de \tag{5.6}$$

The unit loss coefficient (h) is a relative damping unit. It is found by normalizing the energy absorbed by the unit elastic strain energy (U) per cycle. The equations for h is as follows [Lazan 1964]

$$h = \frac{D}{2pU} \tag{5.7}$$

The unit elastic strain energy denoted by U is an average measure of the energy input and released upon loading and unloading the specimen respectively. The value of the unit strain energy is calculated as [Lazan 1968]

$$U = \int_{e=0}^{e_a} s_{mid}(e)de \tag{5.8}$$

The value of s_{mid} at any strain, e_i, is calculated as the average of the stress during loading at e_i and the stress during unloading at e_i [Lazan 1968]. A graphic representation of the s_{mid}-e curve can be seen in Figure 5.8.

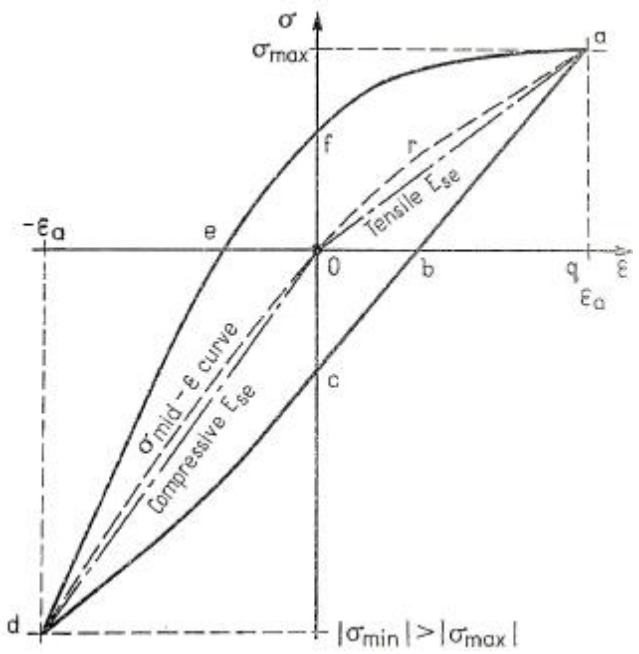

Figure 5.8: Schematic of a hysteresis loop demonstrating the s_{mid}-e curve. The area under this curve represents the specific elastic strain energy (U). Note e in the figure is equivalent to e in this work. [Lazan 1968]

The experimental results contain random noise from the load cell (± 10 N) and a noise at 300 Hz from the hydraulic pump (± 20 N). These have little effect on the results producing only a ± 0.0018 MPa variation in the stress-strain curves (observed stress range from 0 to > 1 MPa). However the noise does result in strain values not being sequential, which causes problems in calculating the area under the curve. To make the calculation easier the loading and unloading curves are curve fit with 4th order polynomials with an average fit coefficient of $R^2 = 0.999$. An example of the curve fitting to the loading and unloading curves with polynomials is shown in Figure 5.9. The area is then calculated by integrating the polynomial. The area in the hysteresis loop is calculated by subtracting the area of the unloading curve from the area of the loading curve. The s_{mid} curve, used to calculate the elastic strain energy, is determined by combining the loading and unloading curves and fitting the full cycle

curve with a 4th order polynomial. This is shown in Figure 5.10. Again the area is calculated by integrating the polynomial. The error in loss coefficient due to variations in calculating the s_{mid} curve is less than 5 %. Curve fitting the loading, unloading and full cycle curves for 190 cycles is time consuming and not required. The rapid change in the hysteresis loop up to the 10th cycle and the subsequent slower changes over the next 180 cycles are captured by performing the preceding procedure on the following selected cycles 2, 5, 10, 20, 30, 50, 70, 80, 100, 120, 130, 150, 170, and 190. The average values of D and h are calculated by summing the values from the selected cycles between the 10th and 190th cycle and dividing by 12. Starting at the 10th cycle eliminates the effect the high values the 2nd and 5th cycle have on the average.

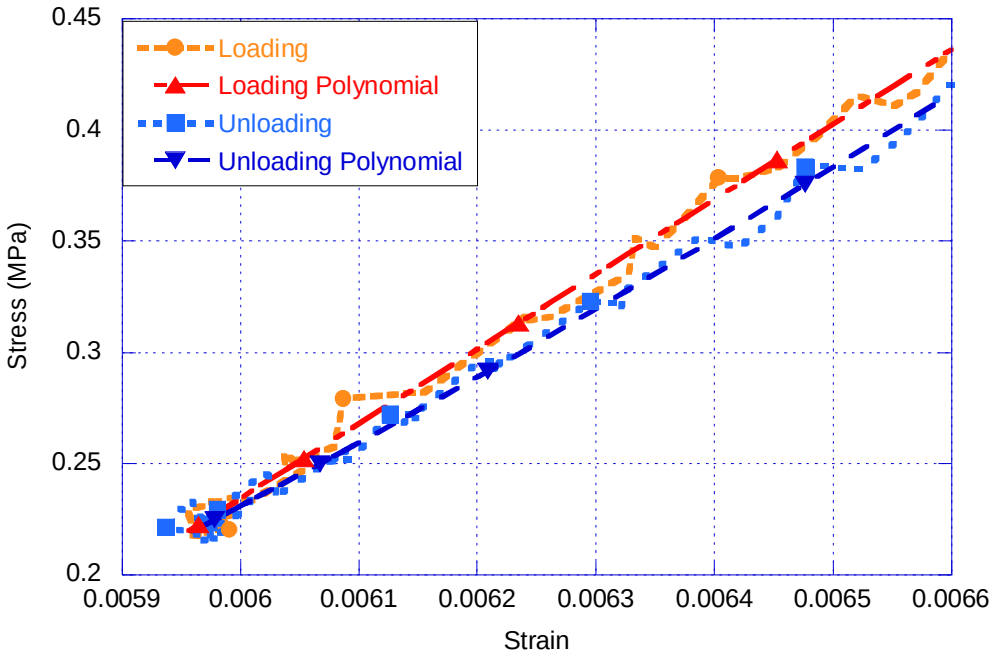

Figure 5.9: An example of the noise level in the loading and unloading stress-strain curves and the resultant 4th order polynomial curve fits utilized in damping calculations.

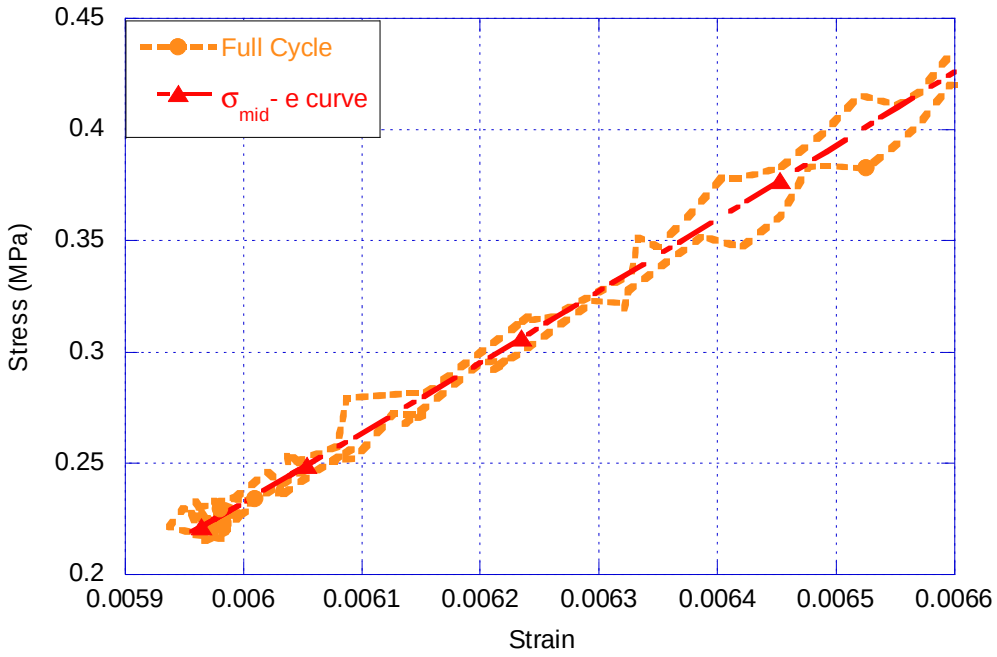

Figure 5.10: An example of the $s_{mid} - e$ curve. Produced by a 4th order polynomial curve fit to the full cycle.

Chapter 6
Experimental Results

6.1 Introduction

The results are categorized according to the experimental testing procedures described in Chapter 5. The materials tested, which encompass aluminum foam, polymer, and aluminum foam-polymer hybrid, are the basis for the subdivision of each experimental test section.

6.2 Static Compression Testing

In this section material response to static loading is quantified using stress-strain curves, energy absorption diagrams (i.e. W vs. s plots) and the cushion factor (C), as described in Chapter 2. Energy absorbed per unit volume (W) is calculated as the area under the stress-strain curve following the procedure outlined in Chapter 2. Tables listing specimen yield strength (s_{ys}), densification stress and strain (i.e. s_d and e_d, respectively), energy absorbed up to densification W_d and C are included in each section.

6.2.1 Aluminum Foam

For static compression testing both age-hardened aluminum and as-fabricated foam are investigated. The repeat of compression testing in as-fabricated and selected aging conditions show the results are generally reproducible. During compression testing the foams are fully densified. The height of the specimens is reduced to approximately 7 mm when a maximum compressive load of 70 kN is applied and approximately 10 mm when a maximum compressive load of 20 kN is applied. Minimal lateral expansion is observed only upon initial loading. This can be seen in Figure 6.1 where lateral expansion occurs up to a strain of approximately 0.13 but remains constant thereafter.

Deformation is observed to occur heterogeneously in discreet crush bands of high localized strain in all aluminum foam specimens. This is shown for an aluminum foam specimen aged for 1 hr at 220˚C in Figure 6.1 where the lines indicate the regions of high strain. The circles show areas with little local deformation despite the macroscopic strain of up to 0.38. Some slight barreling in the compressed specimen is observed due to the initial expansion. A typical compressed aluminum foam specimen can be seen in Figure 6.2.

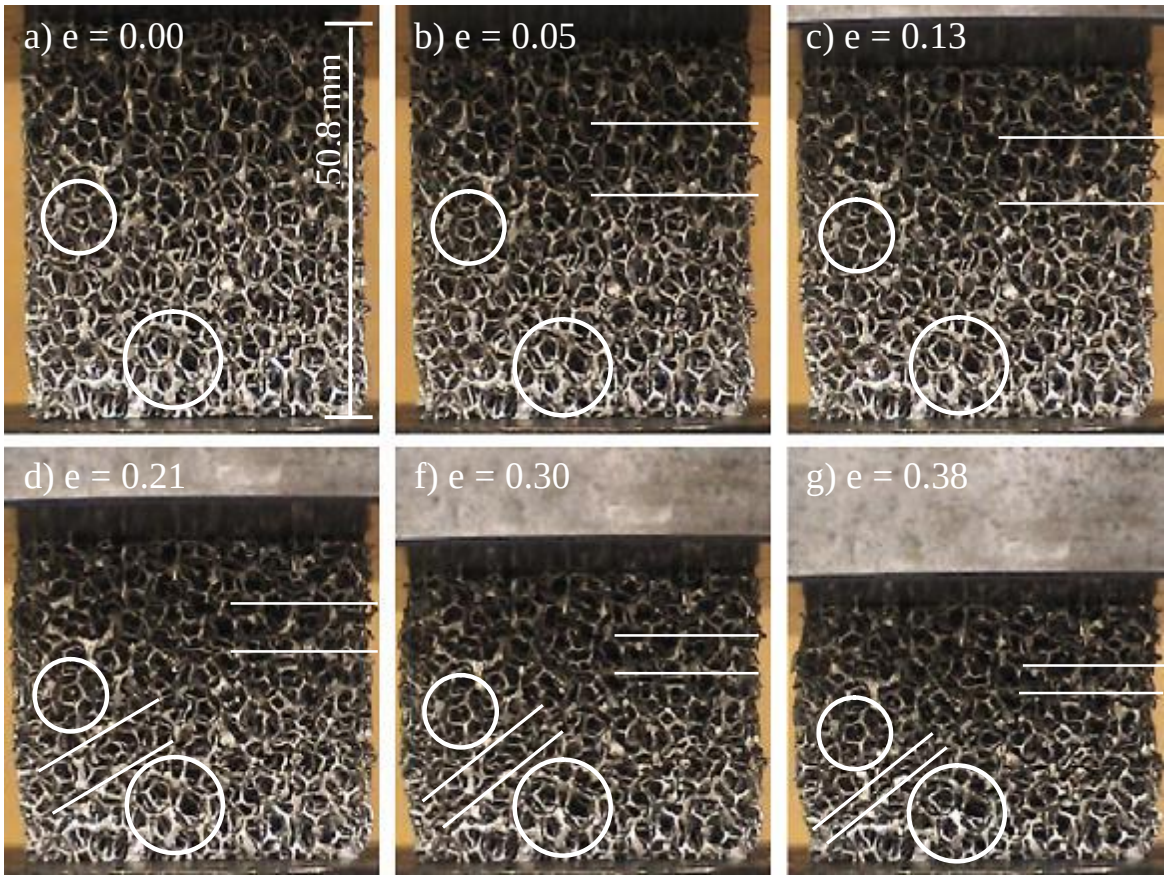

Figure 6.1: Images captured during compression testing of an aluminum foam specimen artificially aged for 1 hr at 220˚C for strains from 0.00 (a) to 0.38 (g). In the circles are examples of cells which show little deformation up to e = 0.038. The lines show examples of crush bands.

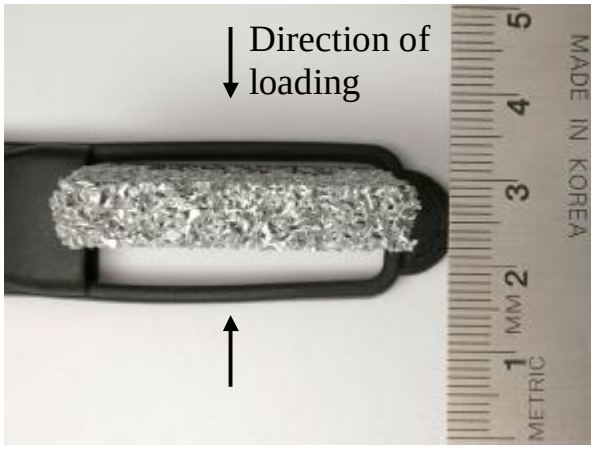

Figure 6.2: Typical aluminum foam specimen after static compression testing.

6.2.1.1 Age-Hardened Aluminum Foam

Age hardening of aluminum foam is performed at 180˚C and 220˚C for select aging times according to the heat treatment procedure described in Section 5.4. The goal is to evaluate the effect of precipitation hardening in the alloy on the yield strength, energy absorption and cushion factor of the foam.

The compression testing results for specimens aged at 180˚C and 220˚C can be seen in Figure 6.3 and Figure 6.4, respectively. For clarity only selected aging times have been included. The results indicate that age hardening treatments increase the yield strength as well as the stress plateau. The specimens aged for 7 hrs at 180˚C, 2 hrs at 220˚C and 4 hrs at 220˚C display stress-strain curves with upper yield points followed by stress valleys. Specimens aged for shorter times (i.e. underaged conditions) have smooth, constantly increasing, stress levels from 0 loading up to and beyond yielding. The stress-strain plateaus generally show small peaks and valleys and a decrease in slope as aging time increases. The specimens aged for 1 hr at 180˚C and 0.5 hr at 220˚C show the steepest slopes. The average yield strength at each aging conditions is listed in Table 6.1. When only a single

test is performed for a given aging condition (i.e. for 1, 4, 5 hours at 180˚C) the values of that test are listed. From Table 6.1 it can be seen that the specimens aged for 5 hrs and 7 hrs at 180˚C have the highest yield strength at 1.25 MPa and 1.26 MPa, respectively, followed by the specimen aged for 4 hrs at 220˚C with a yield strength of 1.16 MPa. All specimens densify between strains of 0.54 and 0.57. The specimens aged at 180˚C densify at somewhat different stresses (1.7 to 2.06 MPa for 2 and 7 hours respectively) and the specimens aged at 220˚C densify at approximately the same stress values (1.83 to 1.94 MPa for 0.5 and 4 hours respectively).

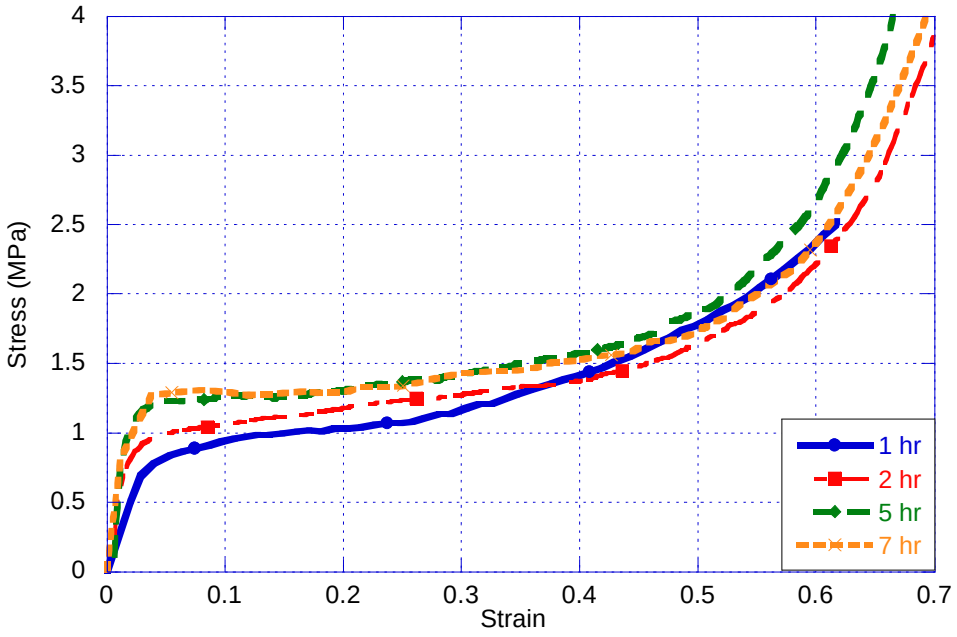

Figure 6.3: Compressive stress-strain curves for aluminum foam specimens age-hardened at 180˚C under static compression.

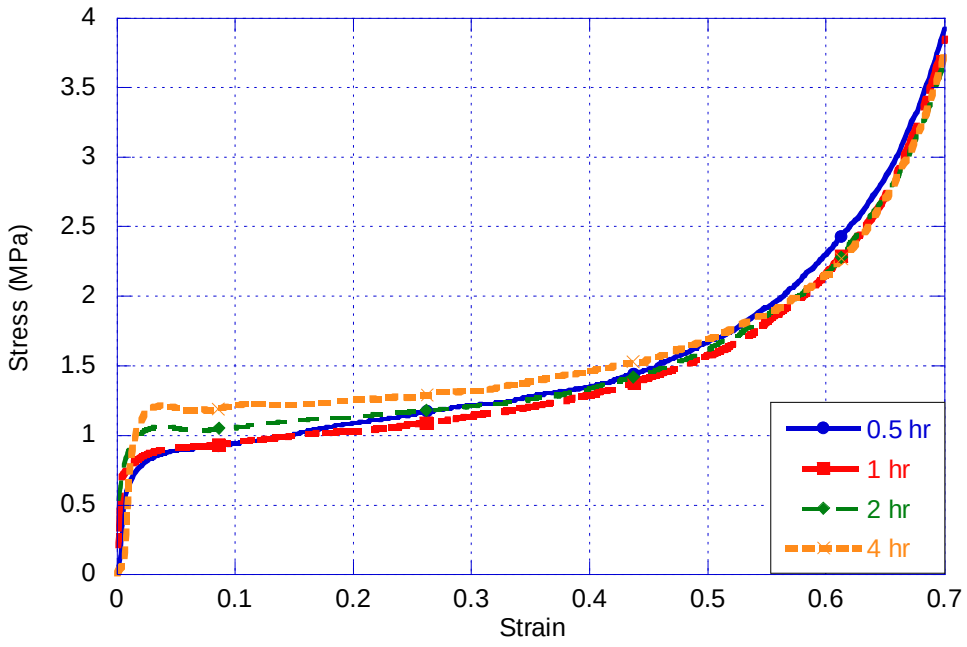

Figure 6.4: Compressive stress-strain curves for aluminum foam specimens age-hardened at 220˚C under static compression.

The increase in magnitude of the stress plateau with increasing aging times leads to a generally higher stress at which energy is absorbed. This can be seen in Figure 6.5 and Figure 6.6 where the vertical portion of the curves is shifted to higher values of stress with increased aging times. As shown in Figure 6.5 the shoulders of the energy curves for foams aged at 180˚C occur at approximately the same stress 2 MPa. This is also seen in Figure 6.6 for the case of aging at 220˚C where the shoulder occurs at a lower stress of 1.9 MPa. These aging conditions, as well as the values obtained for e_d, σ_d, W and C are listed in Table 6.1.

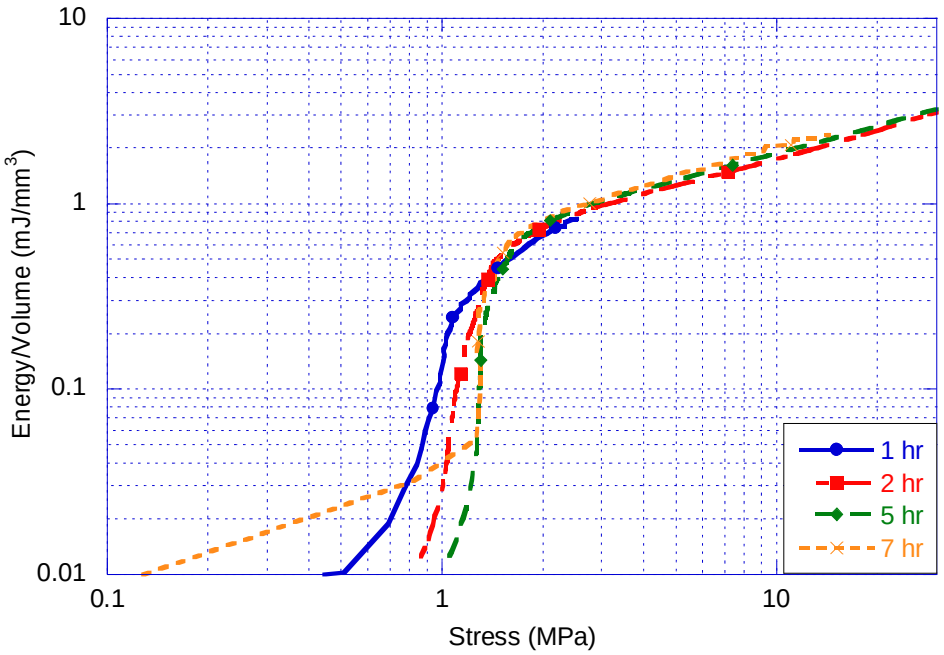

Figure 6.5: Energy absorption curve for aluminum foam specimens age-hardened at 180˚C under static compression.

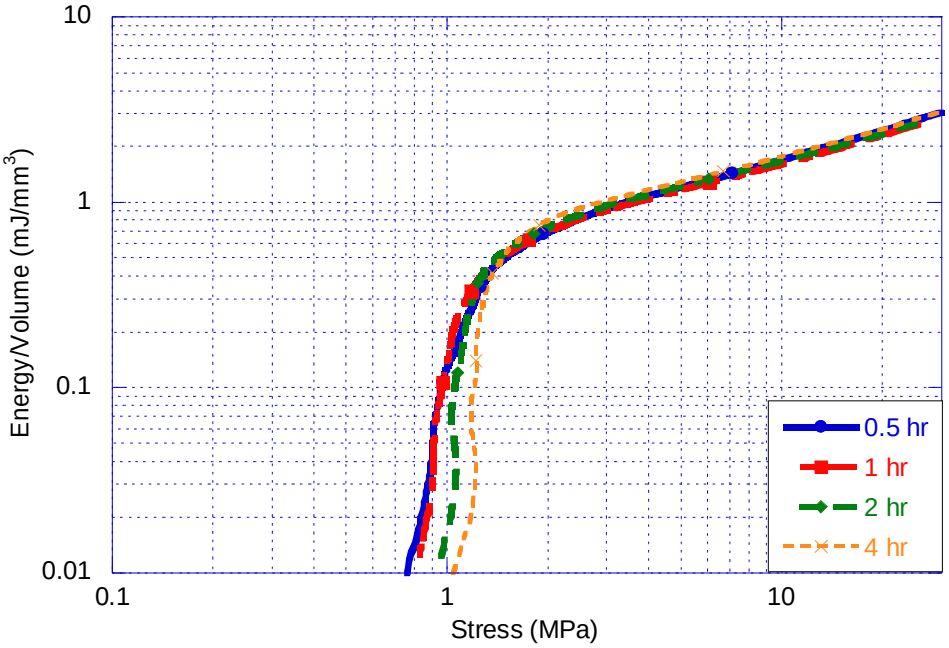

Figure 6.6: Energy absorption curve for aluminum foam specimens age-hardened at 220˚C under static compression.

From Table 6.1 it can be seen that the foams aged for 5 hrs at 180˚C and the 7 hrs at 180˚C absorb the most energy at densification with approximate values of 0.80 mJ/mm^3. At both 180˚C and 220˚C the Cushion factor decreases with increasing aging time. At 180˚C it decreases from 3.0 (aged for 1 hr) to 2.5 (aged for 7 hr). The decrease is less significant in foams aged at 220˚C ranging from 2.8 (aged for 0.5 hr) to 2.6 (aged for 4 hr).

Table 6.1: Properties of age-hardened aluminum foam under static compression.

Specimen Material	Aging Temp. (°C)	Aging Time (hrs)	σ_{ys} (Mpa)	Properties at e_d			
				e	σ_d (MPa)	W (mJ/mm^3)	C
AA Al Foam	180	1	0.84	0.57	2.18	0.737	2.96
AA Al Foam	180	2	0.97	0.54	1.72	0.653	2.64
AA Al Foam	180	4	1.13	0.54	2.00	0.766	2.61
AA Al Foam	180	5	1.25	0.54	2.00	0.783	2.55
AA Al Foam	180	7	1.26	0.55	2.06	0.816	2.53
AA Al Foam	220	0.5	0.91	0.54	1.83	0.648	2.82
AA Al Foam	220	1	1.03	0.54	1.95	0.708	2.75
AA Al Foam	220	2	1.07	0.55	1.87	0.698	2.69
AA Al Foam	220	4	1.16	0.55	1.94	0.749	2.59

Note: AA - Artificially Aged
AF - As Fabricated

Variations of ± 12 % in measured yield strength values, ± 5 % in densification stress and energy absorption values and ± 3 % in densification strain are obtained. Variations in calculated Cushion factors are less than ± 5 %.

6.2.1.2 As-fabricated Aluminum Foam

Average values from compressive tests on three as-fabricated foam specimens are presented in this section. A typical engineering stress-strain curve for an as-fabricated foam can be seen in Figure 6.7.

Also included in the figure are stress-strain curves for peak-age hardened foam at 180˚C (7 hrs) and 220˚C (4hrs). The as-fabricated curve displays an upper yield point at 1.34 MPa stress followed by a drop and a subsequent slow rise in stress (i.e. plateau region) up to densification. Densification in as-fabricated foams occurs at approximately s_d = 1.98 MPa and e_d = 0.56 as determined by the point with the minimum cushion factor. Visual observation of Figure 6.7 confirms these findings. Minor peaks and valleys are observed in the plateau region with a sharp rise in stress upon foam densification. The stress-strain curves of all three foams in Figure 6.7 are all very similar. The as-fabricated foam shows the highest yield strength. The plateau height of the as-fabricated foam is approximately the same height as the 7 hrs 180˚C age hardened foam. Both are higher than the plateau of the 4 hrs 220˚C age hardened foam.

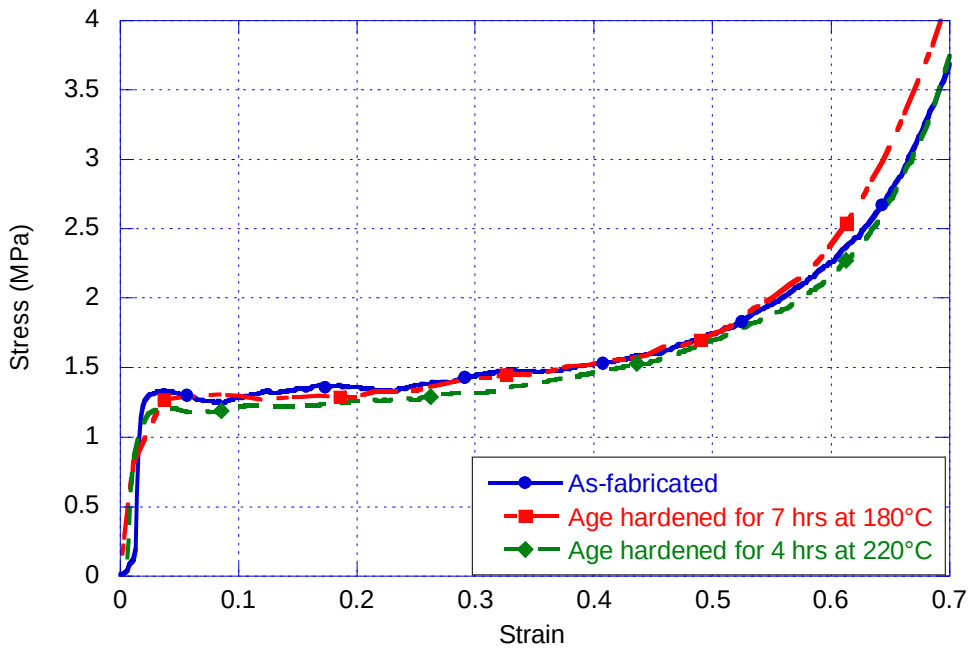

Figure 6.7: Compressive stress-strain curve of the as-fabricated and peak-age hardened aluminum foam under static compression.

The energy absorption curve of a typical as-fabricated foam is shown in **Figure 6.8**. The curve shows that the absorbed energy increases from 0.01 mJ/mm^3 to approximately 0.80 mJ/mm^3 over the plateau region. At the shoulder of the curve, occurring at approximately s_d, the slope transitions from near vertical towards the horizontal. After this point incremental increase in energy absorption is accompanied by a significant increase in stress.

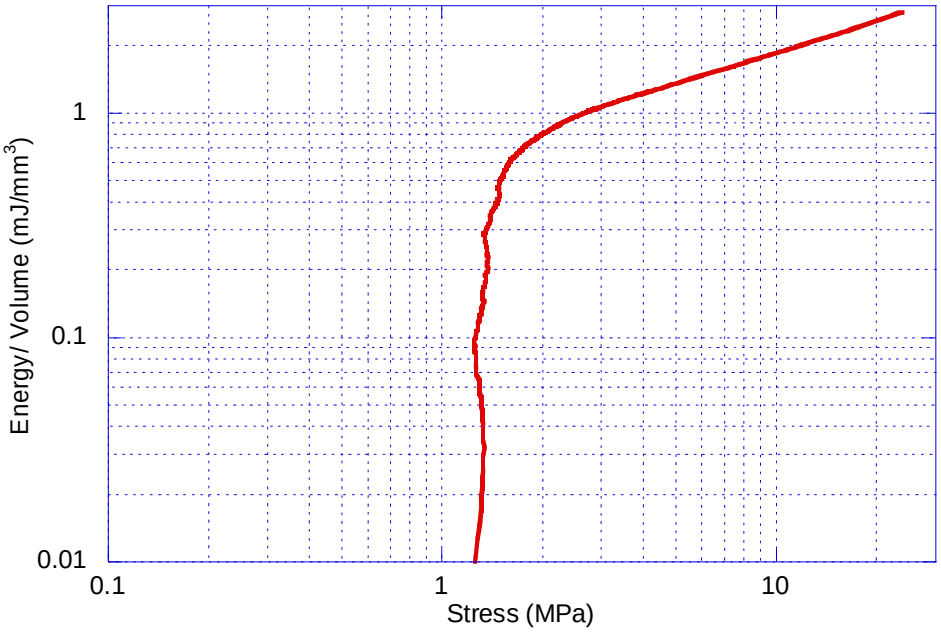

Figure 6.8: Energy absorption curve of as-fabricated aluminum foam under static compression.

Table 6.2 lists the average properties of as-fabricated foams. At densification the as-fabricated foams absorb approximately 0.80 mJ/mm^3, this produces an average cushion factor of 2.5.

Table 6.2: Properties of as-fabricated aluminum foam under static compression.

Specimen Material	Aging Temp. (°C)	Aging Time (hrs)	σ_{ys} (Mpa)	Properties at e_d			
				e	σ_d (MPa)	W (mJ/mm^3)	C
AF Al Foam	N/A	N/A	1.34	0.56	1.98	0.802	2.47

Variations in yield strength, densification stress and energy absorption values are less than ± 2 % for all the values measured.

6.2.2 Polymer

For reasons described in Chapter 4 Elvax® is the polymer chosen for filling the foam. To understand the role of Elvax® in the properties of the hybrid, testing on the polymer is performed under the same conditions as the hybrid material. During compression tests Elvax® expands laterally and showed tearing through the center of the specimen. The polymer sample displays some springback upon unloading. Figure 6.9 shows an Elvax® specimen after compression testing.

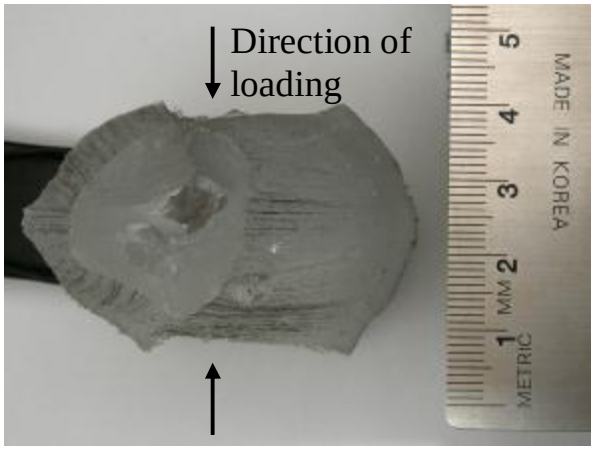

Figure 6.9: Elvax® specimen after static compression testing.

Figure 6.10 shows the stress-strain response of Elvax®. The curve has an initial linear elastic region followed by a sharp rise in stress at a strain of 0.6. No yield point or near-constant stress plateau is observed. Therefore no yield strength value is reported. Elvax®, an already dense solid is not a foam and does not truly densify, similar to the foam however it does have an optimum point for energy absorption therefore the definitions and procedures applied to foams for densification stress,

s_d and strain, e_d are also used on Elvax®. The term densification will still be used to avoid confusion.

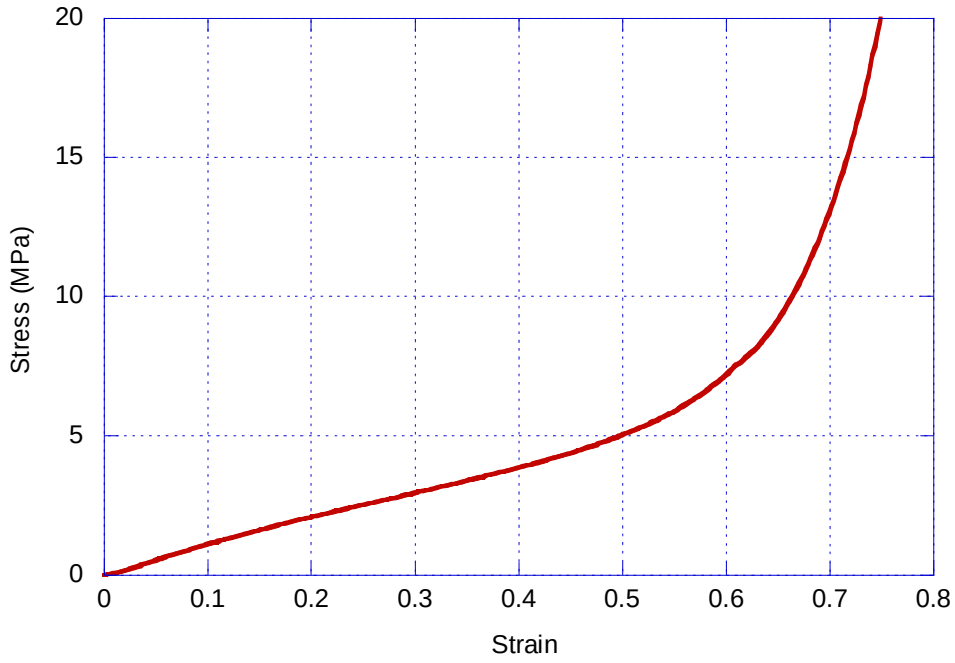

Figure 6.10: Compressive stress-strain curves of solid Elvax® under static compression.

Figure 6.11 shows the energy absorption diagram of Elvax®. As expected the curve does not display any vertical portion. Instead a near constant slope in the log-log plot depicting an increase in the allowable stress required for an increase in energy absorbed is observed up to 4 MPa. From 4 to 8 MPa the slope of the curve decreases until at 8 MPa the curve again shows a near constant slope. This slope is lower than the initial region (i.e. up to 4 MPa) which indicates that for a similar increase in energy absorption a larger increase in stress is observe beyond 8 MPa than before 4 MPa.

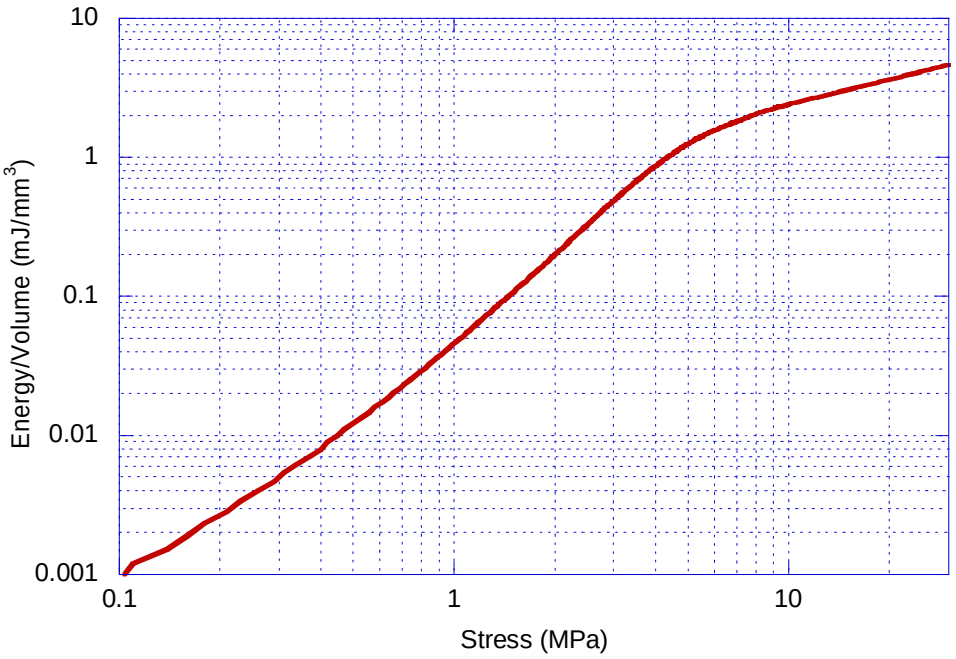

Figure 6.11: Energy absorption curve of solid Elvax® under static compression.

Table 6.3 lists the average values of the properties of interest for solid Elvax®. On average Elvax® densifies at a strain of 0.59 and a stress of 6.5 MPa. It absorbs 1.74 mJ/mm^3 up to densification, this combined with the densification stress yields a Cushion factor of 3.7.

Table 6.3: Properties of solid Elvax® under static compression.

Specimen Material	Aging Temp. (°C)	Aging Time (hrs)	σ_{ys} (Mpa)	Properties at e_d			
				e	σ_d (MPa)	W (mJ/mm^3)	C
Elvax	N/A	N/A	N/A	0.59	6.48	1.743	3.72

The results of compression testing on solid Elvax® were repeatable showing a ± 5 % variation in densification stress and energy absorption values and less than 1 % variation is densification strain. Variations in calculated C values are less than ± 5 %.

6.2.3 Aluminum Foam-Polymer Hybrid

For static compression testing of hybrid materials both an as-fabricated and a 4 hrs at 220˚C age-hardened aluminum foam are infiltrated with polymer and tested. The definitions of s_{ys} and e_d employed for aluminum foam are also used for the aluminum foam-polymer hybrid material. Repeats were not performed on the age-hardened foams.

During compression testing of the hybrid material the specimen deforms laterally similar to solid Elvax®. After compression testing the appearance of the hybrid specimens are again akin to solid Elvax®. The aluminum foam in the hybrid is only partially densified and the damaged hybrid specimens are permanently flattened. The dimensions of the tested specimens normal to the crushing axis expand due to the presence of Elvax®. This can be seen in Figure 6.12 a). Some of the ligaments in the filled foam buckle akin to an unfilled foam, however ligaments in the filled foam also fracture. The result is a discontinuous network of aluminum ligaments distributed throughout the Elvax®. This is shown in Figure 6.12 b).

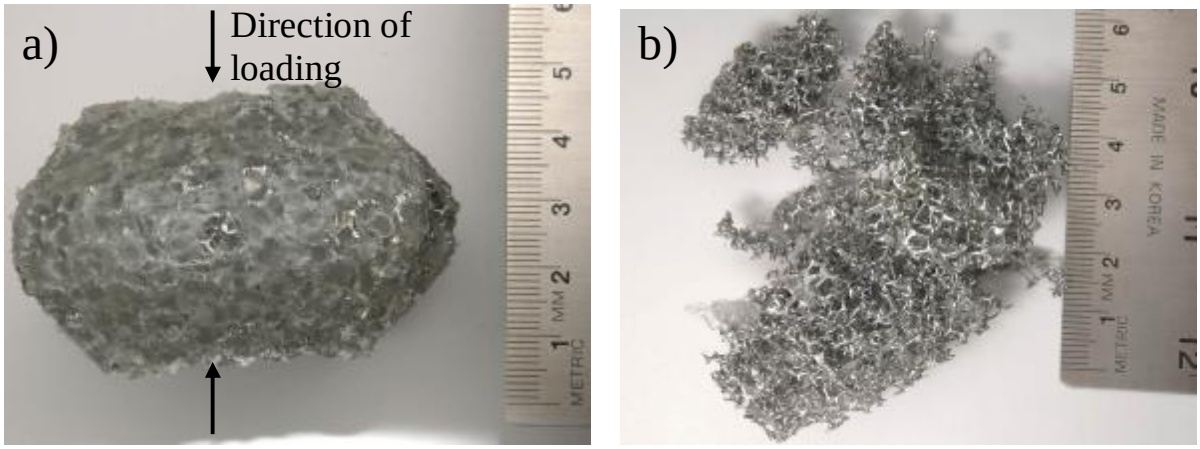

Figure 6.12: Typical aluminum foam-polymer hybrid specimen after static compression testing before (a) and after the polymer has been melted out (b).

The stress-strain curve of the hybrid material is distinct from the materials of which it is constructed, as shown in Figure 6.13. From initial loading (i.e. e = 0) up to a strain of 0.03 the approximately linear stress-strain behaviour of the hybrid material is similar to that of aluminum foam. Between e = 0.03 and e = 0.18 the stress-strain curve retains an approximately linear stress-strain relationship, displaying an observed slope that is slightly elevated compared to the slope of the stress-strain curve for Elvax®. Yet another approximately linear relationship between stress and strain occurs between e = 0.19 and densification (i.e. $e_d \approx 0.57$). The slope of the stress-strain curve of the hybrid between these strains is less than that displayed in the stress-strain curve for Elvax®. From a strain of 0.03 to 0.57 the stress level in the hybrid material quadruples. Beyond densification a sharp rise in stress is observed for the hybrid material and the stress-strain curve of both the hybrid and Elvax® begin to merge. The stress-strain response of the hybrid specimen with an as-fabricated matrix is the same as the hybrid specimen with an age-hardened foam matrix.

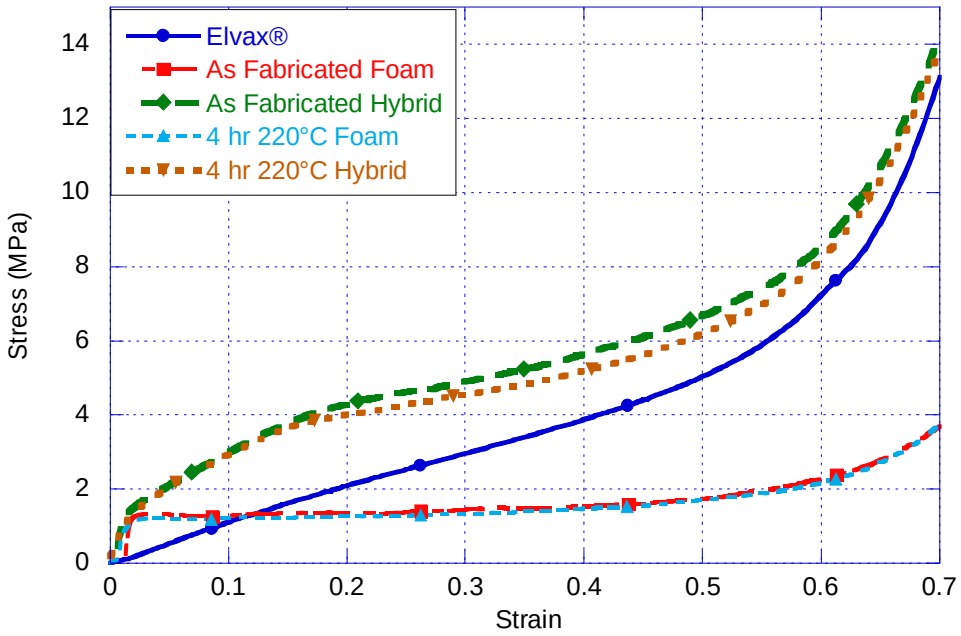

Figure 6.13: Compressive stress-strain curves of aluminum foam-polymer hybrid under static compression. Included are the stress-strain curves of the parent material.

The energy absorption diagram is shown in Figure 6.14. The aluminum foam-polymer hybrid curves do not display a vertical segment, as observed in the base foam material. It does, however, have a steeper slope than solid Elvax® showing a larger increase in energy absorbed for the same stress increase (~ 2.0 mJ/mm^3 compared to ~ 1.6 mJ/mm^3 from 1 to 6 MPa). The shoulder of the energy absorption curve of the hybrid materials occur between 6 and 7 MPa.

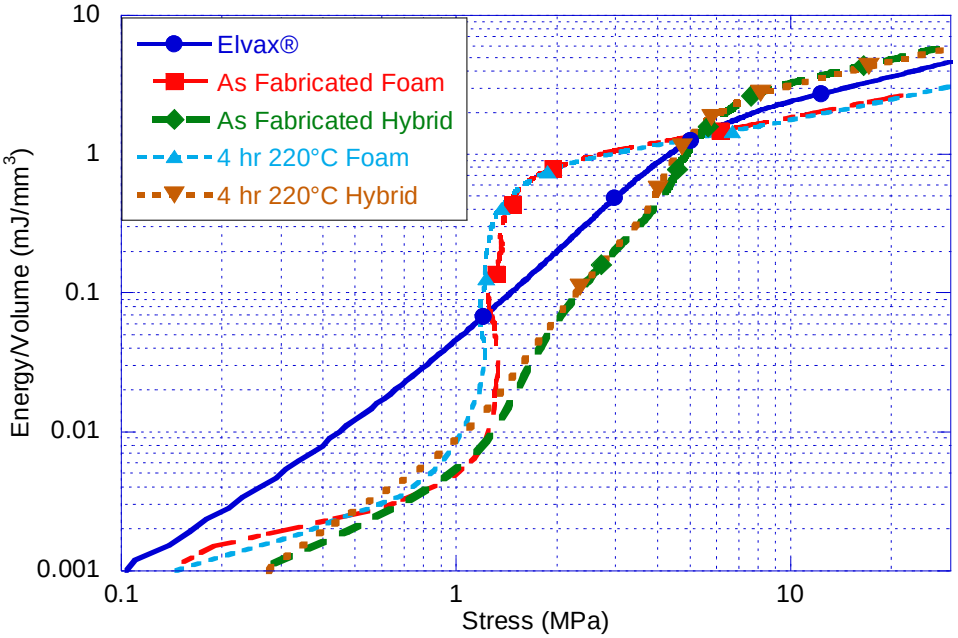

Figure 6.14: Energy absorption curve of aluminum foam-polymer hybrid under static compression. Included are the energy absorption curves of the parent materials.

Table 6.4 lists the properties of the hybrid specimens. The values of the yield strength for the as-fabricated and the age-hardened aluminum foam-polymer hybrid are 2.11 and 2.09 MPa, respectively. The as-fabricated aluminum foam-polymer hybrid densifies at a stress of 7.94 MPa absorbing 2.75 mJ/mm^3. The age-hardened aluminum foam-polymer hybrid densifies at a lower stress of 7.19 MPa

absorbing less energy at 2.46 mJ/mm^3. The Cushion factor at both conditions is however quite similar at approximately 2.9.

Table 6.4: Properties of aluminum foam-polymer hybrid in two aluminum foam conditions (i.e. as-fabricated and artificially aged for 4 hrs at 220˚) under static compression.

Specimen Material	Aging Temp. (°C)	Aging Time (hrs)	σ_{ys} (Mpa)	Properties at e_d			
				e	σ_d (MPa)	W (mJ/mm^3)	C
AF Al Foam Hybrid	N/A	N/A	2.11	0.58	7.94	2.750	2.89
AA Al Foam Hybrid	220	4	2.09	0.56	7.19	2.457	2.93

Note: AA - Artificially Aged
AF - As Fabricated

The variations observed in repeated tests on the aluminum foam-polymer hybrid with the foam in the as-fabricated condition are less than 2% for all values.

6.3 Dynamic Compression Testing

In this section material response to dynamic loading is quantified in the same manner as in static compression testing with the exception of the yield strength. The repeat of dynamic tests on each material are repeatable and show little variation in results (less than ± 4 %).

6.3.1 Aluminum Foam

Both as-fabricated and age hardened (4hrs at 220˚C) aluminum foams are tested dynamically. Upon impact the specimens crush, as they do in static testing with minimal barreling. Specimen height after impact is approximately 9 mm. A typical specimen after dynamic compression testing can be seen in Figure 6.15.

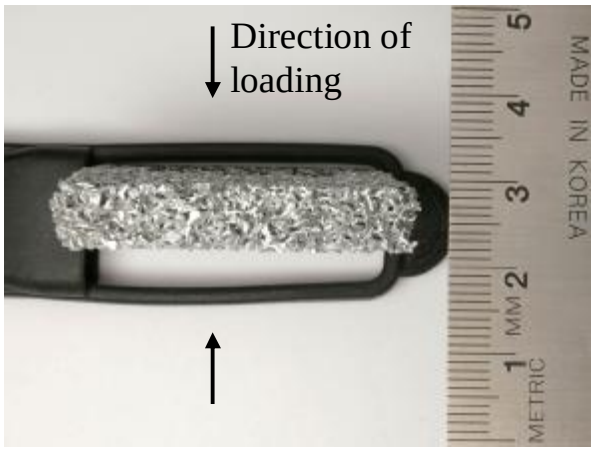

Figure 6.15: A typical aluminum foam specimen after dynamic compression testing

The stress-strain responses of the as-fabricated and age-hardened aluminum foams are shown in Figure 6.16. There is little difference between the responses of the two different aluminum foam conditions. As mentioned in Section 5.5.2 little of the initial linear-elastic regions of the foams are captured. The stress-strain curves are rough, especially up to approximately $e = 0.3$. It is noted that the peaks and valleys occur at approximately the same intervals in both foams and that the amplitude of these fluctuations decreases with increasing strain.

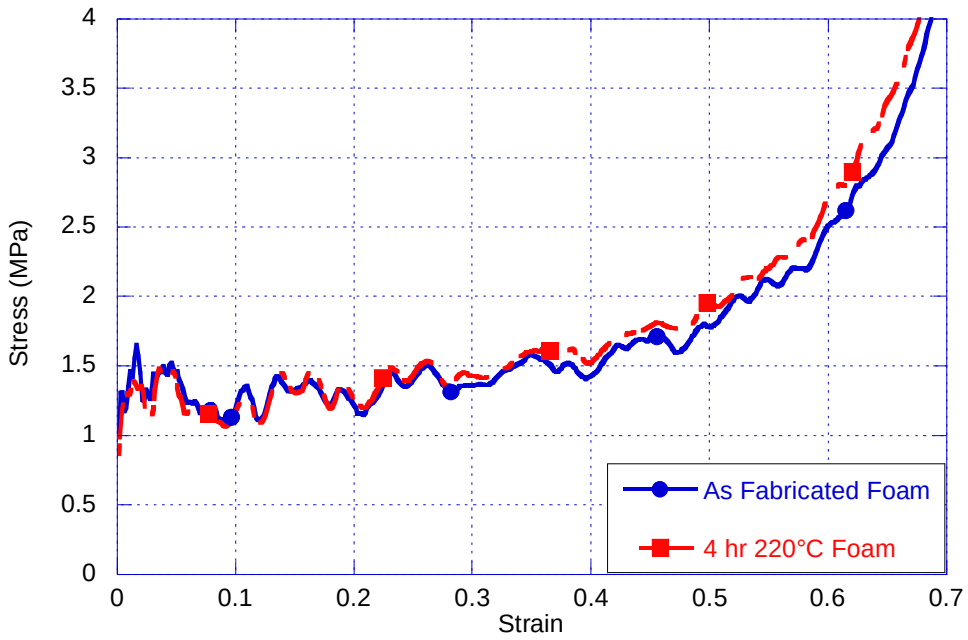

Figure 6.16: Compressive stress-strain curves of aluminum foam in the as-fabricated and age hardened (4hr at 220˚C) conditions tested at de/dt = 100 s^{-1}.

Figure 6.17 shows the energy absorption diagram for the two specimens. The curves have a vertical slope indicating energy absorbed at near constant stress up to the shoulder. The shoulder of the energy absorption diagram occurs at approximately $s_d \approx 2.3$ MPa.

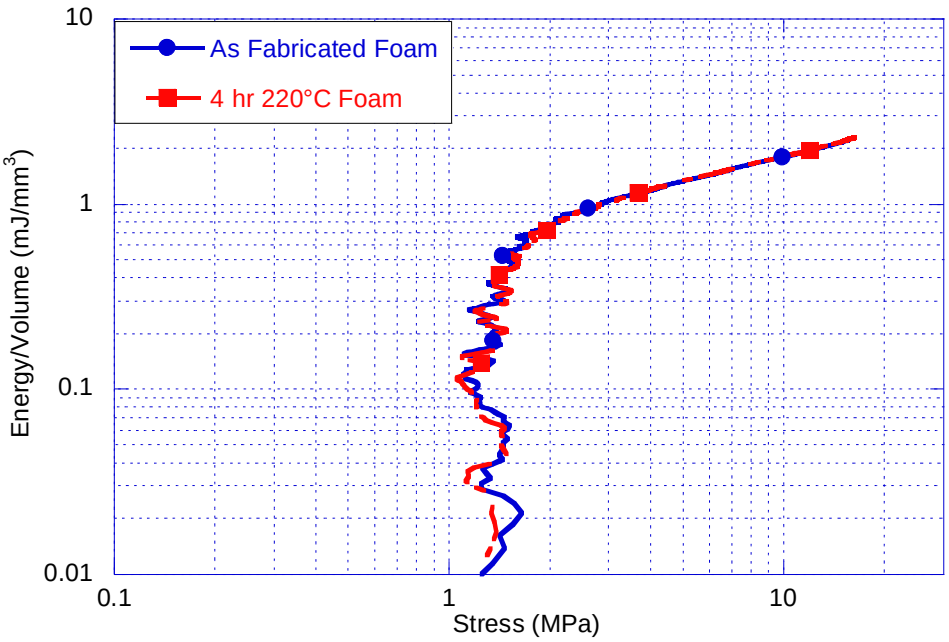

Figure 6.17: Energy absorption curve of aluminum foam in as-fabricated and age hardened (4hr at 220˚C) condition tested at de/dt = 100 s^{-1}.

Table 6.5 lists the average value of the properties of the aluminum foam specimens in both conditions. The as-fabricated aluminum foam absorbs approximately the same energy (W = 0.88 mJ/mm^3) at a lower densification stress ($s_d \approx 2.23$ MPa) than the artificially aged foam (0.87 mJ/mm^3 at $s_d \approx 2.28$ MPa). This results in a lower Cushion factor of 2.53 for the as-fabricated specimen compared to 2.62 for the artificially aged foam.

Table 6.5: Properties of aluminum foam in two conditions (i.e. as-fabricated and artificially aged for 4 hrs at 220˚C) tested at de/dt = 100 s^{-1}.

Specimen Material	Aging Temp. (°C)	Aging Time (hrs)	σ_{ys} (Mpa)	Properties at e_d			
				e	σ_d (MPa)	W (mJ/mm^3)	C
AF Al Foam	N/A	N/A	N/A	0.58	2.23	0.881	2.53
AA Al Foam	220	4	N/A	0.57	2.28	0.871	2.62

Note: AA - Artificially Aged
AF - As Fabricated

6.3.2 Polymer

The Elvax® specimens show little permanent deformation after dynamic testing. Spring back of the specimen is observed after loading. This is seen in Figure 6.18 where the final height of the specimen is close to the 43 mm compared to the initial 44 mm.

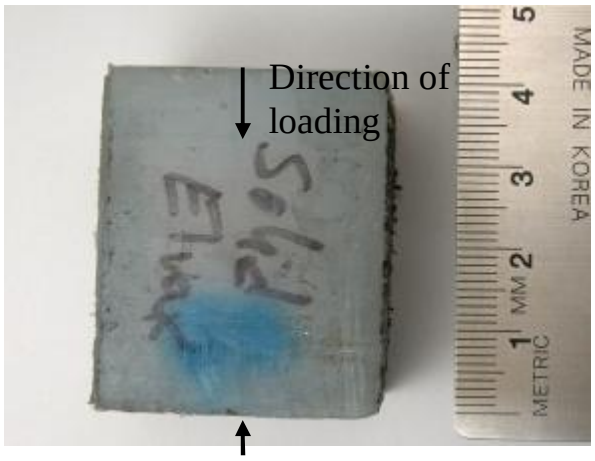

Figure 6.18: Typical Elvax® specimen after dynamic compression testing.

Figure 6.19 displays the dynamic stress-strain response of Elvax®. Dynamic testing of the solid Elvax® specimens halts between approximately $e \approx 0.48$ and 0.53. At the prescribed strain rate

Elvax® shows linear stress-strain behaviour up to the limits of the present testing. Non-linear curve characteristics, such as a plateau and densification are not observed.

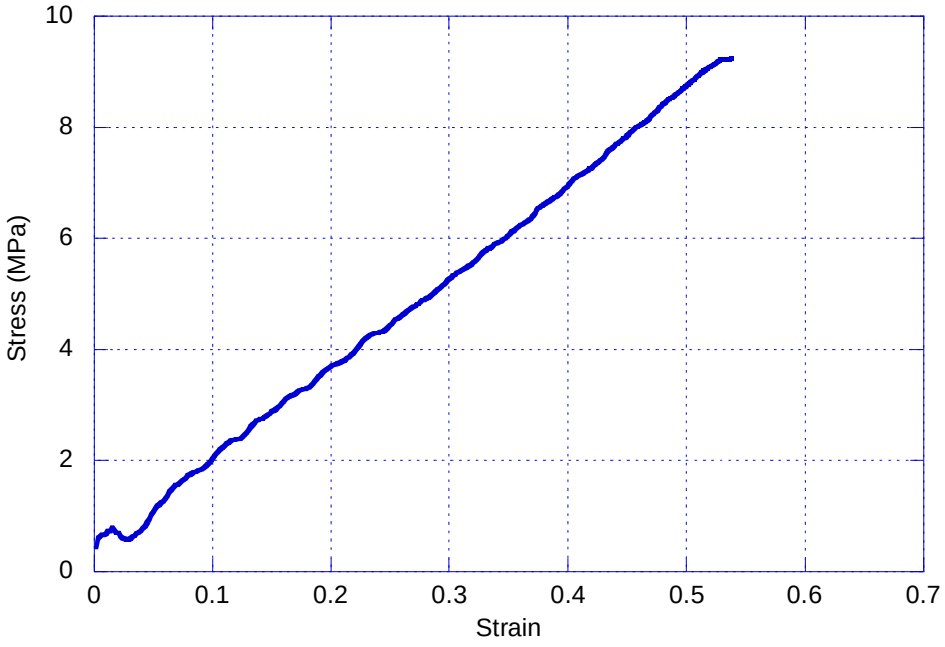

Figure 6.19: Compressive stress-strain curve of solid Elvax® tested at de/dt = 100 s^{-1}.

The energy absorption curve for Elvax® is shown in Figure 6.20. Except the initial fluctuation, the log of the absorbed energy shows a linear increase with log of the stress. Table 6.6 lists the average properties of solid Elvax® at a strain of 0.48 as no data is available beyond this point for all solid Elvax® specimens. The average stress and energy absorbed associated with this strain is approximately 8.14 MPa and 2.1 mJ/mm^3 respectively. The Cushion factor is 3.96.

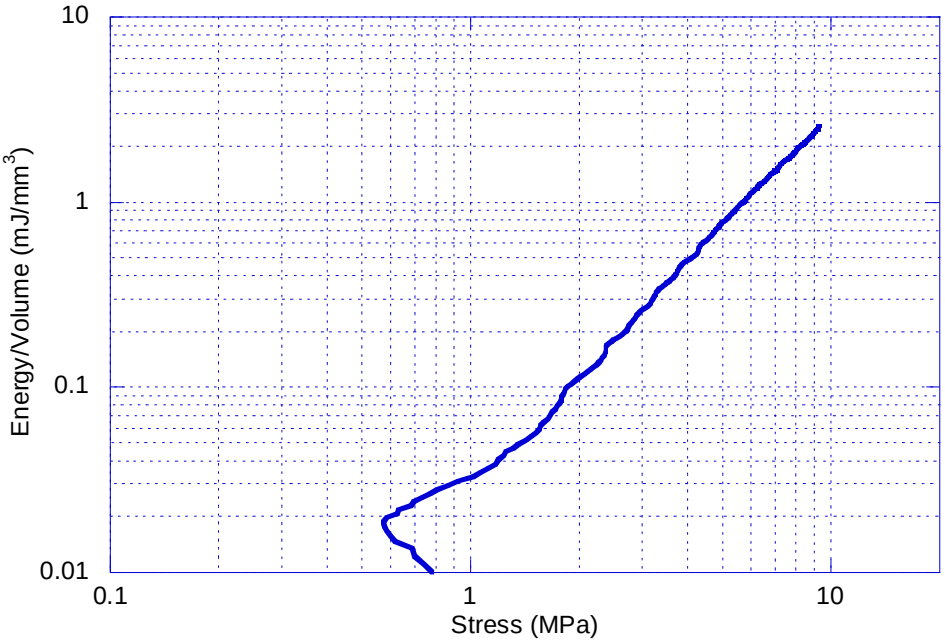

Figure 6.20: Energy absorption diagram of Elvax® tested at de/dt = 100 s^{-1}.

Table 6.6: Properties of solid Elvax® tested at de/dt = 100 s^{-1}.

Specimen Material	Aging Temp. (°C)	Aging Time (hrs)	σ_{ys} (Mpa)	Properties at e_d			
				e	σ_d (MPa)	W (mJ/mm^3)	C
Elvax	N/A	N/A	N/A	0.48	8.14	2.056	3.96

6.3.3 Aluminum Foam-Polymer Hybrid

Dynamic compression testing of hybrid materials is performed on both as-fabricated and age-hardened (4 hrs at 220˚C) aluminum foam infiltrated with polymer.

The post impact specimens have a permanent barrel distortion. The height of the specimens has been reduced by approximately 10 mm, i.e. the final size is 40 mm. Although the aluminum foam has been permanently deformed it is still intact. A typical aluminum foam-polymer hybrid specimen post

dynamic testing with the polymer and after the polymer has been melted out is shown in Figure 6.21 a) and b). A close inspection of the aluminum foam without the polymer shows many of the ligaments have fractured. Arrows in Figure 6.21 c) indicate some of the fractured ligaments.

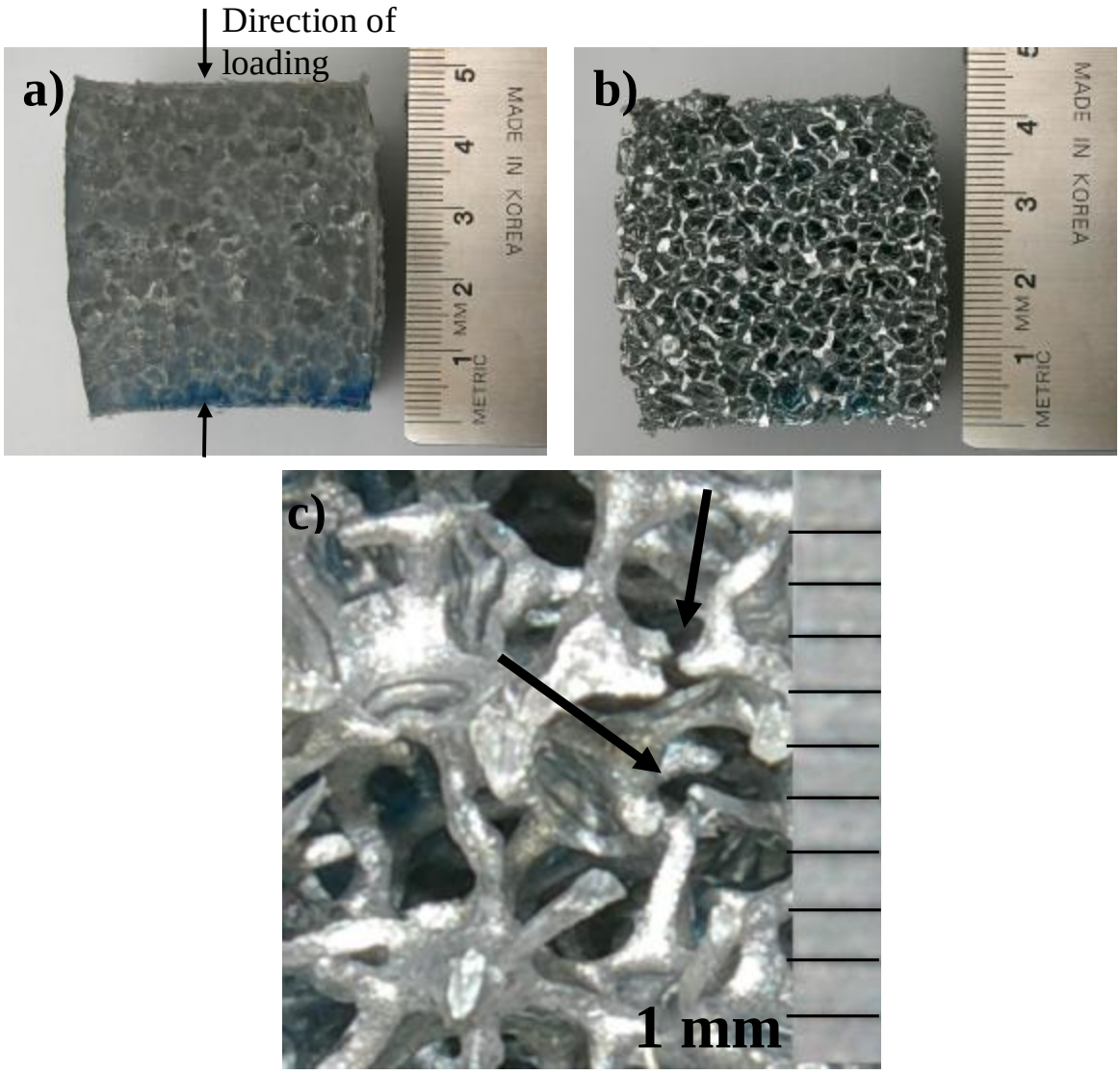

Figure 6.21: Typical aluminum foam-polymer hybrid specimen after dynamic compression testing before (a) and after the polymer has been melted out (b) and (c). Arrows in (c) indicate examples of fractured ligaments.

The results of the dynamic compression test of the hybrid specimens are shown in Figure 6.22. Included with the stress-strain results are the curves of unfilled foam and solid Elvax®. Due to the repeatability of the tests only one stress-strain result for each foam condition is included. It is evident from Figure 6.22 that the stress-strain response of the hybrid under dynamic loading conditions is the same for both aluminum foam conditions. Data collection is halted when the impactor has zero downward velocity, this occurs between strains of approximately e = 0.47 to 0.53. No densification point appears on the curve. Upon initial loading fluctuations with amplitudes as large as 1 MPa are present to 0.1 MPa by e = 0.19. Between these strains a generally linear stress-strain relationship is observed. It is noticed that the difference between the hybrid curve and the solid Elvax® curve is larger at e = 0.19 (~ 3 MPa) than at e = 0.1 (~ 2 MPa). This indicates the slope of the stress-strain hybrid curve is steeper than the slope for the solid Elvax® stress-strain curve. The difference between the hybrid and solid Elvax® curves at e = 0.4 is approximately 2.2 (4 hr 220˚C specimen) to 2.6 MPa (as-fabricated specimen). This indicates that beyond e = 0.19 the slope of the approximately linear stress-strain hybrid curve reduces to below that displayed by the solid Elvax® stress-strain curve.

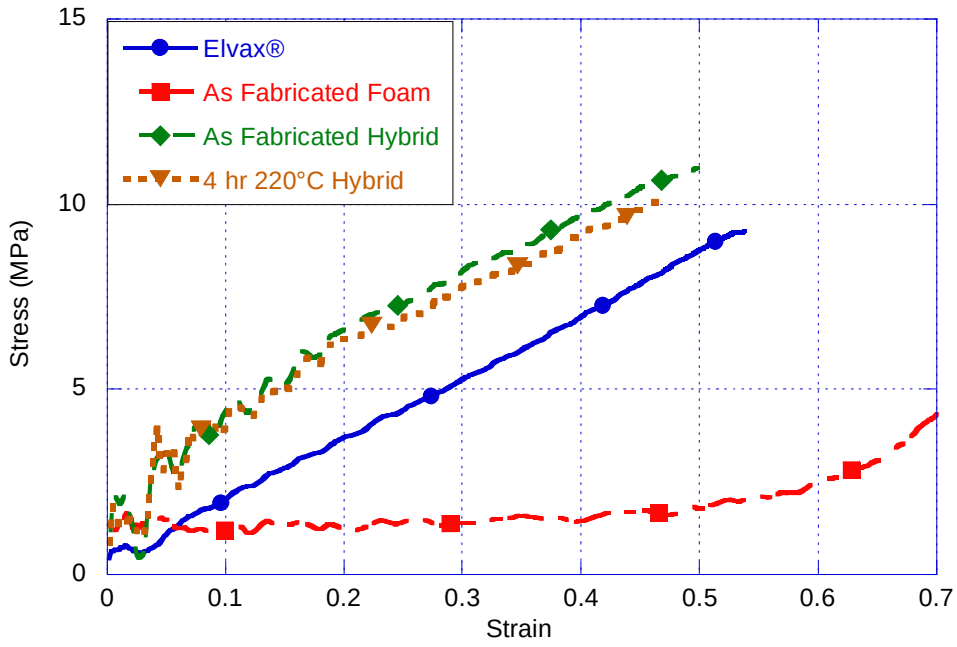

Figure 6.22: Compressive stress-strain curves of aluminum foam-polymer hybrid tested at de/dt = 100 s^{-1}. Included also are the stress-strain curves of the parent material.

The energy absorption diagram for the hybrid material is seen in Figure 6.23. Curves for the parent materials are also included. Ignoring the fluctuations, the hybrid specimens show a near linear increase in the log(W) with log(σ). The slope is steeper than that for solid Elvax® but not vertical like that seen for aluminum foams. The energy absorption of the hybrid specimens increases from approximately 0.1 to 3.0 mJ/mm^3 as the stress increases from 3 MPa to 10 MPa.

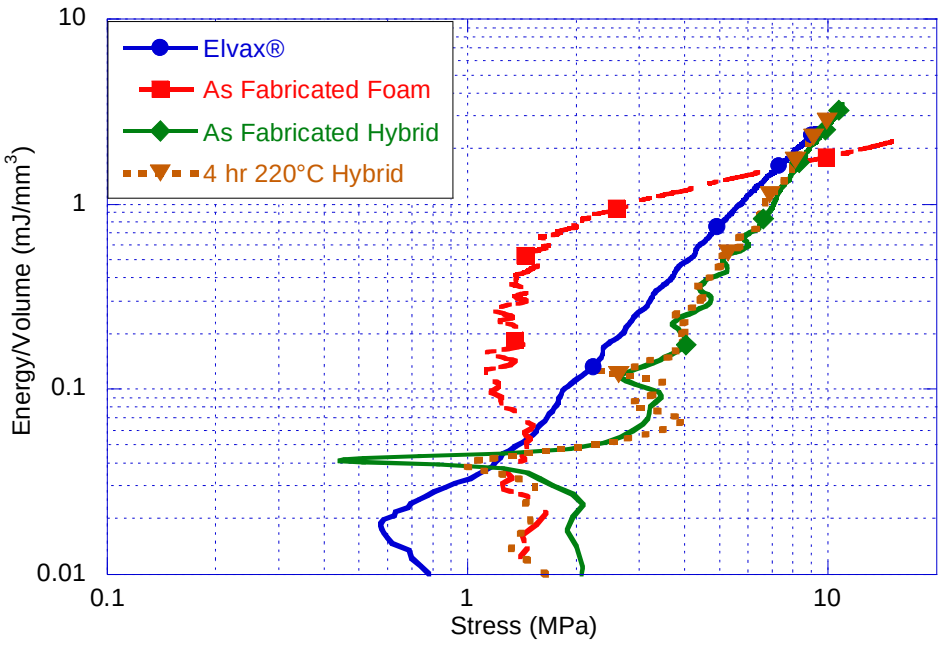

Figure 6.23: Energy absorption curve of aluminum foam-polymer hybrid tested at de/dt = 100 s^{-1}. Included are the results of the parent materials.

Table 6.7 lists the stress values at a strain of 0.47 for the hybrid specimens. A strain of 0.47 was chosen as beyond this strain data is not available for all hybrid specimens. The average stress in as-fabricated aluminum foam hybrid at the selected strain is 10.38 MPa with an average energy absorbed of 3.1 mJ/mm^3. The age-hardened aluminum foam hybrid has an average stress of 10.28 MPa and average energy absorption of 3.1 mJ/mm^3 when compressed to a strain of 0.45. The Cushion factors are approximately 3.3 for the hybrid specimens regardless of foam condition

Table 6.7: Properties of aluminum foam-polymer hybrid in two aluminum foam conditions (i.e. as-fabricated and artificially aged for 4 hrs at 220˚) tested at de/dt = 100 s^{-1}.

Specimen Material	Aging Temp. (℃)	Aging Time (hrs)	σ_{ys} (Mpa)	Properties at e_d			
				e	σ_d (MPa)	W (mJ/mm^3)	C
AF Al Foam Hybrid	N/A	N/A	N/A	0.47	10.38	3.132	3.31
AA Al Foam Hybrid	220	4	N/A	0.47	10.28	3.094	3.32

Note: AA - Artificially Aged
AF - As Fabricated

6.4 Mechanical Damping Results Obtained from Compression-Compression Cyclic Testing

In this section the cyclic stress-strain response, unit damping (D) and the non dimensional loss coefficient (h) of as-fabricated aluminum foam and as-fabricated aluminum foam-polymer hybrid are assessed by way of cyclic testing. The change in cyclic stress-strain response over time is shown in figures containing the stress-strain curves of the 1^{st}, 10^{th}, 100^{th} and 150^{th} cycle. Average values of unit damping and the loss coefficient are listed in tables while selected individual cycle D and h values (cycle numbers listed in Chapter 5.5.3) are plotted vs. number of cycles.

Selected cyclic tests were repeated and a variation of ± 5 % in average unit damping and loss coefficient values are obtained. For the same specimen within the 190 cycle test, values of D at the selected cycles vary by as much as 16 % from the calculated average, while values of h can differ by up to 10 % from the average.

The cyclic stress-strain curves for the D5L and D5H testing conditions applied to aluminum foam (Figure 6.24 and Figure 6.25) and aluminum foam-polymer hybrid (Figure 6.27 and Figure 6.28)

show two general trends. The first trend visible in all four figures is the initial non-symmetric, open hysteresis loop produced in the first loading cycle. Initially upon loading, the specimens display approximately linear stress-strain behaviour. At compressive strains between 0.0073 and 0.0075 the curves representing the first loading cycle in all four specimens (i.e. Figure 6.24, Figure 6.25, Figure 6.27and Figure 6.28) demonstrate a decrease in slope. This decrease in slope is observed to be more pronounced in the aluminum foam specimens than in the hybrid specimens. Upon unloading the curves have shifted to lower stress values. This is apparent from the difference between the start of the loading curves and the end of the unloading curves which is greater in aluminum foam specimens than in the hybrid specimens. From the second cycle on, the hysteresis loops are all closed, i.e. end at the same stress they begin at.

The second trend observed for both aluminum foam and aluminum foam-polymer hybrid materials is the gradual drifting of hysteresis loops. The aluminum foam figures (Figure 6.24 and Figure 6.25) and the hybrid figures (Figure 6.27 and Figure 6.28) show that from the 1^{st} to the 10^{th} to the 100^{th} cycle the hysteresis loops shift towards decreasing stress values. As the cycles increase the hysteresis loop stabilizes and ceases to drift. In all four cases the 100^{th} and the 150^{th} loop are near identical indicating stabilization of the loops occurs at or before the 100^{th} cycle. The drift in stress is seen to be larger at higher strain amplitudes.

6.4.1 Aluminum Foam

Measurement of specimens' dimensions post testing shows that testing under D5L conditions produces no appreciable height difference but a 0.1 mm reduction in height tested under D5H conditions is observed. The cyclic stress-strain curves for D5L and D5H aluminum foam are shown in Figure 6.24 and Figure 6.25, respectively. The shapes of the curves vary significantly between the D5L and D5H conditions. The shapes of the D5L curves (i.e. Figure 6.24) are approximately linear

and do not change with increasing cycles. They show little hysteresis loop area between the loading and unloading curves.

The D5H (i.e. Figure 6.25) curves produce larger hysteresis loops than those tested at D5L conditions. The curves display non-linear stress-strain behaviour at the beginning and end of the loading and unloading curves, respectively. For less than 10 cycles only the initial loading and final unloading stress have a value of 0 MPa. As the number of cycles increase more of the curve displays a stress of 0 MPa. In Figure 6.25 the curves of the 10^{th}, 100^{th} and 150^{th} cycle contains a horizontal line at 0 MPa.

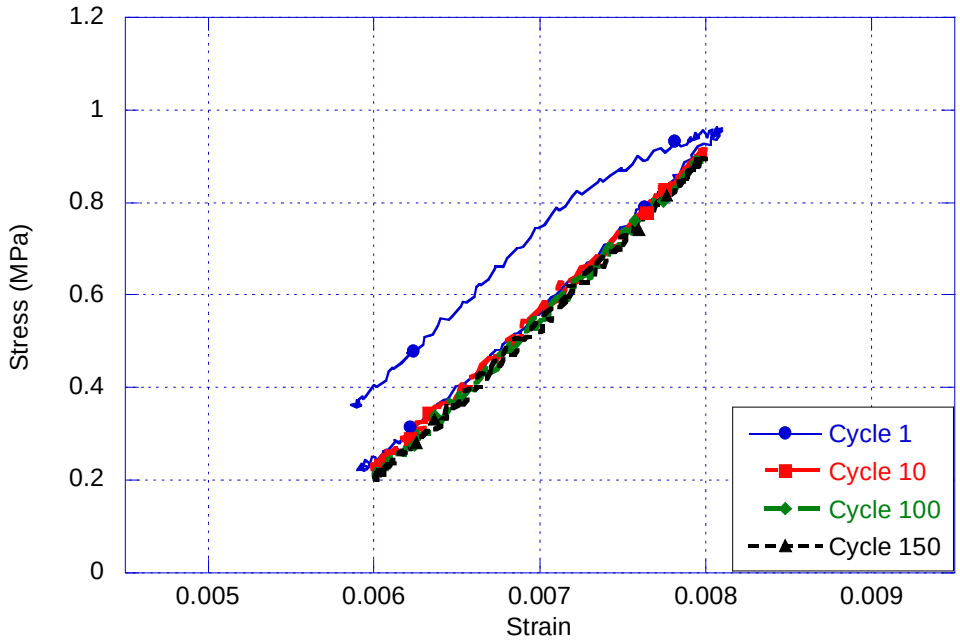

Figure 6.24: Stress-strain curves at selected cycles for aluminum foam specimens tested under D5L condition (ie. 5 Hz, d_M = 0.356 mm and d_A = 0.051 mm).

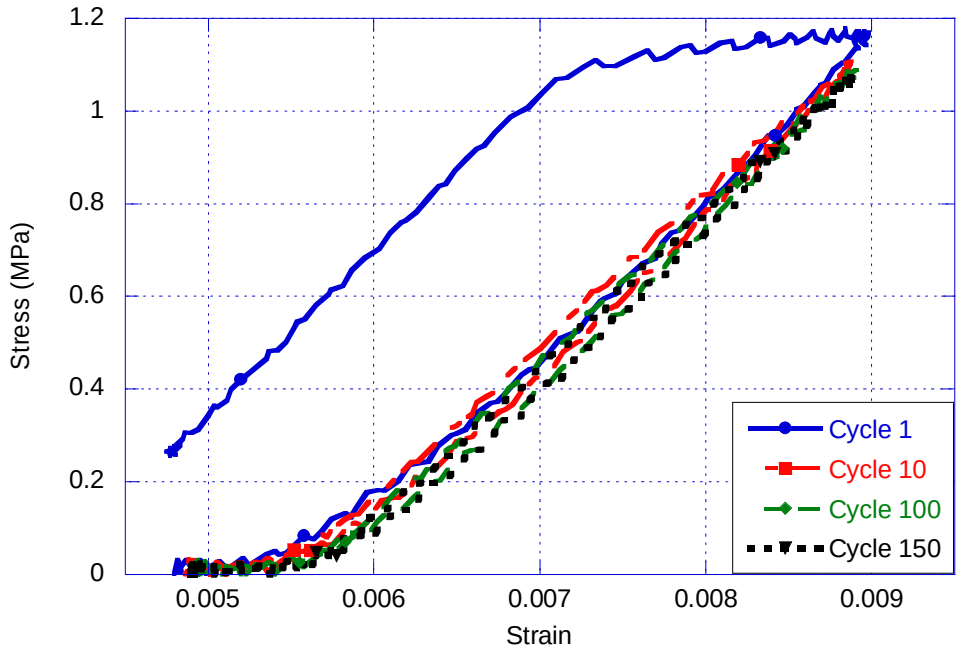

Figure 6.25: Stress-strain curves at selected cycles for aluminum foam specimens tested under D5H condition (ie. 5 Hz, d_M = 0.356 mm and d_A = 0.101 mm).

Table 6.8 lists the average unit damping and loss coefficient values for aluminum foam at the two testing conditions. The aluminum foam tested at the lower amplitude has an average unit damping of D = 2.48 x 10^{-5} mJ/mm^3 and an average loss coefficient of h = 0.0036 over the 190 cycles. At the higher amplitude the foam has an average unit damping of D = 1.53 x 10^{-4} mJ/mm^3 and an average loss coefficient of h = 0.0129. Figure 6.26 shows the evolution of D and h over 190 cycles at both amplitudes. The value of h for the first cycle is not included due to the open hysteresis loop producing uncharacteristically high values. The 2nd cycle values for D and h at both testing conditions are high compared to their respective average values. The unit damping and loss coefficient values stabilize by the 10th cycle for the D5L foam. As such, the average values of both D and h well represents any cycle over the 190 cycles. From Figure 6.26 values for the 190th cycle are

found to be D = 2.33 x 10^{-5} mJ/mm^3 and h = 0.0036. It takes up to the 100th cycle for the D5H foam to stabilize. This results in differences between the values of D and h at any cycle and the average values. For D5H the values of D and h at the 190th cycle are D = 1.32 x 10^{-4} mJ/mm^3 and h = 0.0115. Figure 6.26 also shows that any shift in unit damping values produces an equivalent shift in loss coefficient values at both D5L and D5H testing conditions.

Table 6.8: Aluminum foam average unit damping (D) and loss coefficient (h) over 190 cycles.

Test Condition	D (mJ/mm^3)	η
D5L	2.48E-05	0.0036
D5H	1.53E-04	0.0129

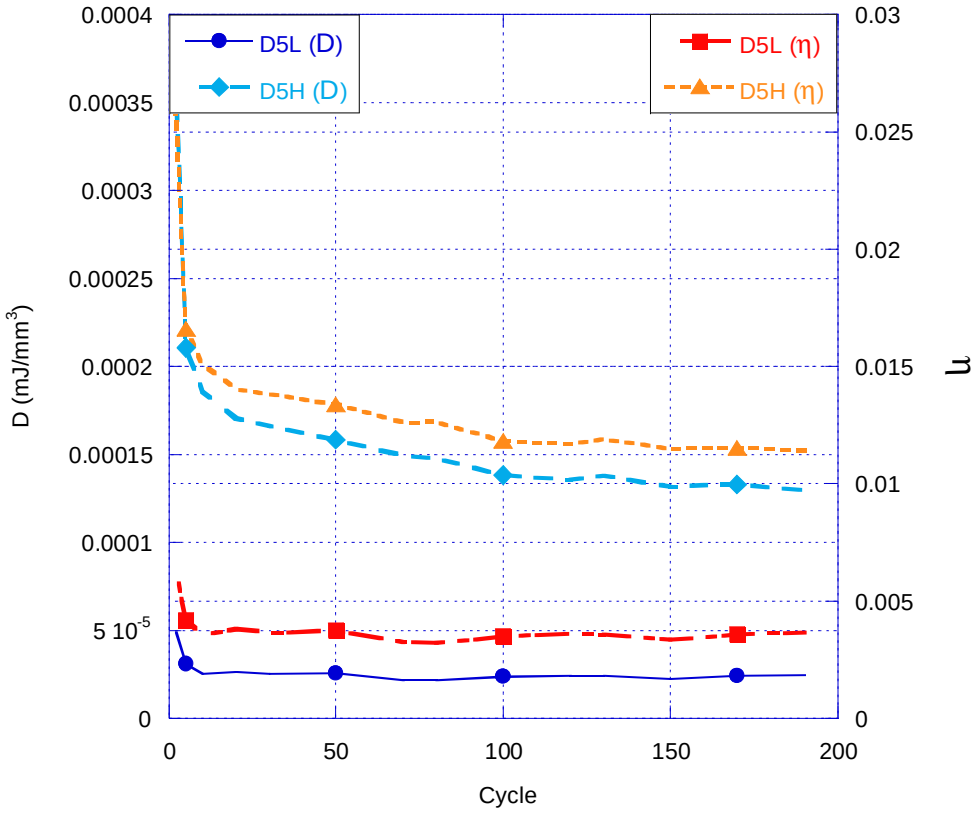

Figure 6.26: Evolution of aluminum foam unit damping (D) and loss coefficient (h) for 190 cycles at D5L and D5H testing conditions.

6.4.2 Aluminum Foam-Polymer Hybrid

Measurements of the hybrid specimens after cyclic testing show no reduction in height for either D5L or D5H test conditions. The results of cyclic testing carried out at D5L and D5H are shown in Figure 6.27 and Figure 6.28, respectively. The D5L hybrid specimen shows little area in the hysteresis loop, as is the case of aluminum foam. In contrast, the hysteresis loop of the D5H hybrid specimen shows significant hysteresis loop area between loading and unloading curves. Also visible in the curves of the hybrid specimen tested under D5H conditions is the lack of any horizontal sections and a minimum compressive stress value of 0.17 MPa.

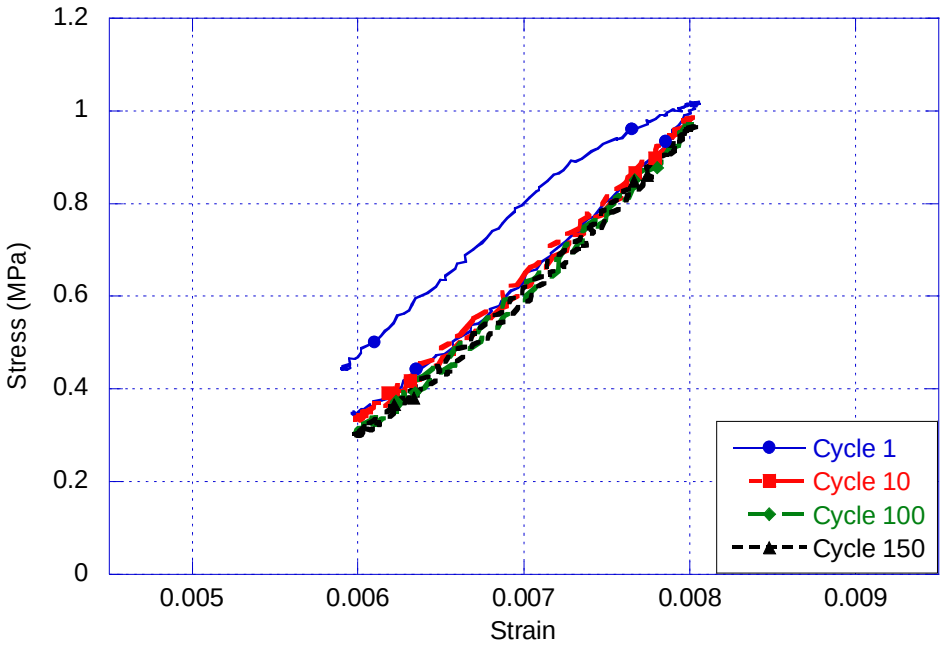

Figure 6.27: Stress-strain curves at selected cycles for aluminum foam-polymer hybrid specimens tested under D5L condition (ie. 5 Hz, d_M = 0.356 mm and d_A = 0.051 mm).

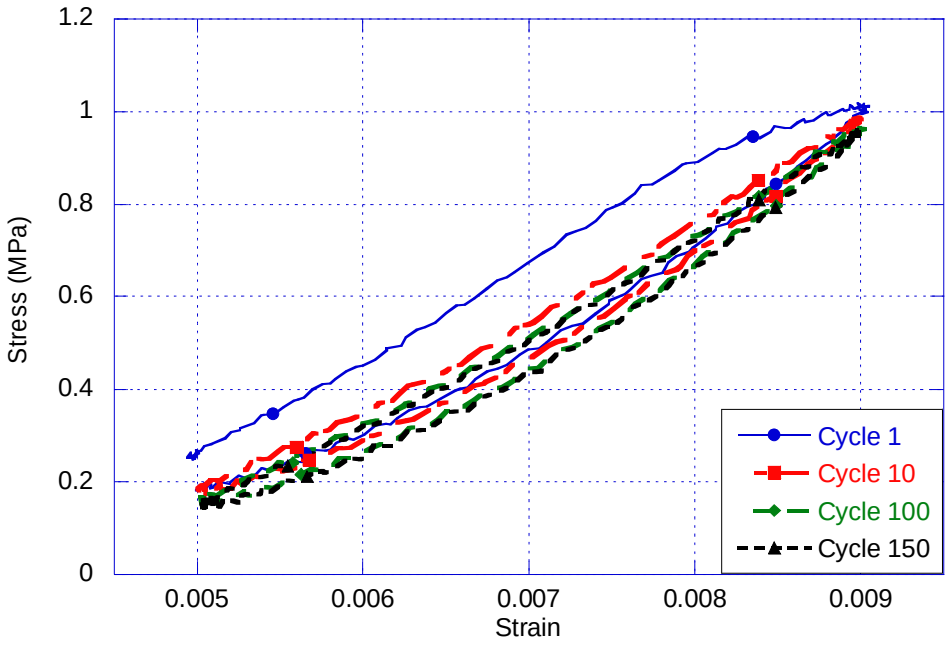

Figure 6.28: Stress-strain curves at selected cycles for aluminum foam-polymer hybrid specimens tested under D5H condition (ie. 5 Hz, d_M = 0.356 mm and d_A = 0.101 mm).

Table 6.9 lists the average values of D and h for the D5L and D5H hybrid specimens. The D5L hybrid specimen has an average unit damping of D = 4.28 x 10^{-5} mJ/mm^3 and an average loss coefficient of h = 0.0053, while the D5H specimen has an average unit damping of D = 2.15 x 10^{-4} mJ/mm^3 and an average loss coefficient of h = 0.0168. The evolution of unit damping and the loss coefficient over the 190 cycles is shown in Figure 6.29. At both D5L and D5H testing conditions the hybrid material shows the stabilization of D and h by the 10th cycle. The flat curves imply that the average values of D and h closely resemble the values obtained at any cycle. This is confirmed by the following values obtained from the 190th cycle for both D and h at both testing conditions from Figure 6.28. For D5L testing conditions D = 4.11 x 10^{-5} mJ/mm^3 and h = 0.0052, and at D5H testing conditions D = 2.10 x 10^{-4} mJ/mm^3 and h = 0.0157. At D5L the curve for D and the curve for h

are remain parallel to each other over the 190 cycles. This is in contrast to the curves for D and h at D5H test conditions which are divergent. This apparent divergence is within experimental error and is not considered significant.

Table 6.9: Aluminum foam-polymer hybrid average unit damping (D) and loss coefficient (h) over 190 cycles.

Test Condition	D (mJ/mm^3)	η
D5L	4.28E-05	0.0053
D5H	2.15E-04	0.0168

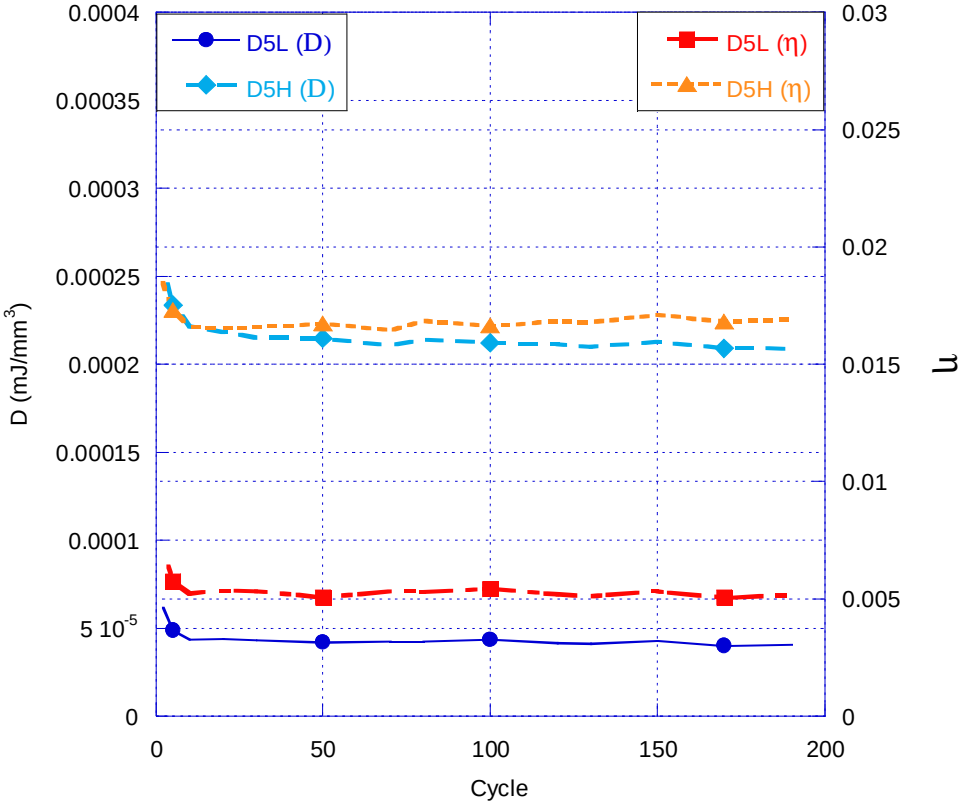

Figure 6.29: Evolution of aluminum foam-polymer hybrid unit damping (D) and loss coefficient (h) for 190 cycles at D5L and D5H testing conditions.

Chapter 7
Discussion

7.1 Stress-Strain Behaviour under Static Compressive Loading

Aluminum Foam

The minimal lateral expansion observed in the aluminum foam specimens during compression can be explained by the porous nature and the cell geometry of aluminum foam. The open cell network of the foam allows air to escape with no resistance and therefore no lateral loads are imposed on the foam. Due to the cell geometry, the ligaments deform by bending and buckling [Gibson and Ashby 1997, Zhou *et al.* 2004b]. The deformed ligaments fill the voids within the foam and cause changes to the geometry of the cell resulting in a redistribution of load to other ligaments in the cell [Zhou *et al.* 2004a]. This change in geometry is likely the cause of the minimal lateral expansion observed.

The observation of the collapse of the foam in discreet crush bands is in agreement with Zhou *et al.* [2004a] who have applied Digital Imaging Correlation (DIC) methods to map surface strain during static compression tests on as-fabricated and T6 Duocel® aluminum foam. Their findings show that early in the plateau region ($e < 0.15$) a single crush band is observed. They relate this first crush band to the initial stress peak (seen in Figure 6.7) and find the causes to be the strain hardening behaviour of the aluminum ligaments and the ligament orientation [Zhou *et al.* 2004a]. The flow stress increase before the peak is caused by the strain hardening of the ligaments. The weakest ligaments deform causing a change in cell structure. This produces instantaneous structure softening and deformation at the center of the crush band. Above a strain of 0.15 multiple crush bands form leading to a gradual rise in flow stress [Zhou *et al.* 2004a]. DIC also shows the majority of deformation in the specimens

is found in the crush bands and adjacent regions [Zhou *et al.* 2004a]. These crush bands expand until at densification, the whole specimen is homogeneously strained. This is seen in Figure 6.2.

All the aluminum foam specimens tested in this study display generally smooth stress-strain curves. These curves show the typical shape, including the linear-elastic, plateau and densification regions of elastic-plastic foams [Gibson and Ashby 1997]. The general shape of the stress-strain curves are consistent with those reported by other researchers for Duocel® aluminum foams [Andrews *et al.* 1999, Zhou *et al.* 2004a and Krishna *et al.* 2005]. This includes the upper yield points and slight peaks and valley observed in the as-fabricated and the higher strength artificially aged foams. However the yield strength values obtained in this study are lower than those reported in literature [Andrews *et al.* 1999, Andrews *et al.* 2001, Zhou *et al.* 2004a, Krishna *et al.* 2007]. For the artificially aged specimens the lower yield strengths are likely the result of differences in the thermal processes, including the quenching process after solution heat treatment. The artificially aged foams tested by Zhou *et al.* [2004a] are water quenched after solutionizing while in this study the slower air cooling has been utilized. Esmaeili *et al.* [2000] have conducted resistivity measurements on AA6XXX series aluminum alloys at various ageing times with differing quench mediums. It was found that samples quenched in a slower quenching medium (i.e. air) had a lower resisitivity. This lower resisitivity was due to the loss of solute to grain boundary precipitation during the quench resulting in lower yield strengths. For the as-fabricated specimens this difference can be attributed to the aluminum foam fabrication procedure. As this process is unknown the exact cause of the lower yield strength values can not be determined.

Artificial aging of the aluminum foam produces differences in the stress-strain curves. The increase in yield strength and plateau height with increasing aging times observed in this study is in agreement with the trends observed by other researchers for AA6XXX based foams [Lehmus and Banhart 2003, Chan and Chan 2004]. This result is expected since the AA6XXX alloys are known to be heat

treatable and, the yield and plateau strength are dependant on ligament material properties [Gibson and Ashby 1997]. Cluff and Esmaeili [2006] performed isothermal calorimetry on AA6101 Duocel® foam and found that the peak-aged condition is achieved in 4 hrs at 220˚C or 7 hrs at 180˚C. This is consistent with the results obtained through compression testing where similar peak yield strength values are obtained for the samples aged for 5 hours and 7 hours at 180°C and the peak yield strength occurs after 4 hours of aging at 220°C.

It is known that a semi-brittle foam produces and upper yield point on the stress-strain curve [Gibson and Asby 1997]. Lehmus and Banhart [2003] attribute the presence of upper yield points on the stress-strain curves of warm aged AA6XXX and AA7XXX closed cell aluminum foams to reduced ductility. The observation of upper yield points on the stress-strain curves for 7 h at 180°C, 2 h and 4 h at 220°C, can also be explained by a gradual loss of ductility as the microstructural state of the alloy approaches overaging [Cluff and Esmaeili 2006]. Although the present stress- strain curves are generally smooth beyond the yield point, the appearance of the upper yield point may denote some reduction in ductility. The reduction in ductility and a transition from ductile to brittle fracture mode has also been reported in a open cell AA6061 foam after age hardening treatment of 18 hours at 160°C [Chan and Chan 2004].

The stress-strain curves produced by the specimens peak-aged at 220˚C and 180˚C both have an upper yield point and similar plateau slopes. However the yield strength of the specimens aged at 180˚C are higher than those aged at 220˚C. This difference is small and falls within the range of scatter for the artificially aged aluminum foam specimens. However, it is also expected that the number density of precipitates that form at the higher aging temperature is smaller [Esmaeili ***et al.*** 2007], leading to a coarser microstructure and therefore a lower yield strength [Esmaeili ***et al.*** 2003]

It can be seen from Figure 6.7 that the stress-strain curves produced by the as-fabricated aluminum foam specimens are similar to those of the peak-aged specimens. From Table 6.1 and Table 6.2 the as-fabricated specimens have higher average yield strength values than the peak-aged foams. Without knowing the aluminum foam fabrication process (i.e. the as-fabricated thermal history) or performing Transmission Electron Microscopy the microstructural differences between these conditions, that cause the differences in yield strength is unknown. However, it is also noted that the difference in yield strength values is with the range of observed scatter.

The scatter in the yield strength values of the age hardened foams (i.e. ± 12 %) is much higher than for the as-fabricated specimens (i.e. ± 3 %). There are two main causes of this. The first is due to the scatter in specimen relative densities. The largest difference in observed in the age hardened specimens was 0.4 % (i.e. ranging from 7.2 to 7.6 %) compared 0.05% (i.e. ranging from 7.33 to 7.38 %) for as-fabricated specimens. Equation (2.14) is found to predict the strength of Duocel® aluminum foam well when a bulk aluminum yield strength of 194 MPa is used [Andrews *et al.* 1999]. An estimate on the contribution of scatter in relative density on yield strength can therefore be found using equation (2.14) and the measured minimum and maximum relative densities. From this the scatter in relative density accounts for approximately only ± 5 % variation in yield strengths. The remaining variation is likely the result of variations in the heat treating procedures and variations due to the testing devices.

The total energy absorbed and the energy absorption efficiency are closely related to the shape of the stress-strain curve. The flatter stress-strain curves produced by artificially aging aluminum foam to peak-aged conditions produces specimens which typically absorb more energy and demonstrate lower Cushion factors (i.e. more efficient energy absorbers) than under-aged aluminum foams. The similar stress-strain curves between the as-fabricated and peak-aged aluminum foams produce similar energy absorption values and Cushion factors.

Having compared the mechanical properties of the peak-aged aluminum foam to the under-aged aluminum foams produced in this study (i.e. by air quenching) it can be concluded that the peak aged specimens provide higher yield strengths, higher plateaus, larger energy absorption and better energy absorption efficiencies (i.e. lower Cushion factors). However, comparing these same peak-aged foams to the as-fabricated foams no enhancement of the mechanical properties is observed. By utilizing as-fabricated foam, the time and cost of artificial aging is avoided. It is therefore better to use an as-fabricated aluminum foam over a peak-aged aluminum foam produced using the thermal processing procedure that is utilized in this study.

Aluminum Foam-Polymer Hybrid

The observations made during the compression testing of the aluminum foam filled with Elvax® (i.e. lateral expansion of the aluminum foam-polymer hybrid and the broken foam ligaments) are similar to those observed by Cheng and Han [2003] during the compression of aluminum foam filled with silicone. Cheng and Han [2003] attribute the lateral expansion of their polymer filled foam to the incompressibility (i.e. maintenance of constant volume during deformation) of the silicone. The lateral expansion observed during the compression testing of pure Elvax® specimens indicates that the polymer used in this study also attempts to maintain its original volume under uniaxial compression. Unlike the foam, which has empty cells accommodating the deforming aluminum, the hybrid is a solid specimen comprised mostly of Elvax® (~ 93 %). The lateral expansion of the aluminum foam-polymer hybrid material can therefore be attributed to the behaviour of the polymer used in filling the foam. The lateral expansion of the polymer is also the cause of the fractured ligaments. The ligaments prevent the polymer from expanding, however when the compressive stress is large enough (producing large forces normal to the loading direction on the ligaments by the expanding polymer) the ligaments fail allowing the polymer to flow out [Cheng and Han 2003]. The implications to the stress-strain curve are discussed in more detail later on. Not noted by Cheng and

Han [2003], but observed in this investigation is the recovery of strain (approximately 0.2) upon unloading of the specimen. This behaviour can again be attributed to Elvax® as it is considered an elastomer at test temperatures displaying recoverable deformation up to large strains, whereas aluminum foam deforms plastically resulting in no strain recovery. The rate of strain recovery in the hybrid and Elvax® are not measured, however it is assumed they will both be similar.

Shown in Figure 6.13 are the stress-strain curves of aluminum foam-polymer hybrid with the aluminum foam in both as-fabricated and 4 hr at 220˚C age hardened condition. Little difference is seen in the stress-strain curves of both hybrid specimens. The largest difference is less than 11 % at a strain of approximately 0.4. With variations in densification stresses in age hardened foams of up to ± 5 % at and in Elvax® specimens of ± 5 %, a 10 % difference between the two hybrids is not significant. It can be concluded that no benefit to the mechanical properties of the aluminum foam-polymer hybrid are obtained by subjecting the aluminum foam to the extra thermal processing performed in this study compared to using as-fabricated aluminum foams. Also repeats on the as-fabricated aluminum foam-polymer hybrid specimen show a difference of 7 % in stress values at strains of approximately 0.2. Based on the convention used for yield strength of aluminum foams the as-fabricated foam hybrid and the age-hardened foam hybrid have yield strengths significantly higher than the values observed for the base foams. The increase in strength is due to the added strength provided by Elvax® and the added strength produced by the interaction between the foam ligaments and Elvax®. The hybrids densify at a strain of 0.57. This is within the range of densification strains of both aluminum foams and Elvax®.

There are both differences and similarities between the stress-strain curves of the hybrid material and the parent materials shown in Figure 6.13. Below a strain of approximately 0.03 the stress-strain curves of the hybrid and the aluminum foam are similar. Above a strain of approximately 0.58 the stress-strain curves of the hybrid and the polymer become similar. In between these two strains the

stress-strain curve of the hybrid is an addition of the sum of the stress-strain curves of the parent materials and an interaction between the parent materials. The hybrid stress-strain curve can be split into four regions. The first three regions are divided based on the changes in slope, indicating a change in deformation mechanisms. The last region is the densification regime in which point of division is based on the point of minimum Cushion factor. These regions can be seen for an as-fabricated aluminum foam-polymer hybrid in Figure 7.1. Included in this figure is the linear summation of the stress-strain curves for as-fabricated aluminum foam and Elvax® (i.e. $\sigma_{sum}(e) = \sigma_{aluminum\ foam}(e) + \sigma_{Elvax®}(e)$). The deformation mechanisms thought to be responsible for the shape of the stress-strain curve are explained region by region below.

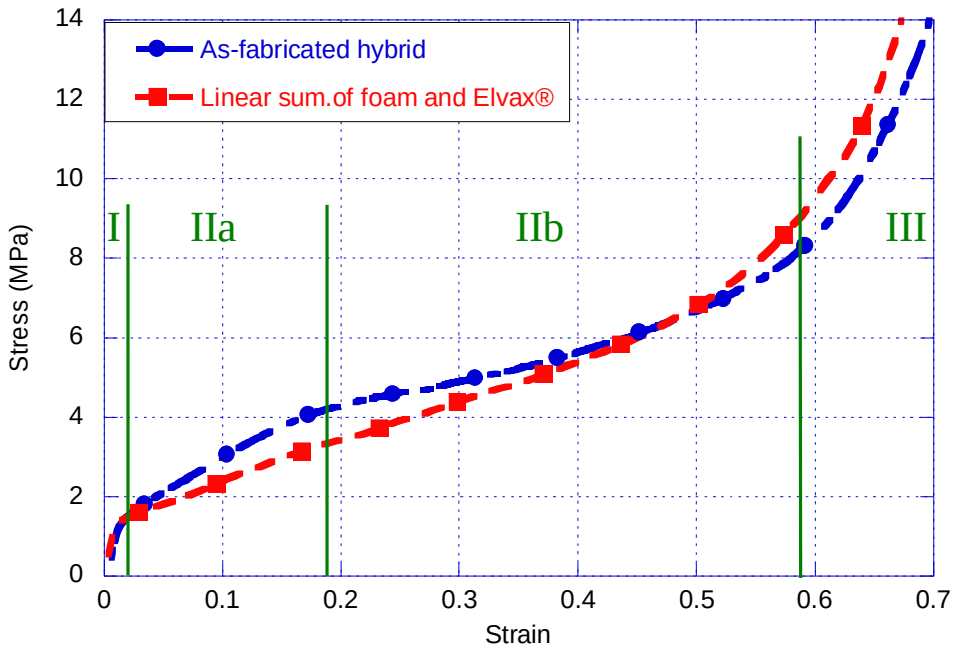

Figure 7.1: Compressive stress-strain curve of as-fabricated aluminum foam-polymer hybrid and a linear summation of the parent material curves under static loading.

A larger view of Region I for an as-fabricated foam-polymer hybrid is shown in Figure 7.2. The stiffness of the hybrid material is almost exactly the same as that shown by the linear summation of both parent materials and is also very similar to the stiffness of the aluminum foam. This is expected since Elvax® displays low stiffness and low stress values compared to the foam at this stage and is not expected to carry much load. Cheng and Han [2003] and Kwon *et al.* [2003] similarly note the little effect the polymer filling has on the stiffness of a filled aluminum foam. Both materials are elastic in this region and so it is expected that the hybrid will also display elastic deformation.

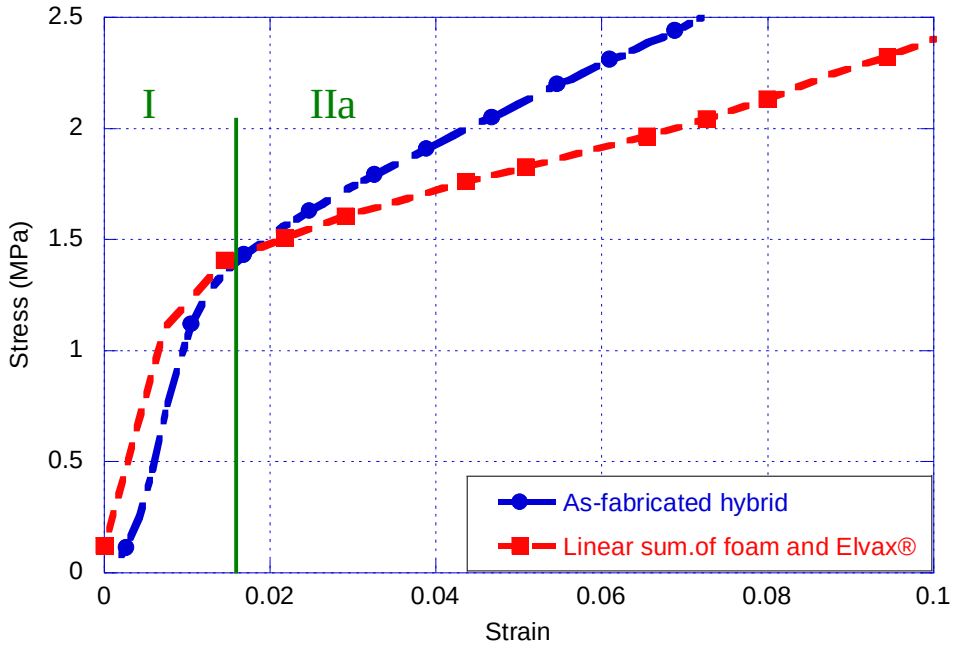

Figure 7.2: Compressive stress-strain curve for Region I of as-fabricated aluminum foam-polymer hybrid and a linear summation of the parent material curves under static loading.

In the beginning of Region IIa, shown in Figure 7.2, the similarity between the stress-strain response of the hybrid and of the linear addition of the foam and polymer quickly disappears. The hybrid displays a much steeper slope than that predicted by the linear addition of the foam and the

polymer. This trend is seen to continue up to a strain of approximately 0.2 in Figure 7.1. Both Cheng and Han [2003], and Kwon *et al.* [2003] attribute the increase in strength to the support provided by the polymer against ligament bending and buckling. It has however been found that a 7 % relative density Duocel® foam under hydrostatic loading shows little increase in yield strength or stiffness, and plastic bending of struts similar to uniaxial compression is observed at a hydrostatic stress of 2.2 MPa [Gioux *et al.* 2000]. Therefore some of the increase in strength must also be due to the effect the ligaments have on the polymer. The prevention of polymer expansion by the ligaments produces a tri-axial compressive pressure on the polymer. Tri-axial compressive pressure is known to increase the apparent stiffness of polymers [Nielsen 1974b]. It is therefore likely that plastic deformation in the foam structure occurs in Region IIa and that the increase in strength is due to resistance to polymer expansion imposed by the aluminum foam ligaments.

Opposite to what occurs in Region IIa, Region IIb shows a decrease in slope below that observed by the linear summation of as-fabricated foam and polymer. This indicates a change in the strengthening mechanisms produced by the foam-polymer interaction. The incompressible nature of the polymer has not changed and it is therefore still exerting pressure on the ligaments. Although deformation mechanisms are not fully understood it is theorized that failure of aluminum foam ligaments would produce a decrease in slope consistent with observed behaviour. First a disconnected cell structure decreases the resistance to polymer expansion, decreasing the apparent stiffness of the polymer in the hybrid. Second as the foam becomes disconnected, fewer ligaments contribute to the load carrying capacity of the foam in the hybrid. It is likely these two factors combine to produce the decrease in slope. At the end of Region IIb, a strain of approximately 0.58, the stress-strain response approaches that of Elvax®. This indicates most of the load is carried by the polymer and not the foam. Also reduction in interconnectivity of the aluminum foam network decreases the resistance to

the recovery of strain in the polymer upon removal of load. This explains the difference between the measured strain upon testing and the observed final strain after unloading.

The response of the hybrid in Region III reinforces the assumptions made about the deformation in Region IIb. In region III we see the hybrid and Elvax® approaching almost the same densification response, indicating further reductions in the load carried by the foam. This indicates ligaments continue to fracture in the densification region. However to confirm the assertions about hybrid deformation mechanisms further investigation is required. This includes strain mapping during deformation and removing the polymer from specimens tested up to strains of 0.1. 0.2 and 0.3 to observe the type of deformation in the foam ligaments.

On first inspection the stress-strain curve presented for the silicone rubber filled aluminum foam produced by Cheng and Han [2003] appears different to the stress-strain curve of the hybrid material produced in this study. Firstly, Cheng and Han [2003] list five regions instead of four. This however is a matter of definition. Cheng and Han [2003] define a transition region between the regions defined in this paper as Regions IIa and IIb. A more important difference is the observation the silicone rubber filled aluminum foam densifies at a higher strain and a lower stress than the aluminum foam it is based on. This contrasts with the similar densification strains and much higher densification stresses observed in the Elvax® filled aluminum foam compared with the aluminum foam parent material in this study. The difference in the observed stress-strain behaviour is due to the difference in parent material choices. Cheng and Han [2003] used a 0.4 % relative density aluminum foam and a polymer that is more compliant than Elvax®. The stress in the silicone rubber is significantly less than the stress in the aluminum foam at all strains. As the aluminum foam fractures at higher strains the stress-strain behaviour of the silicone filled foam approaches that of pure silicone. This indicates that to achieve an aluminum foam polymer-hybrid material that densifies beyond the parent foam and at a lower stress requires a polymer which densifies beyond the parent foam and at a lower stress.

There are still other hybrid systems which utilize aluminum foam such as aluminum foam core sandwich panels and aluminum foam filled extrusions. Typically aluminum foam core sandwich panels are tested in bending [Harte *et al.* 2000, Chen *et al.* 2001, Yu *et al.* 2003, Tagarielli *et al.* 2004]. However it is noted that compressing aluminum foam specimens sandwiched between aluminum face sheets in axial compression do not change the stress-strain behaviour of the base aluminum foam [Zhou *et al.* 2005]. Therefore the differences between the stress-strain curve of Elvax® filled aluminum foam and an aluminum foam core sandwich panel loaded under uniaxial compression are likely similar to the differences previously presented between Elvax® filled aluminum foam and aluminum foam.

The results of uniaxial compression on foam filled extrusions are reported as force-displacement curves by Fuganti *et al.* [2000] and Hanssen *et al.* [2000]. Converting the force-displacement curves to engineering stress-strain curves does not change the shape of curves. It is therefore possible to compare directly the shapes of the force-displacement curves to the stress-strain curves reported in this investigation for the aluminum foam-polymer hybrid material. Two differences between the curves are observed. The foam filled extrusion force-displacement curves contain many force peaks and valleys compared to the relatively smooth stress-strain curve produced by the Elvax® filled aluminum foam. This difference is due to the different mechanisms of deformation present in the two different hybrid systems. The second and more important difference is that the force-displacement curve of the foam filled extrusion produces a plateau with a near horizontal slope that extends beyond the densification strain of the aluminum foam-polymer hybrid material. The foam filled extrusion produced by [Fuganti *et al.* 2000] displays a peak force of 52000 N (~ 8 MPa based on supplied geometry) and a densification strain of 0.69 (recall from chapter 2 that the stroke efficiency (S_E) defined by Fuganti *et al.* [2000] and Hanssen *et al.* [2000] is equivalent to the definition of densification strain utilized in this work). This is in contrast to the stress-strain behaviour of the foam-

polymer hybrid which shows a quadruple of the stress value from the end of the linear elastic region (i.e. from 2 MPa at e = 0.03) up to the densification strain (i.e. 8 MPa at e_d = 0.58). Although the densification stresses in the two hybrid materials are approximately the same the densification strain in the foam filled extrusion occurs later by more than 0.1 strain. The implications of this are that the foam filled extrusion is a more efficient energy absorbing material. A comparison of the energy absorption properties of both hybrids is performed later on.

The distinct shape of the aluminum foam-polymer hybrid stress-strain curves from the stress-strain curves of the parent materials result in differences in energy absorption behaviour. This is clearly demonstrated in Figure 6.14. The hybrid material absorbs more energy at densification but is less efficient (i.e higher Cushion factor) than the aluminum foam it is based on. The higher strength observed in Regions IIa and IIb of the hybrid stress-strain curve are responsible for the larger amount of energy absorbed. The steeper average slope of these regions compared to the near horizontal stress plateau observed in the aluminum foam stress-strain curves result in the lower efficiencies. The hybrid material shows improvement in both the total energy absorbed and the energy absorption efficiency at densification compared to pure Elvax®. This is the result of the similarity between the average slope of Regions IIa and IIb in the hybrid stress-strain curve and the slope of pure Elvax® over these same strains with stress-strain curve of the hybrid demonstrating a higher strength. Based on energy absorption efficiency it is clear that the aluminum foam is a better energy absorbing material than the aluminum foam-polymer hybrid material. However an aluminum foam-polymer hybrid material in which the densification stress is lower and the densification strain is higher than the parent foam, similar to the one produced by Cheng and Han [2003], would have a higher energy absorption efficiency than the base aluminum foam. However, when dealing with two materials demonstrating significant differences in densification stress, such as as-fabricated aluminum foam (~ 2 MPa) and as fabricated aluminum foam-polymer hybrid (~ 8 MPa), choosing a material for an

energy absorption application is more complicated than picking the material with the highest energy absorption efficiency. The total amount of energy, maximum allowable force, contact area and volumetric constraints are all important factors in choosing the best material. The effect these factors have on material choice is highlighted using the following two impact scenarios.

The first impact scenario (IS1) is the impact of a head on the A pillar of a car. This scenario defined by Kretz *et al.* [2002] requires the absorption of 100 J of energy and a peak deceleration not to exceed 200 g (or 1960 m/s^2). The mass of an average head equals 4.5 Kg [McIntosh *et al.* 1995]. Utilizing Newton's second law of motion (i.e. Force = mass × accelearation) the maximum load that can be transmitted to the head is approximately 8800 N. For the purpose of this comparison we will assume the impact volume has a circular contact area with a diameter of 75 mm and a maximum allowable length of 30 mm. Based on the peak load and the geometry and following equation (5.1), the maximum allowable stress in the material is 2 MPa. A sketch of the impact volume for IS1 is shown in Figure 7.3 a).

The second impact scenario (IS2) is that for an automotive crash box. Fuganti *et al.* [2000] define an energy absorption of 5000 J is required with a peak load not exceeding 50 kN. In this comparison the impact volume has an area of 79 mm x 79 mm (for the crash box to fit inside the bumper) and a maximum allowable length of 350 mm. The peak allowable stress in the material is therefore a minimum of 8 MPa. A sketch of the impact volume for IS2 is shown in Figure 7.3 b).

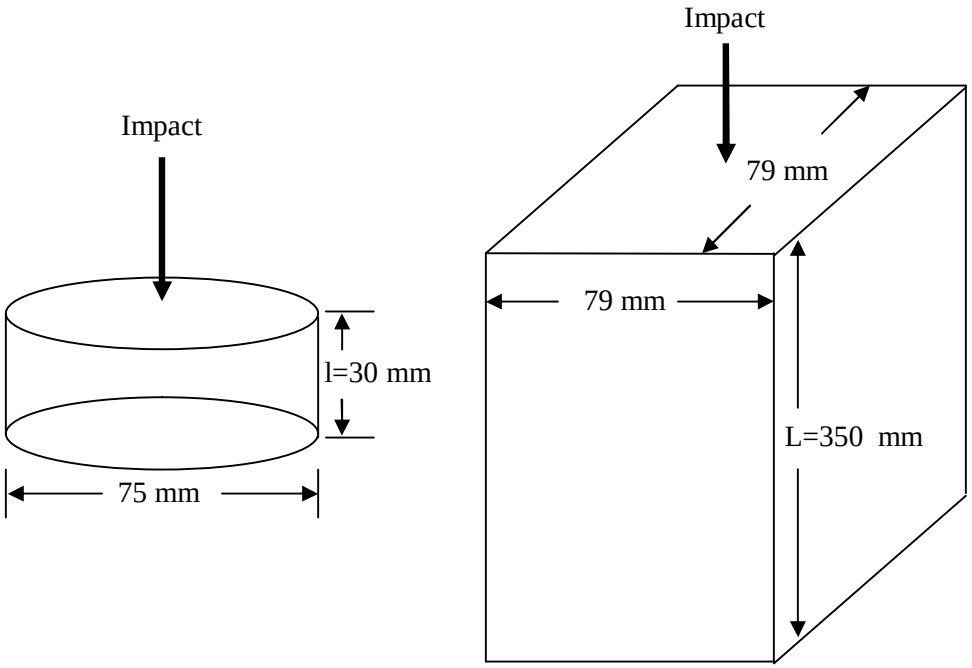

Figure 7.3: Schematic of impact volume for a) IS1 and b) IS2

In order to evaluate both the aluminum foam and the aluminum foam-polymer hybrid the amount of energy per unit volume (*W*) absorbed is read from Figure 6.14 for both materials with the aluminum foam in as-fabricated condition. Employing the specified area (*A*) of each impact scenario, W and the target energy absorption (*U*) the length required to fulfill the energy absorption requirements, *l*, is determined by the following calculation:

$$l = \frac{U}{A \times W} \tag{7.1}$$

Table 7.1 lists W for both materials at the maximum allowable stress levels in each impact scenario and the required length.

Table 7.1: Energy absorbed per unit volume (W) at the maximum allowable stress level and the required length to absorb the impact energy of IS1 and IS2 for aluminum foam and aluminum foam-polymer hybrid under static loading.

Material	IS1 (U = 100 J)			IS2 (U = 5000 J)		
	W (mJ/mm^3)	A (mm^2)	l (mm)	W (mJ/mm^3)	A (mm^2)	l (mm)
Aluminum Foam	0.80	4417.9	28.3	1.70	6240.0	471.3
Aluminum foam-polymer hybrid	0.07	4417.9	323.4	2.75	6240.0	291.4

It is clear from Table 7.1 that in IS1 (i.e. at low stress levels) the aluminum foam-polymer hybrid material does not meet the size requirements (i.e. calculated l > required l = 30 mm). The same is true for aluminum foam (calculated l > required l = 350 mm) in IS2 (i.e. at high stress levels). It can be concluded that for energy absorption applications under static loading conditions where a low stress level (i.e. ~ 2 MPa) is required the aluminum foam is the better choice, however at higher stress levels (i.e. ~ 8 MPa) the aluminum foam-polymer hybrid outperforms aluminum foam alone and is the better choice.

In a situation where two materials exhibit similar densification stress but one material has a higher energy absorption efficiency the more efficient material allows for a more compact energy absorber volume. This can be seen by comparing the aluminum foam-polymer hybrid produced in this study with the foam filled extrusion produced by Fuganti *et al.* [2000]. The higher efficiency of the foam filled extrusion results in a crash box length of only 210 mm [Fuganti *et al.* 2000], compared to 291 mm for the aluminum foam polymer hybrid. In this application where the ideal is to minimize the length of the crash box the foam filled extrusion is a better choice. However the macroscopic heterogeneity of the foam filled extrusion means its energy absorption behaviour varies significantly depending on its dimensions [Hanssen 2000]. The aluminum foam-polymer hybrid however is

macroscopically homogenous and can therefore be made to fit a variety of high stress energy absorption applications with greater ease. It is noted that in the preceding comparison factors such as cost, weight and rebound have not been discussed. It is recommended that upon further study of this material these factors be investigated in the comparison of the alumiunum foam-polymer hybrid with aluminum foam and other hybrid materials of interest.

7.2 Stress-Strain Behaviour under Dynamic Compressive Loading

Aluminum Foam

It is assumed that the lack of the initial linear-elastic regime observed in the stress-strain curves of the aluminum foam specimens is attributed to experimental conditions and not to a possible change in initial aluminum foam deformation mechanisms. This assumption is supported by the results of Deshpande and Fleck [2000], Dannemann and Lankford Jr. [2000], McArthur *et al.* [2003] and Lee *et al.* [2006] who all show a linear-elastic region in aluminum foams tested at much higher strain rates using a Compressive Split Hopkinson Bar. The fluctuations in the curves appear to have a periodic nature to them with the magnitudes and locations of the peaks occurring at almost the same strains in both specimens. Lifshitz *et al.* [1994] and Shin *et al.* [1999] find that the high frequency ringing in one of the natural modes of vibration of the impactor are present in the results and the fluctuations do not represent actual loads placed on the specimen. Based on this it is concluded that the fluctuations observed in Figure 6.15 are due to noise and are not an indication that the foam deforms in a brittle fashion.

From Figure 6.16 it is seen that both the as-fabricated and the peak-aged (4 hrs at 220˚C) aluminum foam specimens produce nearly identical stress-strain curves with the peak-aged foam showing a higher densification stress. This contrasts with the higher yield and plateau strengths observed in the as-fabricated aluminum foams over the similar peak-aged foams tested under static loading. However,

the magnitude of the increase in strength in the as-fabricated foams under static loading is less than the amplitude of the noise observed in the dynamic stress-strain curves. Indicating the change in the stress-strain behaviour is insignificant.

As a result of the similarities in the stress-strain curves of the as-fabricated aluminum foams and the artificially aged (4 hrs at 220˚C) aluminum foams the energy absorption values are also similar. The total energy absorbed up to densification is identical for the two foam conditions with the as-fabricated foams showing a higher efficiency owing to the higher densification stresses observed in the artificially aged specimens.

Dynamic testing of as-fabricated and peak-aged aluminum foams indicate no benefit to aluminum foam mechanical properties is produced by the extra processing required for artificial aging.

Aluminum Foam-Polymer Hybrid

Unlike during static compression testing where the hybrid and the polymer specimens had similar appearances after testing, Figure 6.18 and Figure 6.21 a) show that while the polymer displays near full recovery of strain the hybrid demonstrates permanent deformation characterized by a loss in height and barreling. As in the case of static testing the lateral expansion and the strain recovery that is observed in the hybrid is attributed to the polymer filling. The full strain recovery in the polymer specimens indicate that the permanent deformation in the hybrid specimens are likely due to the plastic deformation of the aluminum foam component and not the polymer component of the hybrid. The strain that is recovered can be explained by the broken struts seen in Figure 6.21 c) which reduce the resistance to strain recovery in the polymer component.

The full strain recovery in the polymer and the maintenance of a semi-connected network of struts in aluminum foam component of the hybrid are a consequence of the materials not achieving densification during testing. This is evidenced by the Cushion factor being the lowest at the last

collected data points and the lack of a sharp increase in stress in the stress-strain curves for both materials shown in Figure 6.22. Previous testing performed on another elastomer (polyurethane rubber) by Doman [2004] shows that the sharp increase in stiffness, defined as densification in this investigation, occurs up to strain rates of 1200 s^{-1}. In the current study the lack of densification is caused by the full absorption of impact energy in the specimens prior to densification. Assuming that polymer and hybrid densification are similar as they are in static testing using a larger impact energy would allow the test to continue past the strains shown and it is expected that the materials would show the typical sharp increase in stress and minimum Cushion factor associated with densification.

Shown in Figure 7.4 is the stress-strain curve of an as-fabricated aluminum foam-polymer hybrid specimen compared to the linear addition of as-fabricated aluminum foam and Elvax® stress-strain curves. The observed behaviour of a larger slope in the hybrid compared to the linear addition prior to 0.2 and the lower slope after 0.2 is similar to the behaviour observed in Regions IIa and IIb in the static stress strain curve. It is therefore likely that the same deformation mechanisms that occur under static loading also occur for dynamic loading. Also visible at the beginning of the hybrid stress-strain curve are fluctuations. These fluctuations are attributed to the vibrations in the impact head, as they are in the aluminum foam stress-strain curves, since the magnitudes and the locations of the peaks are very similar in the stress-strain curves of both the as-fabricated and the age-hardened aluminum foam-polymer hybrids tested. Different from the aluminum foams where noise is present beyond densification, the hybrid stress-strain curves show a decrease in amplitude to almost zero by a strain of 0.2. This strain coincides with the beginning of Region IIb and hence the fracture of aluminum foam ligaments in the hybrid material. Based on the little noise present in the polymer stress-strain curve compared to noise still present beyond densification in the aluminum foam it is speculated that the elimination of noise in the hybrid at 0.2 strain is due to the increase in the stress supported by the polymer due to ligament fracture.

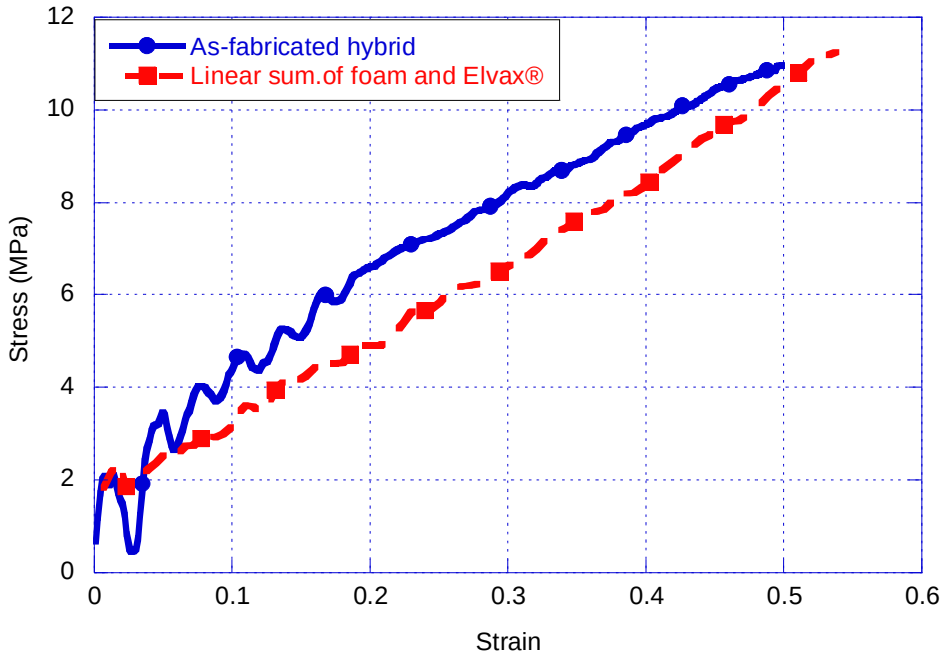

Figure 7.4: Compressive stress-strain curve of as-fabricated aluminum foam-polymer hybrid including a linear sum of the parent material curves under dynamic loading.

The similarity between the stress-strain curves of the as-fabricated aluminum foam-polymer hybrids and the peak-aged (4hr at 220˚C) aluminum foam-polymer hybrids is consistent with previous findings of this investigation that when both aluminum foam conditions display similar stress-strain curves there is also little difference in the two hybrid materials. From this, the conclusion drawn for static and dynamic compression testing of aluminum foam and static compression testing of aluminum foam-polymer hybrid that no benefit in mechanical properties is obtained by the artificial aging treatment utilized in this study also holds for dynamic loading of the hybrid.

To compare the energy absorption properties of the aluminum foam-polymer hybrid to those of aluminum foam, the impact scenarios (i.e. IS1 and IS2) defined in Section 7.1 will be utilized with energy absorption values obtained from Figure 6.23. The results are listed in Table 7.2. It is clear that at the lower stress application (i.e. IS1) the aluminum foam outperforms the hybrid material which

requires more than 15 times the allotted specimen length to fully absorb the impact energy. The stress level in IS2 (i.e. 8 MPa) occurs at the point of intersection between the aluminum foam and the hybrid energy curves. It therefore not surprising that both the foam and the hybrid require the same specimen length to absorb the impact energy in IS2, however neither meets the length requirement. By decreasing the contact area to 70 mm x 70 mm the crash box can still fit within the bumper and the maximum allowable stress in the crash box material is increased to approximately 10 MPa. This allows the hybrid material to operate at a stress level where the energy absorption efficiency is higher. By definition the stress at which the energy absorption efficiency is highest is the densification therefore if the densification stress of the hybrid were known the area of the crash box could be optimized to produce a length shorter than 310 mm. Further testing on the hybrid to obtain the densification stress at the present strain rate is required before an optimized energy absorption device can be made form this material.

Table 7.2: Energy absorbed per unit volume (W) at the maximum allowable stress level and the required length to absorb the impact energy of IS1 and IS2 for aluminum foam and aluminum foam-polymer hybrid under dynamic loading.

Material	IS1 (U = 100 J)			IS2 (U = 5000 J)		
	W (mJ/mm^3)	A (mm^2)	l (mm)	W (mJ/mm^3)	A (mm^2)	l (mm)
Aluminum Foam	0.80	4417.9	28.3	1.70	6240.0	471.3
Aluminum foam-polymer hybrid	0.05	4417.9	452.7	1.70	6240.0	471.3

It can be concluded that for a strain rate of 100 s^{-1} aluminum foam performs better than the aluminum foam-polymer hybrid at low stress energy absorption applications (i.e. ~ 2 MPa). At higher stress levels which correspond to the densification stress of the hybrid material the performance of the aluminum foam is poor and the hybrid material is the much better choice.

7.3 Effect of Strain Rate on Stress-Strain Behaviour

Aluminum Foam

Figure 7.5 shows the stress vs. strain curves obtained from both dynamic testing and static testing of the as-fabricated foam. It can be seen that the foams do not show any significant strain rate sensitivity up to a rate of 100 s^{-1}. This is agreement with the results published by Deshpande and Fleck [2000], Dannemann and Lankford Jr. [2000], McArthur *et al.* [2003] and Lee *et al.* [2006]. Deshpande and Fleck [2000] used the simple cubic cell model by Gibson and Ashby [1997], shown in Figure 2.4, to show that the strain rate at the cell edges, where the deformation takes place, is an order of magnitude lower than the macroscopic strain rate. This, in combination with strain rate insensitivity observed in the strength of AA6XXX alloys up to strain rates of 10^3 s^{-1} [Lindholm *et al.* 1971], explain the lack of strain rate sensitivity of Duocel® aluminum foam at the strain rates tested. One result of this is that the aluminum foam deforms by way of ligament bending and buckling in the same manner as observed at static strain rates [Deshpande and Fleck 2000].

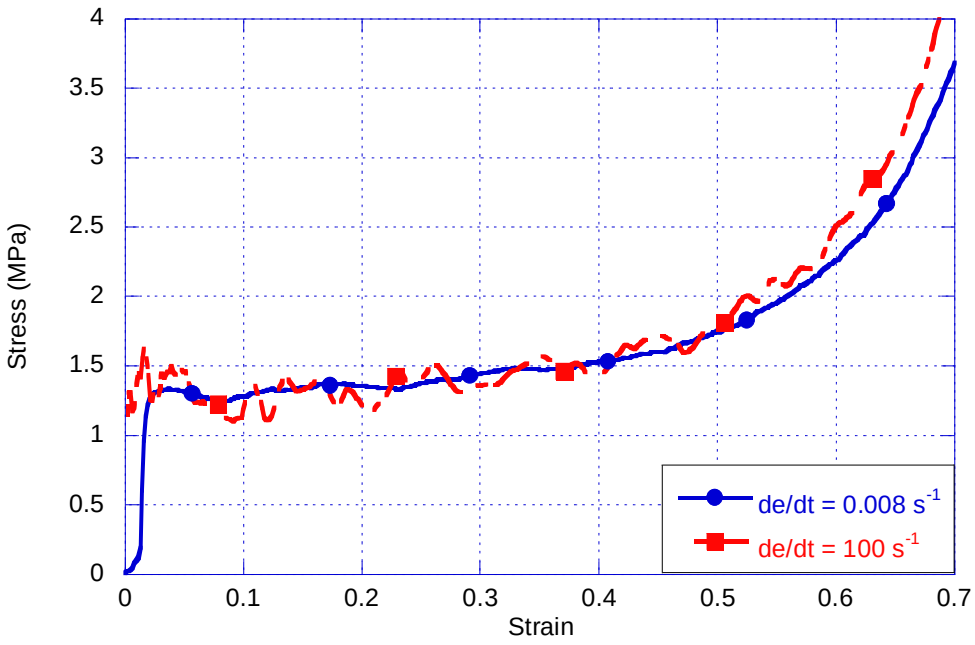

Figure 7.5: Compressive stress-strain results of as-fabricated aluminum foam at static (0.008 s^{-1}) and dynamic (100 s^{-1}) strain rates.

The energy absorption in the aluminum foam is unchanged with strain rate. This can be seen by the fact that the same volume of foam is required for IS1 regardless of strain rate. This property makes designing energy absorbing devices with this material much easier as variations in impact rate do not affect the energy absorbed.

Aluminum Foam-Polymer Hybrid

Figure 7.6 shows the response of as-fabricated aluminum foam-polymer hybrid at static and dynamic loading conditions. It is apparent that the dynamic stress-strain curve displays an increased stress over the static stress-strain curve when deformed to the same strain. This is the result of steeper slopes in the dynamic stress-strain curve compared to the slopes in the equivalent regions of the static stress-strain curve. Out of the two parent materials only the polymer displays strain rate sensitivity,

shown in Figure 7.7. Polymers are visco-elastic in nature and at higher loading rates less time allowed for stress relaxation in the viscous component causes an increase in the apparent stiffness [Kaelble 1964]. This rate sensitive behaviour in the polymer is also responsible for an increase in the additional strength produced by the interaction between the foam ligaments and the polymer. This is seen by the larger difference in strength between the hybrid curve and the linear combination of foam and Elvax® under dynamic loading (Figure 7.4) compared to static loading (Figure 7.1).

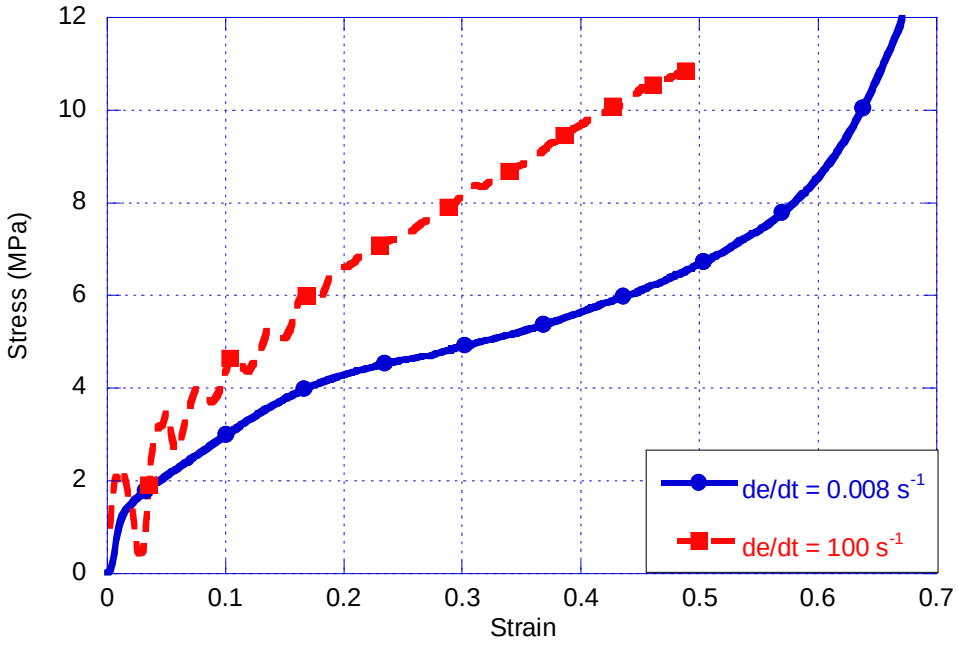

Figure 7.6: Compressive stress-strain results of as-fabricated aluminum foam-polymer hybrid at static (0.008 s^{-1}) and dynamic (100 s^{-1}) strain rates.

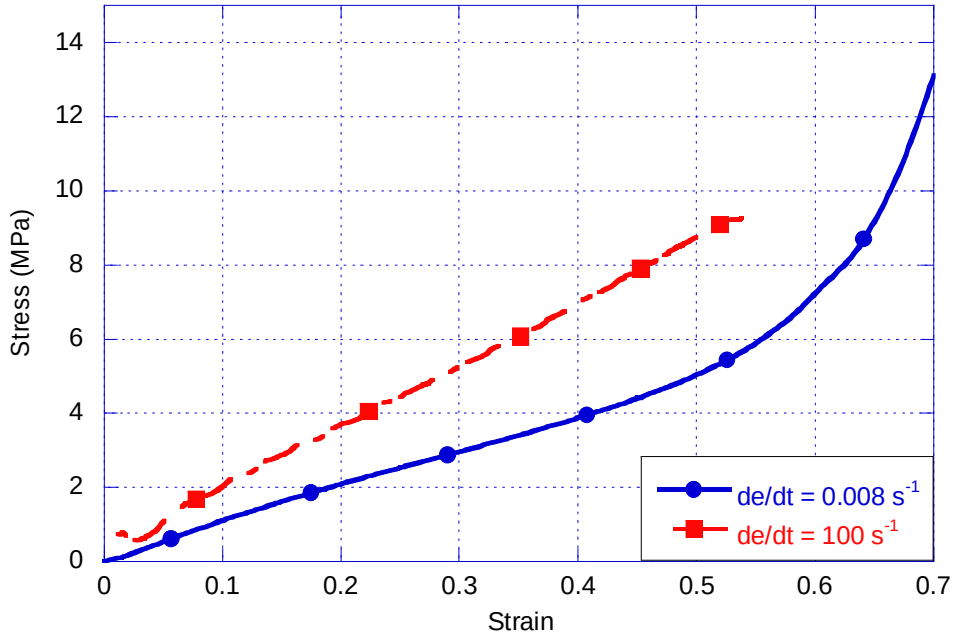

Figure 7.7: Compressive stress-strain results of Elvax® at static (0.008 s^{-1}) and dynamic (100 s^{-1}) strain rates.

The difference the rate sensitivity has on the energy absorption can be seen by comparing the length required for IS2 at both static and dynamic tests. It is clear that the specimen requires a much longer length for dynamic testing to absorb the same amount of energy. However if the area of the part is made smaller to accommodate the higher densification stress at dynamic rates the length requirement can still be achieved. Polymer rate sensitivity also indicates that in aluminum foam-polymer hybrid materials, where the energy absorption efficiency is higher than the parent material under static conditions (e.g. aluminum foam-polymer hybrid produced by Cheng and Han [2003]), may not be more efficient at higher loading rates. These issues highlight the importance of knowing the rate of impact and utilizing material data from the same impact rate when designing an energy absorbing device that is strain rate dependant. It is suggested that further testing on the Elvax® filled

aluminum foam at multiple strain rates be performed to asses its applicability in applications with known impact rates.

7.4 Mechanical Damping of Aluminum Foam and Aluminum Foam-Polymer Hybrid

Aluminum Foam

The initial open hysteresis loops displayed by the aluminum foam specimens are the result of strain hardening produced by microplastic yielding in the aluminum foam struts [Golovin *et al.* 2004b]. Microplastic yielding displays a non-linear stress-strain response and it occurs between the true elastic region and the yield stress as shown in Figure 2.5. Scanning electron microscopy performed on Duocel® aluminum foam which has been loaded-unloaded into this non-linear region by Zhou *et al.* [2004b] shows that dislocation slip bands are formed on select ligaments even though no observable deformation occurs. This is consistent with the findings for the D5L aluminum foam sample that no difference in height was measured. This however contradicts the loss of 0.1 mm in height in the case of the D5H aluminum foam sample. It is therefore thought that the plateau region of just under 0.002 strain in length (equal to a little less than 0.1 mm) in Figure 6.25 indicates the occurrence of plastic deformation in the specimen upon initial loading. Thus it is the production of dislocation slip bands during plastic deformation in the D5H specimen that is responsible for the initial open hysteresis loop.

Cyclic tension-compression tests under load control performed by Golovin *et al.* [2004b] on Alporas® closed cell aluminum foam show a gradual shift of the "zero" point in the stress-strain hysteresis loops towards compressive stresses and strains. The shift results in lower compressive stresses for the same strain. Golovin and Sinning [2003] attribute this shift to the accumulation of deformation in the specimens in the compression part of the tension-compression tests. In this

investigation, a shift in the level of compressive strain is not observed since testing was performed under displacement control and thus the maximum and minimum strains are fixed. However, a shift to lower compressive stresses is observed. It is speculated that this shift might also be due to the accumulation of deformation similar to the foams tested by Golovin and Sinning [2003] and Golovin *et al.* [2004b]. It is also speculated that the stabilization observed is due to the decreasing stress level. Due to the work hardening of the foam caused by deformation larger stresses are required to produce similar amounts of deformations. Since the stress is decreasing the amount of deformation per cycle decreases until the stress level is not high enough to produce any further deformation. It is thought that the higher strain amplitudes produce larger deformations and thus producing shifts in the stress-strain curves that are greater at higher amplitudes.

The cause of the horizontal line with a near constant stress level of 0 MPa at the bottom of the D5H stress-strain curve is unknown. It is likely from the fact that 0 MPa is attained when the platen must lose contact with the foam specimen. Only 0.1 mm of plastic deformation is measured in the D5H specimens and experimental setup ensures that the minimum compression on the specimen is 0.25 mm. The length of the line increases with testing potentially indicating a loss of specimen height. This is not an isolated occurrence as it happens when the testing is repeated. It is noted that the average damping values calculated from each repeated test show good agreement with each other. To determine the cause of this occurrence further investigation is required.

The decrease in the amount of energy dissipated (i.e. D) by the D5H aluminum foams throughout testing is the result of the lengthening horizontal line with near constant stress of 0 MPa. The increase in this line reduces the area within the stress-strain curve. Stabilization in D at approximately 100 cycles is a result of the stabilization in the shifting stress-strain hysteresis loop which also stabilizes the length of the horizontal line at 0 MPa. The variation in D over the length of the test causes a lower value of D for the stabilized (taken from the 190^{th} cycle) foam than the average value. The D5L

specimen shows little difference between the average value of D and the value at the 190^{th} cycle due to the approximately constant value of D from the 10^{th} cycle up to the 190^{th} cycle. For the purposes of comparison the stabilized value of D will be utilized. Comparing the stabilized values of D at both D5H and D5L test conditions the D for D5H is larger than the D displayed by the D5L specimens. This result is the consequence of the higher amplitude of testing. Higher strain amplitudes result in larger stress-strain hysteresis loops.

Comparing the stabilized values of h for D5H and D5L test conditions shows that h is larger for the D5H specimens. This indicates the aluminum foam displays amplitude dependant damping. This is consistent with many other damping studies performed on aluminum foam [Yu and He 1994, Banhart *et al.* 1996, Fu-sheng *et al.* 1997, Liu *et al.* 1998, Golovin and Sinning 2003, Golovin and Sinning 2004, Golovin *et al.* 2004a and Golovin *et al.* 2004b]. However, the strain amplitudes investigated in this study ($> 10^{-3}$) are larger than the strain amplitudes utilized in many of the other studies ($\leq 10^{-4}$) [Yu and He 1994, Banhart *et al.* 1996, Fu-sheng *et al.* 1997, Liu *et al.* 1998]. According to Golovin and Sinning [2003] the amplitude dependant damping mechanisms change from reversible dislocation motion (according to the Granato and Lücke [1956] vibrating string dislocation model) for strain amplitudes $\leq 10^{-4}$ to damping due to microplastic deformation for strain amplitudes $> 10^{-4}$. It is suggested that aluminum foam due to its cellular structure and heterogeneous deformations displays amplitude dependant damping, with the high amplitude D5H specimens showing higher values of D and h than the D5L specimens. However, for a better understanding of the damping mechanisms that are occurring in the Duocel® aluminum foam testing up to 10^6 cycles and more detailed analysis should be performed.

Aluminum Foam-Polymer Hybrid

It has previously been shown by looking at the stress-strain curves of both the hybrid and aluminum foam that at the low strain values utilized in testing the majority of the stress is supported by the aluminum foam. Therefore the open hysteresis loops seen in the hybrid are caused by microplastic deformation in the aluminum foam. However in testing at high amplitudes (i.e. D5H) the support provided by the polymer against ligament bending inhibits the plastic deformation seen in the D5H aluminum foam specimens, instead resulting in microplastic yielding in the hybrid specimen. Therefore, in both D5H and D5L hybrid specimens it is suggested that the open hysteresis loop is due to the creation of dislocation slip bands in the aluminum foam component due to microplastic yielding in the foam.

The creation of new slip bands in the hybrid specimens due to microplastic yielding is thought to be responsible for the shifting stress-strain hysteresis loops, similar to aluminum foam. Again similar to aluminum foam it is suggested that the larger shifts in stress-strain hysteresis loops in the D5H hybrid specimens is due to the increase in microplastic yielding over the D5L hybrid specimens.

Comparing h of the two amplitudes shows that the D5H specimens have a higher loss coefficient than the D5L specimens. The hybrid therefore displays amplitude dependant damping similar to the aluminum foam. Typically polymers do not show amplitude dependant damping [Nielsen 1974a]. It is therefore likely that the amplitude dependence is due to the aluminum foam component of the hybrid.

The hybrid is found to absorb more energy than aluminum foam at equivalent strain amplitude levels. This indicates that the there is more than just dislocation damping in the hybrid. A combination of both damping in the polymer and damping at the aluminum foam-polymer interfaces are likely responsible for the increase in damping in the hybrid over the base aluminum foam. Polymers which are known to have high damping abilities dissipate energy by the viscous sliding of

polymer chains [Kaelble 1964]. Interface damping is thought to be one source of damping in woodceramics filled with magnesium [Xian-Qing *et al.* 2002]. In areas where wetting is good and the bond is strong the deformation of the foam will produce higher local deformations in the polymer increasing the dissipated energy while in areas where the bond is weak friction produced by the relative motion the ligament and the polymer will again result extra energy dissipation [Lavernia *et al.* 1995]. The strength of the bond between the polymer and the aluminum foam is unknown and therefore the exact mechanism is unknown however an increase in damping occurs in both cases.

The result that the hybrid is a better damper than the aluminum foam under both amplitudes is promising. However, due to the strain rate dependence on the stress-strain curve of the polymer a different result may occur if the testing frequency is altered. As it stands the hybrid is a better choice than the aluminum foam in applications where the strain amplitudes and frequency are similar to the values used in this investigation. To expand on the range of potential applications it is suggested that testing at smaller amplitudes and over a range of frequencies be performed. Due to the microplastic yielding in the aluminum foam component further investigations into the stability of hybrid material beyond 190 cycles is also recommended.

Chapter 8
Conclusions and Recommendations

8.1 Conclusions

The aims of the present work were to (a) design a new metal-polymer hybrid material utilizing open-cell aluminum foam that could be recycled, and (b) to assess the potential enhancement in the mechanical properties of the hybrid material in comparison with the base aluminum foam and polymeric filling material. Goal (a) was accomplished using a thermoplastic polymer with a high MI. Goal (b) was achieved by experimental analysis of foam, polymer and fabricated hybrid samples using static and dynamic compressive testing, as well as cyclic compressive testing for damping property analysis. The important conclusions on the mechanical behaviour assessment are as followsl:

- When heat treatment is applied to the foam samples, artificial aging up to the peak-aged condition produces an enhancement to mechanical properties, including yield strengths and plateau strengths, energy absorption and energy absorption efficiency, over under-aged specimens.
- Comparing the mechanical properties under static loading conditions of the as-fabricated aluminum foam to the solutionized, air quenched and peak-aged aluminum foams it is seen that no benefit to the mechanical properties of the as-fabricated aluminum foam are achieved by aging.
- Similar to the findings for aluminum foam no benefit in mechanical properties is observed in the peak-aged aluminum foam-polymer hybrid compared to the as-fabricated aluminum foam-polymer hybrid. It is concluded the extra heat treatment procedure is not required.

- The hybrid shows four distinct stress-strain regions upon deformation. Region I is linear-elastic and shows a good approximation to the linear combination of polymer and foam stress-strain curves. The polymer filling has little effect on the stiffness of the hybrid. Region IIa shows an interaction effect between the polymer and the foam resulting in an increase over the strength predicted by the linear combination of polymer and foam curves. This is due to the polymer supporting the ligaments from bending and the ligaments preventing the polymer from expanding laterally. Some plastic deformation is still expected. In Region IIb the aluminum foam ligaments fail reducing the slope by allowing the polymer to expand laterally and reducing the area of aluminum foam capable of carrying load. By the end of Region IIb the hybrid stress-strain curve approaches the stress-strain curve for the polymer indicating the aluminum foam has little effect on the hybrid strength. Densification occurs in Region III. The polymer and hybrid curves are almost the same.
- Based on energy absorption efficiency the aluminum foam is a better energy absorbing material than the aluminum foam-polymer hybrid produced in this study.
- For static energy absorption applications where the maximum allowable stress is 2 MPa the aluminum foam is the better choice of the two materials. For a maximum allowable stress of 8 MPa the hybrid is the better choice.
- As in the case of static loading, under dynamic loading no benefit to the mechanical properties is observed in the peak-aged aluminum foams over the as-fabricated aluminum foams.

- Similar to the aluminum foam, under dynamic loading no benefit to the mechanical properties are observed in the peak-aged aluminum foam-polymer hybrid compared to the as-fabricated aluminum foam-polymer hybrid.
- For energy absorption applications at $100s^{-1}$ the aluminum foam is the best material to utilize in comparison to the hybrid when the maximum allowable stress is 2 MPa. If the maximum allowable stress is approximately the densification stress of the hybrid (above 10 MPa) the hybrid is the better choice.
- Similar to other studies on aluminum foam, the stress-strain curve of the aluminum foam in this study is found to be strain rate independent.
- Unlike aluminum foam the stress-strain curve of the aluminum foam-polymer hybrid is found to be strain rate dependant. The dependence on the rate of testing is due to the visco-elasticity in the polymer component of the hybrid.
- Aluminum foam is found to display amplitude dependant damping. This finding is in agreement with the other studies on aluminum foam damping.
- The aluminum foam-polymer hybrid is also found to display amplitude dependant damping. The hybrid also shows an increase in damping over the base aluminum foam. This increase is suggested to be due to the additional damping in the polymer and damping at the foam-polymer interface.

8.2 Recommendations

The following recommendations for future work involving both this hybrid and new hybrid materials are summarized below:

- In order to confirm the deformation mechanisms it is recommended that loading of the hybrid specimens up to a strain of 0.15 (i.e. middle of Regions IIa) and unloading, while measuring the unloading curve, be performed. The polymer should then be melted out and the resultant foam network be analyzed under SEM. The same procedure should be performed up to a strain of 0.3 (i.e. middle of Region IIb).
- The aluminum foam-polymer hybrid should be tested under more strain rates up to densification to asses potential applications
- The promising damping properties of the hybrid material should be investigated further. Tests at strain amplitudes equivalent to potential service amplitudes should be performed to narrow down potential applications.
- Finally it is recommended that the use of higher relative density foam filled with Elvax® be investigated to see if the energy absorption efficiency the hybrid can be improved.

References

Aklonis J, Macknight W and Shen M. (1972). *Introduction to Polymer Viscoelasticity*, Wiley-Interscience, New York, New York.

Andrews EW, Gioux G, Onck P and Gibson LJ. (2001), *International Journal of Mechanical Sciences*; 43: 701.

Andrews E, Sanders W and Gibson LJ. (1999), *Materials Science and Engineering A*; 270: 113.

Ashby MF. (1983), *Metallurgical Transactions A*; 14A: 1755.

Ashby MF. (1992), *Materials Selection in Mechanical Design*, Pergamon Press, Oxford, UK.

Ashby MF and Bréchet YJM. (2003), *Acta Materialia*; 51: 5801.

ASM. (1992), Properties *and Selection: Nonferrous Alloys and Special-Purpose Materials*, ASM Handbook Vol. 2, Tenth Edition, ASM International.

Banhart J. (2001), *Progress in Materials Science*; 46: 559.

Banhart J and Baumeister J. (1998), *Journal of Materials Science*; 33: 1431.

Banhart J, Baumeister J and Weber M. (1996), *Materials Science and Engineering A*; 205: 221.

Bart-Smith H, Bastawros AF, Mumm DR, Evans AG, Sypeck DJ and Wadley NG. (1998), *Acta Materialia*; 46: 10: 3583.

Barbosa RV, Neto RB, Mauler RS, Gorga CJP, Schneider CG and Simanke AG. (2005), *Journal of Applied Polymer Science*; 97: 1371.

Beals JT and Thompson MS. (1997), *Journal of Material Science*; 32: 3595.

Bin J, Zajun W and Naiqin Z. (2007), *Scripta Materialia*; 56: 169.

Boczkowska A, Konopka K and Kurzydlowski KJ. (2006), *Journal of Materials Processing Technology*; 175: 40.

Boyce MC, Kear K, Socrate S and Shaw K. (2001), *Journal of the Mechanics and Physics of Solids*; 49: 1073.

Brydon AD, Bardenhagen SG, Miller EA and Seidler GT. (2005), *Journal of the Mechanics and Physics of Solids*; 53: 2638.

Cantwell WJ, Compston P and Reyes G. (2000), *Journal of Materials Science Letters*; 19: 2205.

Cao XQ, Wang ZH, M HW, Zhao LM and Yang GT. (2006), *Transactions of Nonferrous Metals Society of China*; 16: 1: 159.

Chan KC and Chan SH. (2004), *Materials and Manufacturing Processes*; 19: 3: 407.

Chen C, Harte AM and Fleck NA. (2001), *International Journal of Mechanical Sciences*; 43 1483.

Cheng HF and Han FS. (2003), *Scripta Materialia*; 49: 583.

Chirwa EC, Latchford J and Clavell P. (2003), *International Journal of Crashworthiness*; 8: 1: 107.

Cluff D and Esmaeili S. (2006), *Journal of Material Science*; Submitted.

Cronin D, (2006), ME725 Course notes.

Dannemann KA and Lankford Jr J. (2000), *Materials Science and Engineering A*; 293: 157.

Deshpande VS and Fleck NA. (2000), *International Journal of Impact Engineering*; 24: 277.

Despois JF, Mueller R and Mortensen A. (2006), *Acta Materialia*; 54: 4129.

Dharmasena KP and Wadley HNG. (2002) *Journal of Materials Research*; 17: 3: 625.

Dieter GE. (1986), *Mechanical Metallurgy*, 3rd ed., McGraw-Hill, Boston, MA, USA.

Doman D. (2004), *Modeling of the High Rate Behaviour of Polyurethane Rubber*, Waterloo, University of Waterloo, Department of Mechanical Engineering, MASc. thesis.

DuPont™. (2005a), "DuPont Packaging and Industrial polymers: DuPont™ Elvax® 205W", Doc. Ref. nn3bjbm8.pdf, April 2005 Copyright 2005 E.I. du Pont de Nemours and Company, Inc.

DuPont™ .(2005b), *DuPont Industrial Polymers: DuPont™ Elvax®*, Nov. 2005, http://www.dupont.com/industrial-polymers/elvax/H-49653-1/H-49653-1.html (Sept. 9, 2005).

Esmaeili S, Poole WJ and Lloyd DJ. (2000), *Materials Science Forum*; 331-337: 995.

Esmaeili S. (2002), *Precipitation Hardening Behaviour of AA6111*, Vancouver, The University of British Columbia, Department of Metals and Materials Engineering, Ph.D. thesis.

Esmaeili S, Lloyd DJ, Poole WJ. (2003) *Acta Materialia*; 51: 3467-3481

Esmaeili S, Vaumousse D, Zandbergen MW, Poole WJ, Cerezo A and Lloyd DJ. (2007) *Philosophical Magazine*; In Press.

Feng Y, Zhu Z , Tao N and Zhen H. (2003) *Chin Shu Hsueh Pao*; 39: 8: 817.

Feng XQ, Tian Z, Liu YH and Yu SW. (2004), *Applied Composite Materials*; 11: 33.

Found MS, Howard IC and Paran AP. (1998), *Composites Structures*; 42: 353.

Fuganti A, Lorenzi L, Hanssen AG and Langseth M. (2000), *Advanced Engineering Materials*; 2: 4: 200.

Fu-sheng H, Zhen-gang Z and Chang-song L. (1997), *Scripta Materialia*; 37: 9: 1441.

Fraunhofer USA—Delaware (2002), *Metal Foams for Improved Crashworthiness of High Speed Rail Passenger Equipment*, HSR IDEA, Contract No. HSR-20, Final Report, National Academy of Sciences, High Speed Rail IDEA Program, Washington, DC, USA.

Gibson LJ and Ashby MF. (1997), *Cellular Solids: Structure and Properties*, 2nd ed., Cambridge University Press, Cambridge, UK.

Gioux G, McCormack TM and Gibson LJ. (2000), *International Journal of Mechanical Sciences*; 42: 1097.

Golovin IS, Sinning HR. (2003), *Journal of Alloys and Compounds*; 355: 2.

Golovin IS and Sinning HR. (2004), *Materials Science and Engineering A*; 370: 504.

Golovin IS, Sinning HR, Arhipov IK, Golovin SA and Bram M. (2004a), *Materials Science and Engineering A*; 370: 531.

Golovin IS, Sinning IS, Göken J and Riehemann W. (2004b), *Materials Science and Engineering A*; 370: 537.

Gong L and Kyriakides S. (2006), *Journal of Applied Mechanics*; 73: 807.

Goodall R, Weber L and Mortensen A. (2006) *Journal of Applied Physics*; 100: 044912

Granato AV. (1964), "Internal Friction Studies of Dislocations". In *Internal Friction, Damping and Cyclic Plasticity: a symposium presented at the sixty-seventh annual meeting*, ASTM, Philadelphia, USA.

Granato A and Lücke K. (1956), *Journal of Applied Physics*; 27: 6: 583.

Hanssen AG, Langseth M and Hopperstad OS. (2000), *International Journal of Impact Engineering*; 24: 347.

Hanssen AG, Hopperstad OS, Langseth M and Ilstad H. (2002a), *International Journal of Mechanical Sciences*; 44: 359.

Hanssen AG, Langseth M and Hopperstad OS. (2002b), *Advanced Engineering Materials*; 4: 10: 771.

Hart AM, Fleck NA and Ashby MF. (1999), *Acta Materialia*; 47: 8: 2511.

Hart AM, Fleck NA and Ashby MF. (2000), *Advanced Engineering Materials*; 2: 4: 219.

Hsiao HM and Daniel IM. (1998), *Composites Part B*; 29B: 521.

Kaelble DH. (1964), “Micromechanisms and Phenomenology of Damping in Polymers”. In *Internal Friction, Damping and Cyclic Plasticity: a symposium presented at the sixty-seventh annual meeting*, ASTM, Philadelphia, USA.

Kanahashi H, Mukai T, Yamada Y, Shimojima K, Mabuchi M, Aizawa T and Higashi K. (2001), *Materials Transactions*; 42: 10: 2087.

Khonakdar HA, Wagenknecht U, Jafari SH, Hässler R and Eslami H. (2004), *Advances in Polymer Technology*; 23: 4: 307.

Kiratisaevee H and Cantwell WJ. (2003), *Journal of Sandwich Structures and Materials*; 5: 53.

Koehler JS. (1952) *Imperfections in Nearly Perfect Crystals*. Wiley and Sons, New York

Koza E, Leonowicz M, Wojciechowski S and Simancik F. (2003), *Materials Letters*; 58: 132

Kretz R, Hausberger K and Götzinger B. (2002), *Advanced Engineering Materials*; 4: 10: 781

Krishna BV, Bose S and Bandyopadhyay A. (2007), *Materials Science and Engineering A*; 452-453: 178.

Kromm FX, Quenisset JM, Harry R and Lorriot T. (2002), *Advances in Engineering Materials*; 4: 371.

Kwon YW, Cooke RE and Park C. (2003), *Materials Science and Engineering A*; 343: 63.

Lavernia EJ, Perez RJ and Zhang J. (1995), *Metallurgical and Materials Transactions A*; 26: 2803.

Lazan BJ. (1964), “Damping Studies in Materials Science and Materials Engineering”. In *Internal Friction, Damping and Cyclic Plasticity: a symposium presented at the sixty-seventh annual meeting*, ASTM, Philadelphia, USA.

Lazan BJ. (1968), *Damping of materials and members in Structural mechanics*, Pergamon Press, Oxford, UK.

Lee S, Barthelat F, Moldovan N, Espinosa HD and Wadley HNG. (2006), *International Journal of Solids and Structures*; 43: 53.

Lehmus D, Banhart J and Rodriguez-Perez MA. (2002), *Materials Science and Technology*; 18: 474.

Lehmus D and Banhart J. (2003), *Materials Science and Engineering* A; 349: 98.

Lehmus D, Marschner C and Banhart J. (2002), *Journal of Materials Science*; 37: 3447.

Li K, Gao XL and Subhash G. (2006), *Journal of the Mechanics and Physics of Solids*; 54: 783.

Lifshitz JM, Gov F and Gandelsman M. (1995), *International Journal of Impact Engineering*; 16: 2: 201.

Lindholm US, Bessey RL and Smith GV. (1971), *Journal of Materials, JMLSA*; 6: 1: 119.

Liu CS, Zhu ZG, Han FS and Banhart J. (1998), *Journal of Materials Science*; 33: 1769.

Lu TJ and Ong JM. (2001), *Journal of Materials Science*; 36: 2773.

Maiti SK, Gibson LJ and Ashby MF. (1984), *Acta Metallurgica*; 32: 11: 1963.

McArthur J, Salisbury C, Cronin D, Worswick M and Williams K. (2003), *Shock and Vibration*; 10: 179.

McCullough KYG, Fleck NA and Ashby MF. (1999), *Acta Materialia*; 47: 8: 2323.

McIntosh et al. (1995) "Head and Neck Injury Resulting from Low Velocity Direct Impact", 37th Stapp Car Crash Conference Proceedings, No. 933112, pp. 43-57.

Miyoshi T, Itoh M, Mukai T, Kanahashi H, Kohzu H, Tanabe S and Higashi K. (1999), *Scripta Materialia*; 41:10: 1055.

Miyoshi T, Mukai T and Higashi K. (2002), *Materials Transactions*; 43: 7: 1778.

Montanini R. (2005), *International Journal of Mechanical Sciences*; 47: 26.

Morrow J. (1964), "Cyclic Plastic Strain Energy and Fatigue of Metals". In *Internal Friction, Damping and Cyclic Plasticity: a symposium presented at the sixty-seventh annual meeting*, ASTM, Philadelphia, USA.

Mukai T, Kanahashi H, Miyoshi T, Mabuchi M, Nieh TG and Higashi K. (1999), *Scripta Metallurgica*; 40: 921.

Mukai T, Miyoshi T, Nakano S, Somekawa H and Higashi K. (2006), *Scripta Materialia*; 54: 533.

NASA. "Lightweight Energy Absorbers for Blast Containers", NASA Tech Briefs: MFS-31563, National Aeronautics and Space Administration.

Nieh TG, Higashi K and Wadsworth J. (2000), *Materials Science and Engineering A*; 283: 105.

Nielson LE. (1974a), "Mechanical Properties of Polymers and Composites: Volume 1", Marcel Dekker Inc., NY, NY, USA.

Nielson LE. (1974b), "Mechanical Properties of Polymers and Composites: Volume 2", Marcel Dekker Inc., NY, NY, USA.

Nowick AS. (1964), "Anelastic Phenomena in Metals and Nonmetallics". In *Internal Friction, Damping and Cyclic Plasticity: a symposium presented at the sixty-seventh annual meeting*, ASTM, Philadelphia, USA.

Nowick AS and Berry BS. (1972), *Anelastic Relaxation in Crystalline Solids*, Academic Press, NY, NY, USA.

Olurin OB, Fleck NA and Ashby MF. (2000), *Materials Science and Engineering A*; 291: 136.

Paek JW, Kang BH, Kim SY and Hyun JM. (2000) *International Journal of Thermophysics*; 21: 2: 453.

Paul A and Ramamurty U. (2000), *Materials Science and Engineering A*; 281: 1.

Prielipp H, Knechtel M, Claussen N, Streiffer SK, Müllejans H, Rühle M and Rödel J. (1995), *Materials Science and Engineering A*; 197: 19.

Radford DD, McShane GJ, Deshpande VS and Fleck NA. (2006), *International Journal of Solids and Structures*; 43: 2243.

Ruan D, Lu G, Chen FL and Siores E. (2002), *Composite Structures*; 57: 331.

Salisbury C. (2006) Personal communication.

Salyer IO and Kenyon AS. (1971), *Journal of Polymer Science: Part A-1*; 9: 3083.

San Marchi C and Mortensen A. (2001), *Acta Materialia*; 49: 3959

Shahbeyk S, Petrinic N and Vafai A. (2007), *International Journal of Impact Engineering*; 34: 573.

Shen Y, Golnaraghi F and Plumtree A. (2001), *International Journal of Fatigue*; 23: 6: 491.

Shin HS, Lee HM and Kim MS. (2000), *International Journal of Impact Engineering*; 24: 571.

Sierakowski RL and Hughes ML. (2006), *Composite Science and Technology*; 66: 2500

Song Z and Nutt S. (2005), *Advanced Engineering Materials*; 7: 1-2: 73.

Sugimura Y, Meyer J, He MY, Bart-Smith H, Grenstedt and Evans AG. (1997), *Acta Materialia*; 45: 12: 5245.

Tagarielli VL, Fleck NA and Deshpande VS. (2004), *Advanced Engineering Materials*; 6: 6: 440.

Tan PJ, Reid SR, Harrigan JJ, Zou Z and Li S. (2005), *Journal of the Mechanics and Physics of Solids*; 53: 2174.

Travitzky NA. (2001), *Journal of Materials Science*; 36: 4459.

Tilbrook MT, Moon RJ and Hoffman M. (2005), *Materials Science and Engineering A*; 393: 170.

Vaidya UK, Pillay S, Bartus S, Ulven CA, Grow DT and Mathew B. (2006), *Materials Science and Engineering A*; 428: 59.

Wang Q, Fan Z and Gui L. (2006), *International Journal of Solids and Structures*; 43: 2064.

Wegner LD and Gibson LJ. (2000), *International Journal of Mechanical Sciences*; 42: 925.

Wegner LD and Gibson LJ. (2001), *International Journal of Mechanical Sciences*; 43: 1061.

Werther DJ, Howard AJ, Ingraham JP and Issen KA. (2006), *Scripta Materialia*; 54: 783.

Xie XQ, Fan TX, Zhang D, Sakata T and Mori H. (2002), *Materials Research Bulletin*; 37: 1133.

Yi F, Zhu Z, Zu F, Hu S and Yi P. (2001), *Materials Characterization*; 47: 417.

Yu CJ, Eifert HH, Banhart J and Baumeister J. (1998) *Materials Research Innovations*; 2: 181.

Yu X and He D. (1994), *Materials and Mechanical Engineering (China)*; 18: 26.

Yu JL, Wang X, Wei ZG and Wang EH. (2003), *International Journal of Impact Engineering*; 28: 331.

Zhang X, Hong C, Han J and Zhang H. (2006), *Scripta Materialia*; 55: 565.

Zhihua W, Hongwei M, Longmao Z and Guitong Y. (2006), *Scripta Materialia*; 54: 83.

Zhou W, Hu W and Zhang D. (1998), *Scripta Materialia*; 39: 12: 1743.

Zhou J, Gao Z, Cuitino AM and Soboyejo WO. (2004a), *Materials Science and Engineering A*; 386: 118.

Zhou J, Shrotriya P and Soboyejo WO. (2004b), *Mechanics of Materials*; 36: 781.

Zhou J, Gao Z, Allameh S, Akpan E, Cuitino AM and Soboyejo WO. (2005a), *Mechanics of Advanced Materials and Structures*; 12: 201.

Zhou J, Allameh S and Soboyejo WO. (2005b), *Journal of Materials Science*; 40: 429.